Nonphotochemical hole-burning imaging studies of *in vitro* carcinoma and normal cells utilizing a mitochondrial specific dye

by

Richard Joseph Walsh

A dissertation submitted to the graduate faculty

in partial fulfillment of the requirements for the degree of

DOCTOR OF PHILOSOPHY

Major: Analytical Chemistry

Program of Study Committee:

Gerald J. Small, Major Professor

Dennis Johnson

R. Sam Houk

Patrica Thiel

Marit Nilsen-Hamilton

Iowa State University

Ames, Iowa

2002

Graduate College

Iowa State University

This is to certify that the doctoral dissertation of

Richard Joseph Walsh

has met the dissertation requirements of Iowa State University

Major Professor

For the Major Program

TABLE OF CONTENTS

To Crista and the one on the way

ABSTRACT

Low temperature Nonphotochemical Hole Burning (NPHB) Spectroscopy of the dye rhodamine 800 (MF680) was applied for the purpose of discerning differences between cultured normal and carcinoma ovarian surface epithelial (OSE) cells. Both the cell lines were developed and characterized at the Mayo Clinic (Rochester, MN), with the normal cell line having been transfected with a strain of temperature sensitive Simian Virus 40 Large T Antigen (SV40) for the purpose of extending the life of the cell culture without inducing permanent changes in the characteristics of the cell line. The cationic lipophilic fluorophore rhodamine 800 preferentially locates in *in situ* mitochondria due to the high lipid composition of mitochondria and the generation of a large negative membrane potential (relative to the cellular cytoplasm) for oxidative phosphorylation.

Results presented for NPHB of MF680 located in the cells show significant differences between the two cell lines. The results are interpreted on the basis of the NPHB mechanism and characteristic interactions between the host (cellular mitochondrial) and the guest (MF680) in the burning of spectral holes, thus providing an image of the cellular ultrastructure. Hole growth kinetics (HGK) were found to differ markedly between the two cell lines, with the carcinoma cell line burning at a faster average rate for the same exposure fluence. Theoretical fits to the data suggest a lower degree of structural heterogeneity in the carcinoma cell line relative to the normal cell line. Measurement of changes in the permanent dipole moment ($f\Delta\mu$) were accomplished by measurement of changes in hole width in response to the application of an external electric field (the Stark effect), and found that $\Delta\mu$

values for the carcinoma line were 1.5× greater than those of the SV40 antigen-free normal analogs. These findings are interpreted in terms of effects from the mitochondrial membrane potential. Results for HGK on the scale of single cells is also presented. Trends observed for large populations of cells (5×10^5 to 2×10^6) were concurrently observed for individual cells, with the carcinoma cell line burning at a faster average rate relative to the normal cell line.

CHAPTER 1. GENERAL INTRODUCTION

Research into the cause, diagnosis, and treatment of cancer has spanned much of modern human history, with no panacea having yet been found. Countless investigators have and continue to search for the answers of how and why cancer forms, and how it can be identified and stopped. And with very good reason: cancer remains the second leading cause of mortality in the United States through the year 1998, only outranked by heart disease (source: Centers for Disease Control).

Cancer is defined as an abnormal growth of cells, which tend to proliferate in an uncontrolled way, and, in some cases, to metastasize. Cancer is composed of over 100 different and distinctive types of the disease, and can involve any tissue of the body. Cancer arises due to the natural checks of growth being defeated, which is most often caused by an insult to the genetic code in control of these processes. All life, however, depends fundamentally on interpretation of genetic code. Because of this, profound and dire as it may sound, cancer can *never* be eliminated from occurring; as long as an organism is growing and dividing (the quality of life), mistakes are possible and cancer must be factored into this possibility. This, in my opinion, is the "bad news". The "good news", however, is that the human race has been able to identify normal, controlled growth and uncontrolled cancerous growth, and in some instances eliminate the self-destructive latter type.

Success in treating cancer has been obtained to a limited extent by the application of three types of treatment: chemical (or chemotherapy), radiological, and surgical. Each has its merits and downfalls. Chemotherapy destroys any type of actively dividing cell in the body, leaving the patient extremely weakened due to the destructive nature to portions of the body in constant regeneration: blood cells

(red and white), digestive tract, etc. Further, chemotherapy has limited application due to the acquisition of chemical resistance by cancerous tissue [1].

Radiology is dependent on knowledge of the location of cancerous tissue, and the correct dosage of energy to destroy the genetic makeup of the unwanted tissue. Radiological treatments are subject to similar side effects as chemotherapy, and run the risk of only temporarily weakening cancerous growth and in rare cases stimulating new cancerous growth (oncogenesis) [2,3]. Further, radiological treatments are extremely risky for young cancer patients, as the radiology can have extreme negative consequences for developing nervous tissue (especially brain).

Surgical removal of cancerous tissue does not suffer from the aforementioned side effects, however surgery can present undesirable side effects of its own and usually involves recuperation time. Surgical removal of tissue is not always possible (i.e. brain tumors), and may not be successful in removing all of the cancerous tissue. Treatments are also not limited to individual use; chemotherapy may be combined with radiological, surgical, or both, or any other possible combination. Medical literature tends to be fairly rigorous at tracking statistical success of each type of cancer and associated treatments, and treatments progress with time.

Three pretreatment factors currently can be identified which help determine an individual's likelihood of surviving the onslaught of cancer: lifestyle, genetics, and detection. Lifestyle is obviously most controllable. The popular media is full of interpretations of scientific studies (usually, anyway) aimed at prescribing foods to avoid (foods high in fat, char-grilled meats, etc.) and include (foods rich in anti-oxidants, such as cooked tomatoes, broccoli etc.), and habits to avoid (sunbathing,

tobacco, etc.) and include (sunscreen, regular visits to a physician). With the realization that an individual's genetic code could provide clues to cancer susceptibility in the early 1990's with the discovery of the BRCA-1 breast cancer gene [4], cancer research has largely expanded to include deciphering carcinogenesis on the genetic scale, with various genes being found that are highly prone to error. Ultimately, an individual can and should build a portfolio of family health history for the purpose of discussion with a medical professional and subsequent education of preventative and diagnostic tactics. As an aside, genetic testing for cancer susceptibility may someday become routine, barring future ethical and/or legal obstructions. This could potentially greatly expand an individual's arsenal for cancer prevention, as each individual would have a look into his or her "oncogenetical future" (their statistical likelihood of contracting any of the given forms of cancer in their lives based on their genetic and proteomic makeup). Lastly, detection, the factor which unilaterally determines cancer survival and which is the underlying objective of the work presented in this thesis, plays an extremely large part in the treatment of cancer, depending solely on timing: the earlier the diagnosis, the better the chances for proper treatment and eradication (source: National Cancer Institute).

The basic premise of the work presented herein is contained within this ideal: investigation of better cancer detection techniques will lead to improved detection rates, with early prognosis being the ultimate objective. Research presented in this thesis seeks to improve and add to cancer detection methods currently in use, and the means by which to accomplish this is the application of nonphotochemical hole-burning (NPHB) imaging. NPHB is analogous to magnetic resonance imaging

(MRI), in that pure optical dephasing times (T_2^*) are measured instead of proton relaxation times (T_1), with the common relation existing between the two in total dephasing time (T_2). NPHB is inherently sensitive to the nanoenvironment in which a fluorophore resides. Therefore, the objective of the work presented here will contain the following: to find and target structural differences between normal and carcinoma cells; to utilize relevant, valid normal and carcinoma cell lines; and to present the ability of NPHB imaging for resolving and quantifying those structural differences. Further explanation will be reserved for future chapters.

The organization of this thesis will be as follows: chapter two will cover pertinent biological aspects concerned with the research presented in chapters four and five. Chapter three shall introduce the topic of NPHB, and elaborate on the application to biological systems for the study of cellular anomalies. Chapter four is a manuscript submitted for publication and currently in press, and chapter five is a manuscript to be submitted for publication, both of which detail results obtained from NPHB of a rhodamine dye in normal and carcinoma *in vitro* ovarian surface epithelial cells. Chapter six will conclude the work presented and offer insight into possible future experimentation based on the accomplishments presented in chapters four and five. Finally, Appendixes A-E will include additional laboratory work completed by the candidate, including results of single cell NPHB, as well as supplemental background information necessary for reproducing any of the work presented in this thesis. Research performed by the candidate but not included in this thesis includes a published manuscript [5] of work completed while in the group of Therese Cotton, with the assistance of George Chumanov.

References

1. Gupta, S.; Tsuruo, T., (Eds.); *Multidrug resistance in cancer cells : molecular, biochemical, physiological, and biological aspects*, J. Wiley: Chichester ; New York, **1996**.

2. Wheldon, E. G.; Lindsay, K. A.; Wheldon, T. E., *Int. J. Radiat. Biol.* **2000**, *76*, 699.

3. Lindsay, K. A.; Wheldon, E. G.; Deehan, C.; Wheldon, T. E., *Br. J. Radiol.* **2001**, *74*, 529.

4. Friedman, L. S.; Ostermeyer, E. A.; Lynch, E. D.; Szabo, C. I.; Anderson, L. A.; Dowd, P.; Lee, M. K.; Rowell, S. E.; Boyd, J.; King, M. C., *Cancer Res.* **1994**, *54*, 6374.

5. Walsh, R. J.; Chumanov, G., *Appl. Spec.* **2001**, *55*, 1695.

CHAPTER 2. PERTINENT BIOLOGY

The work presented in this thesis could not have been made possible except for the extraordinarily unique cellular organelle present in nearly every type of cell in the human body: mitochondria. As such, a large portion of this chapter will be devoted to the history of research on mitochondria and development of the basis for its importance in the work presented in chapters 4 and 5. The remainder of the chapter will be devoted to the subject cell lines used in this research.

2.1. Mitochondria

A look into any biology text of the past century will reveal a basic list of components for most eukaryotic animal cells: the plasma membrane, cytoplasm, and nucleus, which define the cell boundary, account for the volume of the cell, and contain the "command center" of the cell, respectively. Contained within the cytoplasm are the organelles, the analogical machinery of the cell: the aforementioned nucleus, endoplasmic reticulum (smooth and rough), Golgi apparatus, mitochondria, microtubules, microfilaments, ribosomes, and lysosomes, to name but a few. Each of these organelles has evolved into a highly specialized piece of machinery, and although volumes exist about each one, it is the mitochondria which piques our interest in this discussion.

Commonly called the "powerhouse of the cell", mitochondria have been determined to be the place where oxidative phosphorylation occurs. Composing ~20% of the volume of most cells [1], they assume various shapes and sizes, some being spherical, ranging from 0.5-5 μm in diameter, and others being elongated and cylindrical, reaching lengths of 10 μm with cross sections of 10s-100s of nanometers

[2]. Unfortunately, typical sizes of mitochondria are just below the limits of resolution by regular light microscopy in terms of being able to resolve substructure.

The first scientific studies of mitochondria began in the 1880s by Altmann, who discovered a fixation method (bichromate-osmic acid) that preserved the mitochondria, in opposition to the typical fixation methods of the late 19th and early 20th century, when fixatives generally had high acetic acid content, an extremely destructive chemical to mitochondria. Altmann published his findings in a book of colored lithographs with variously stained tissues, revealing "bioblasts", his term for mitochondria [3]. This period also marks a confusing time in the nomenclature and the existence and purpose of mitochondria, as the aforementioned staining techniques halted the cellular life processes, even leading some researchers to doubt the existence of mitochondria. By 1920, however, the trend in cell biology was shifting to observe cells that were perturbed as little as possible. Arguments over the existence of mitochondria in the cell were dispelled with the introduction of the mitochondrial specific stains crystal violet by Benda (who, incidentally, also introduced the term "mitochondria" from the Greek *mitos* and *chondros*) [4], Janus green B by Michaelis [5], and the detailed documentation of mitochondria in fresh *non-fixed* material by Lewis and Lewis [6]. Subsequently, the focus of research began shifting to the study of mitochondrial structure and function.

The structure of the mitochondria was clearly elucidated for the first time with the advent of the transmission electron microscope, and a representative structure is given in Figure 2.1. Palade [7-9] and Sjostrand [10,11] revealed that mitochondria have their own phospholipid - based dual membrane (differentiated simply as "outer"

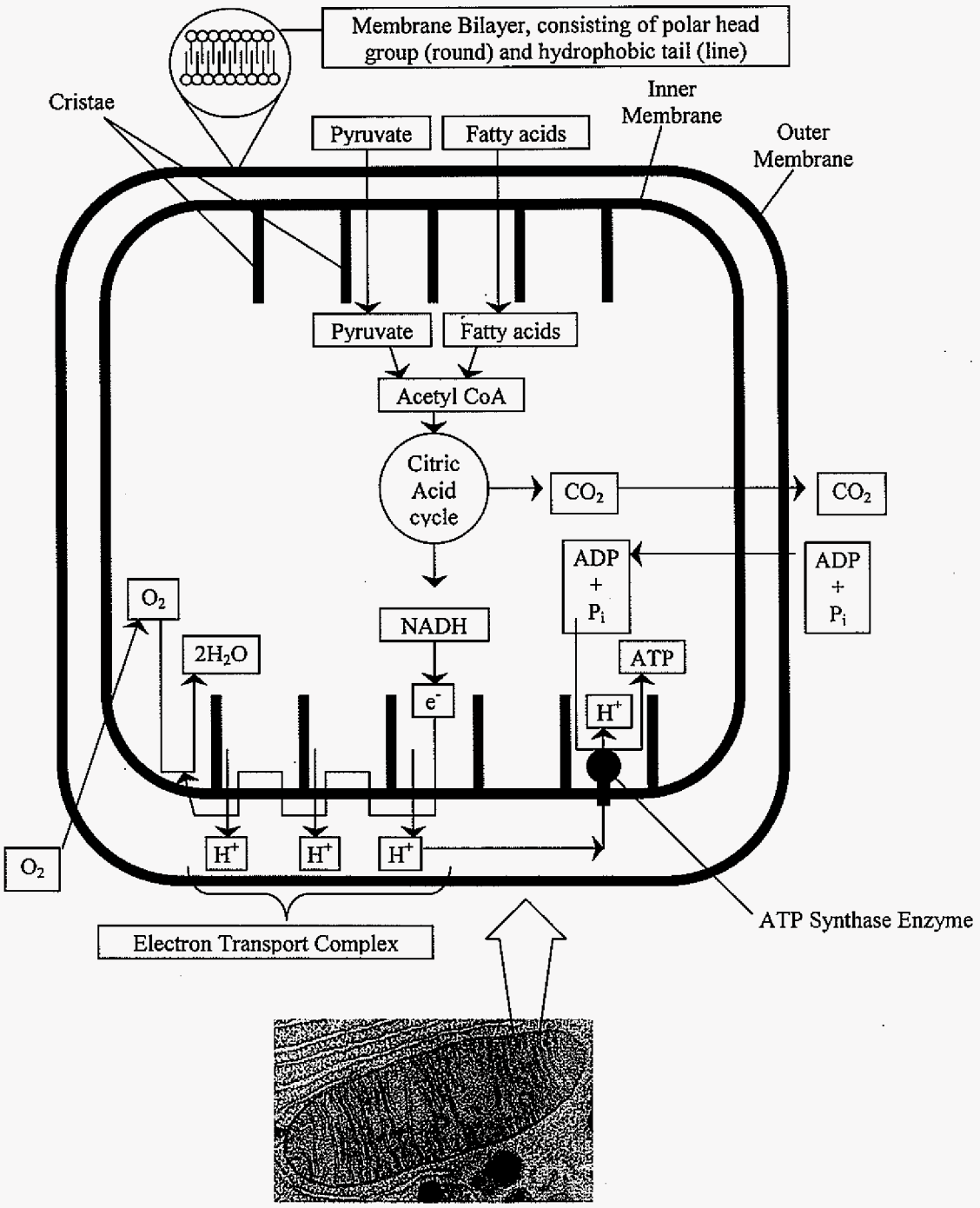

Figure 2.1 Cross section of mitochondrion structure, with representative proteins and related biochemical processes.

and "inner" membranes). Convolutions of the inner membrane into the center of the mitochondrial body give rise to the most characteristic feature of mitochondria, the cristae. The morphology of the cristae serves to increase the surface area of the inner membrane and this is where the proteins responsible for phosphorylation reside. A rough calculation shows the effectiveness of the design: the minimum surface area that would cover a sphere with a volume of 1 μm^3 with a radius *r* equal to 0.62 μm (volume = $4/3\pi r^3$) is 4.83 μm^2. A lipid bilayer membrane 0.006 μm thick with a surface area of 166.6 μm^2 would occupy the same volume. The theoretical gain in surface area is then 166.6/4.83 or ~35 fold increase. Estimates of the inner-membrane surface area to unit volume ratio for rat liver mitochondria are ~16.5, and ~61 for rat heart mitochondria [12]. It then follows that the number of cristae, and hence the density of cristae, is generally higher in tissues which experience high energy demands, i.e. muscle and neurons [13].

Without going into great detail, it is important to mention that mitochondria generate a membrane potential by enacting a proton gradient between the mitochondrial matrix and the intermitochondrial membrane. This is important for two reasons: (1) the membrane potential has become the focus of numerous investigations whereby the magnitude of the potential has been found to differ in mitochondria derived from cancerous tissue relative to normal tissue [14,15] and (2) the lipid-rich, anionic environment poses a favorable site for lipophilic, carbocationic, fluorescent dyes to locate [16-20]. The latter has sparked interest in such dyes for use as chemotherapeutic and photodynamic therapeutic agents (see references).

The generation of the membrane potential is inherently related to the main function of mitochondria: for oxidative phosphorylation, or the creation of adenosine triphosphate (ATP) from adenosine diphosphate (ADP). The process by which this occurs provides one of the most controversial and interesting periods in mitochondrial research history. In 1961, Paul Mitchell initially proposed the chemiosmotic theory, which (correctly) attempted to explain biological energy transformation [21,22]. Many theories abounded as to how this process took place, and most researchers hypothesized that intermediates were formed in a coupling mechanism that eluded discovery. Mitchell conceded that such intermediates likely did not exist, and that if the oxidoreduction in the cytochrome system is organized across a membrane in an anisotropic fashion, protons can be produced on one side of the membrane and consumed on the other side (adapted from Tyler [12]):

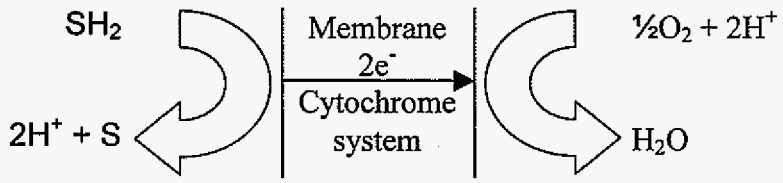

Respiratory-chain reactions provide the energy for the above process, with the return of protons across the membrane coupled with ATP synthesis. The driving force of ATP synthesis was postulated on the basis of both an electrical potential ($\Delta\psi$) and a pH difference ($pH_{out} - pH_{in}$, or ΔpH) across the coupling membrane, to collectively give the proton-motive force (Δp):

$$\Delta p = \Delta\psi - Z\,\Delta pH \qquad 1)$$

where Z represents 2.303RT / F. The theory was not widely accepted after its introduction, but perhaps because of this high level of ridicule, chemiosmosis was scientifically scrutinized and eventually became the accepted mechanism of energy coupling.

One very unique feature of mitochondria is the fact that they contain their own DNA (mtDNA), which has been found to be a remnant of their evolutionary past: mitochondrial gene sequences trace back to a division of Proteobacteria, confirming the once hypothetical eubacterial origin of this organelle. The human version of this sequence is not very large (relative to nuclear DNA) at about 16.5 kbp, but with the high number of mitochondria per cell (100s-1000s), there tend to be high levels of copies contained in a cell (10^3-10^4). These genes are responsible for encoding 13 respiratory chain subunits, 22 transfer RNAs, and two ribosomal RNAs [23]. Although not all processes contained in mitochondria are currently fully understood, it is reasonable to assume that most or all of the components necessary for the start of cancer exist here: short gene sequences that, if they become altered, can have dire effects due to their high encoding use and lack of regulation for damaged code, and the location of reactive oxygen species (ROS) being developed as byproducts of oxidative phosphorylation in close proximity to this code and able to cause alterations, not to mention control of production and delivery of aforementioned basic cellular energy components. Add to this the recent realization that mitochondria are possibly linked to – or in control of – apoptosis (programmed cell death) [13,24], and it seems certain that mitochondria are linked in some way to the early transformation of a cell to a cancerous state.

From here it should be noted that although there may be a close resemblance between mitochondria of a given tissue, their appearance can deviate markedly between different tissues. This raises an interesting point: mitochondria are able to change their shape, and may assume any given shape depending on the needs presented by the tissue. To be fair, however, it should be recognized that it is not fully understood if mitochondria are in control of their shape or if forces external to the mitochondrial body are what determine this. Nonetheless, despite the variability of the external shape the internal structural organization is highly conserved [25].

Structural controls and the proteins involved in oxidative phosphorylation are important to understanding the complexity of the processes which take place inside the mitochondria, and recent thorough reviews are available from Yaffe [26], Wallace [27], Bereiter-Hahn [1,25], and Scheffler [13]. For our purposes, it is important to mention that alterations in mitochondria have been linked to numerous diseases, including but not limited to Parkinson's and Alzheimer's disease [28], liver disease, muscular dystrophy, cardiomyopathy, diabetes, ageing, and cancer [26,27].

In the case of cancer, it has been found that the abnormalities tend to be extraordinary and can include some or all of the following: (1) Changes in size and formations of bizarre shapes, including branching, forming annular rings, s-shaped configurations, semicircular structures, or forming "giant" mitochondria; (2) Changes in mitochondrial number, membrane lipid composition, and membrane potential; (3) Changes in the ultra structure architecture, such as apparent thickening of the mitochondrial cristae; (4) Alteration of the energy-linked function and loss of electron

transport components; and (5) relocation of mitochondria in the cell to abnormal positions, such as penetrating the nuclear envelope [29,30]. In addition to these macro-scale modifications, the aforementioned mtDNA has also been found to have correlated mutations with tumors in cancer patients in a recent study presented by Sidransky et al [23].

Through mitochondria, the premise for finding a discernable difference in the structural makeup of errant cells has been found. Discussion of our second objective (to utilize relevant, valid normal and carcinoma cell lines) shall be the topic of the duration of this chapter.

2.2. Model Subjects in Developing Cancer Diagnostics

Research concerning the development of diagnostic tools for any sort of disease detection is ultimately governed by the ability to obtain relevant samples, both minimally transformed standard samples and valid samples of the disease. In particular, cell culture has often been labeled as a point of contention with regard to research relevance [31]. Recent advances in cell culture techniques have begun to provide better test subjects, however, and the success of the research presented in this dissertation has hinged on the use of two human ovarian surface epithelial (OSE) cell lines that have been scientifically characterized [32,33]. The development and background of each cell line is detailed here in an attempt to expand the relevance of the findings presented in chapters 4 and 5.

2.2.1. OV167: A Human Ovarian Surface Epithelial Cell Line

Calling into question the relevance of research based on their use, cancerous cell models often (unintentionally) include immortalized cell lines with genetic

variances from the source tissue. The OV167 carcinoma cell line used in this study was developed to overcome this difficulty, and the characterization of the cell line was based on the insulin-like growth factor (IGF) system [34-36]. The IGF system is implicated heavily in breast and endometrial carcinogenesis [37-44]. Briefly, the IGF system is composed of peptides very similar in structure to insulin. These peptides are able to bind with specific membrane bound receptors, which, in the case of IGF type I, are able to transduce primary signals for cell metabolism, mitogenesis, transformation, and resistance to apoptosis [45-47]; hence, there are apparent ramifications for the beginning of cancer and tumor growth. Intertwined with IGF's are IGF-binding-proteins (IGFBPs), which are present throughout most bodily fluids. One of the roles of IGFBPs appears to be protecting circulating IGFs, allowing them to be shuttled to their binding sites [47]. It is important to realize the IGF system is a part of normal, functioning ovaries. It is unknown the level of involvement the system plays in the ovarian surface epithelium, from which it is believed most (~90%) ovarian carcinomas develop and from which the OV167 cell line was derived.

As such, the characterization of the OV167 cell line (among others) as presented by Conover et al. [32] is summarized here, with simplifications. The characterization serves as a reference point between normal ovarian epithelial tissue function and characterizations of other pertinent carcinomas, namely breast and endometrial, for which numerous characterizations exist (vide supra). The findings of the characterization are as follows.

The OV167 cell line tested positive for keratin proteins, a marker documented to decrease upon propagation of ovarian cells in culture. IGF-I was detected in

OV167, but not IGF-II. IGFBPs, specifically IGFBP-2, IGFBP-4, and IGFBP-6 were found to exist in substantial quantities, comparable to IGFBPs specifically binding to highly responsive fibroblasts, osteoblasts, and human breast cancer cell lines. Activation of IGFs by IGF type I receptor stimulates growth in numerous malignant cells, and mitogenic and differentiation-related responses to externally added IGF were examined for the OV167 cell line. The cells could be stimulated in growth by added protagonists of IGFs in serum free growth medium, indicative of the aforementioned IGF system overriding growth controls. Lastly, analysis of the secretion of CA-125 antigen found moderate elevations in the OV167 cell line. CA-125 is an antigen expressed by the coelomic epithelium, and significance lies in the fact that over 80% of epithelial ovarian cancers express overabundance, making it a marker for tumor activity [48,49].

Lending further credence, similar studies that sought to create and characterize OSE cell lines have been published, with promising results. Maines-Bandiera et al. [50] were able to successfully transform three human OSE cell lines, with two of the lines expressing keratin and being CA-125 negative, having an increased growth potential and reduced serum dependence, and were determined to be non-tumorigenic when implanted into nude mice. Likewise, Nitta et al. [51] were able to culture several new OSE malignant carcinoma lines not directly derived from cancer cells via SV40 transfection, for the purpose of establishing a model system by which to investigate the mechanisms of cytogenic and molecular changes of normal OSE cells through the various steps of transformation.

All things considered, the OV167 cell line characterized in Conover et al. has retained the cytogenetic characteristics of a primary tumor and can serve as a valid model for studying human epithelial ovarian cancer cell biology. As such, this cell line was deemed ideal for the work presented in this thesis, as the cells are well-characterized and present reliable yet simple growth properties mimicking those of tumor cells.

2.2.2. OSE(tsT)-14: A Simian Virus 40 - Transfected Normal Human Ovarian Surface Epithelial Cell Line

Comparative normal cells, by contrast, are not as easily cultured, as normal human cells tend to have very limited life spans in culture [52] and are easily subject to genetic variation from the parent tissue. The repercussions of these complications are clear: cells cultured for the purpose of playing the role of normal comparatives are mutated and more like the cancer cells with which they are being compared to than to the original normal cells they are supposed to be, in effect making any comparison meaningless. The most credible source of normal cells, unfortunately, are those freshly obtained from a patient and grown minimally (if at all) in culture - one to two passages, four at most. Since this is not always a possibility, cell biologists have devised methods to circumvent the difficulty encountered by researchers not readily able to obtain normal cells on a regular basis, if at all.

One of the most popular ways of creating a normal cell culture that can be grown to high passage number with minimal variation is to transfect the cell culture with Simian Virus 40 (SV40), a polyomavirus of rhesus macaque origin [53]. SV40

has a rather interesting history, first discovered as a contaminant of polio vaccines [54]. Soon after this discovery, the potential for astounding consequences were realized when SV40 was shown to be tumorigenic in rodents and also used to transform many types of cultured cells [55-59]. Between the years 1955-1965, millions of people were inadvertently inoculated, and only time would tell how drastic the mistake would be. Today, the debate continues as the recipients of the virus reach middle-age, and there are numerous recent literature citations [60-66] that show possible elevations in cancer occurrence, but all studies call for continued monitoring and analysis. Even links to acquired immune deficiency syndrome (AIDS) have been raised [67,68], but any true corroboration beyond coincidence has yet to be demonstrated. A truly ironic thought, however, is the fact that the need may someday exist to inoculate against SV40!

To digress, some good has arisen from the aforementioned dilemma: SV40 transfection has allowed for incalculable advances: the determination of the first complete nucleotide sequence of a eukaryotic viral genome, the recognition of enhancers involved in transcriptional regulation, the phenomenon of alternative splicing, identification of tumor suppressor protein p53 (vide infra), elucidation of viral effects on cell cycle regulation and identification of a protein nuclear localization signal [66,69-71]. More to the point of the research presented in this thesis, SV40 allows for an accurate comparison between normal and cancerous cells. The method by which this is accomplished requires further elaboration, and a synopsis of the mechanisms of SV40 is presented here.

SV40 transfection of a cell involves at least three different proteins, the most recognizable being p53. Dubbed the "guardian of the genome" [72], p53 has numerous roles, the most heavily chronicled being that of a tumor suppressor by controlling the initiation of programmed cell death or apoptosis after irreversible DNA damage has occurred [73,74]. p53 is involved in an extraordinary number of protein signaling interactions within the cell, and a complete listing of all interactions is well beyond the scope of this discussion. Excellent reviews are available from Shen [75], Janus [76], Attardi [77], Jayaraman [78], and Hupp [79]. Accordingly, p53 is in control of cell cycle arrest in either G1 or G2 phase (see Appendix B for an explanation of cell growth phase cycles), leading to apoptosis. This is in response to cellular accumulation of DNA defects, and serves the purpose of eliminating the erroneous genetic code and the propagation of dangerous cells which could continue to multiply and threaten the normal cell population [80]. Another aspect of p53's control is in ensuring genomic integrity through DNA damage monitoring and activation of proteins which perform DNA repair when such processes are required. There is also speculation p53 is involved directly in the repair process, and that p53 is not latent in its unstimulated state (vide infra), as is commonly thought [76]. Lastly, studies have found p53 plays critical roles in preventing embryonic developmental disorder processes [81]. Clearly, p53 holds an extraordinarily important role in carcinogenesis.

Summary figures of the multiple roles of p53 are presented in Figures 2.2 and 2.3. Figure 2.2 shows the possible stress signaling sent to p53, often mediated through Arf or Mdm2 (an E3 ligase that catalyzes ubiquitination-degradation of p53).

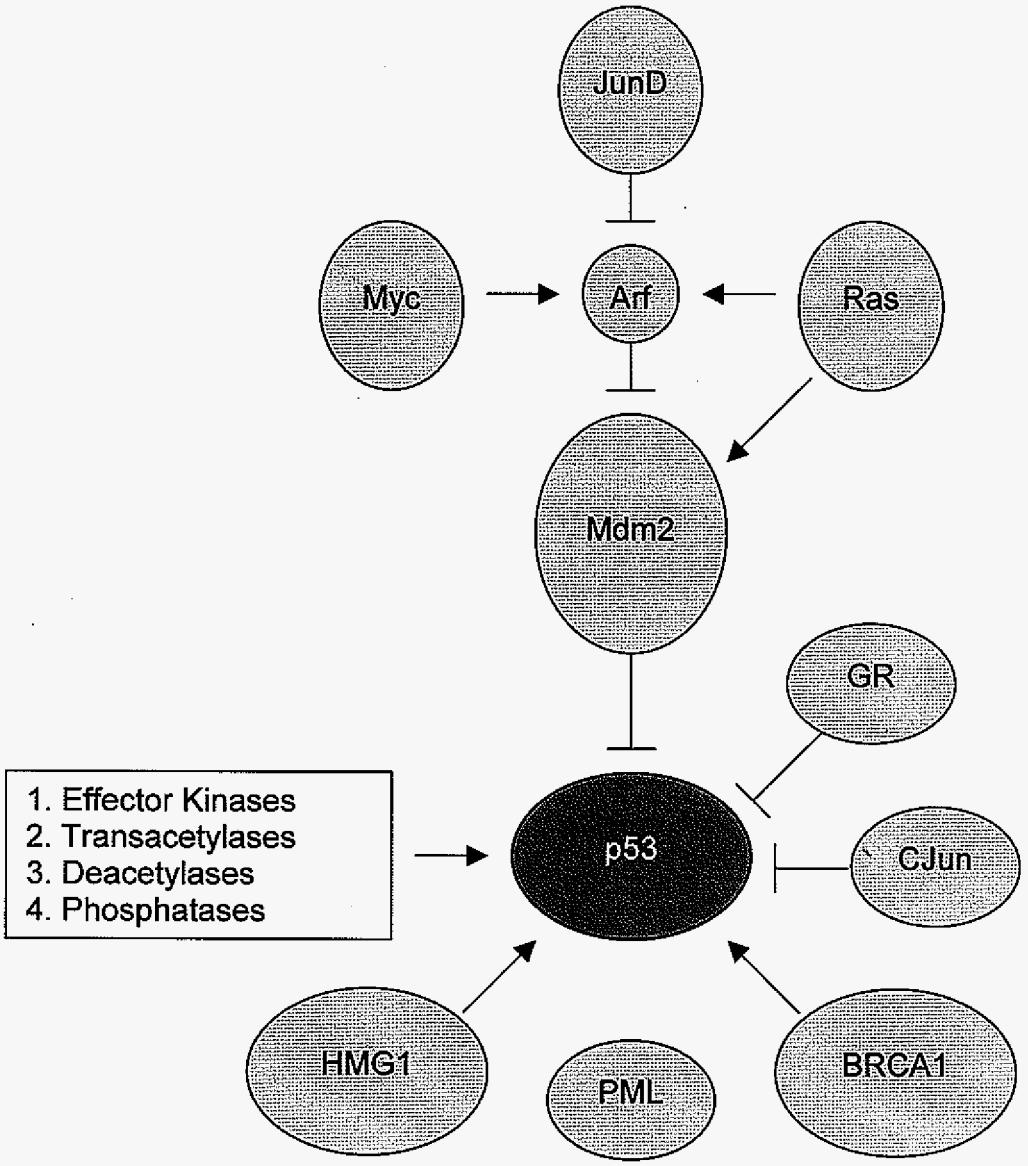

Figure 2.2 Stress signals sent to p53. Oncogenes trigger activation through the Arf-Mdm2-p53 pathway (with the exception of Ras, which can signal directly); other stress signals function by alternate pathways. Adapted from Bargonetti and Manfredi [53].

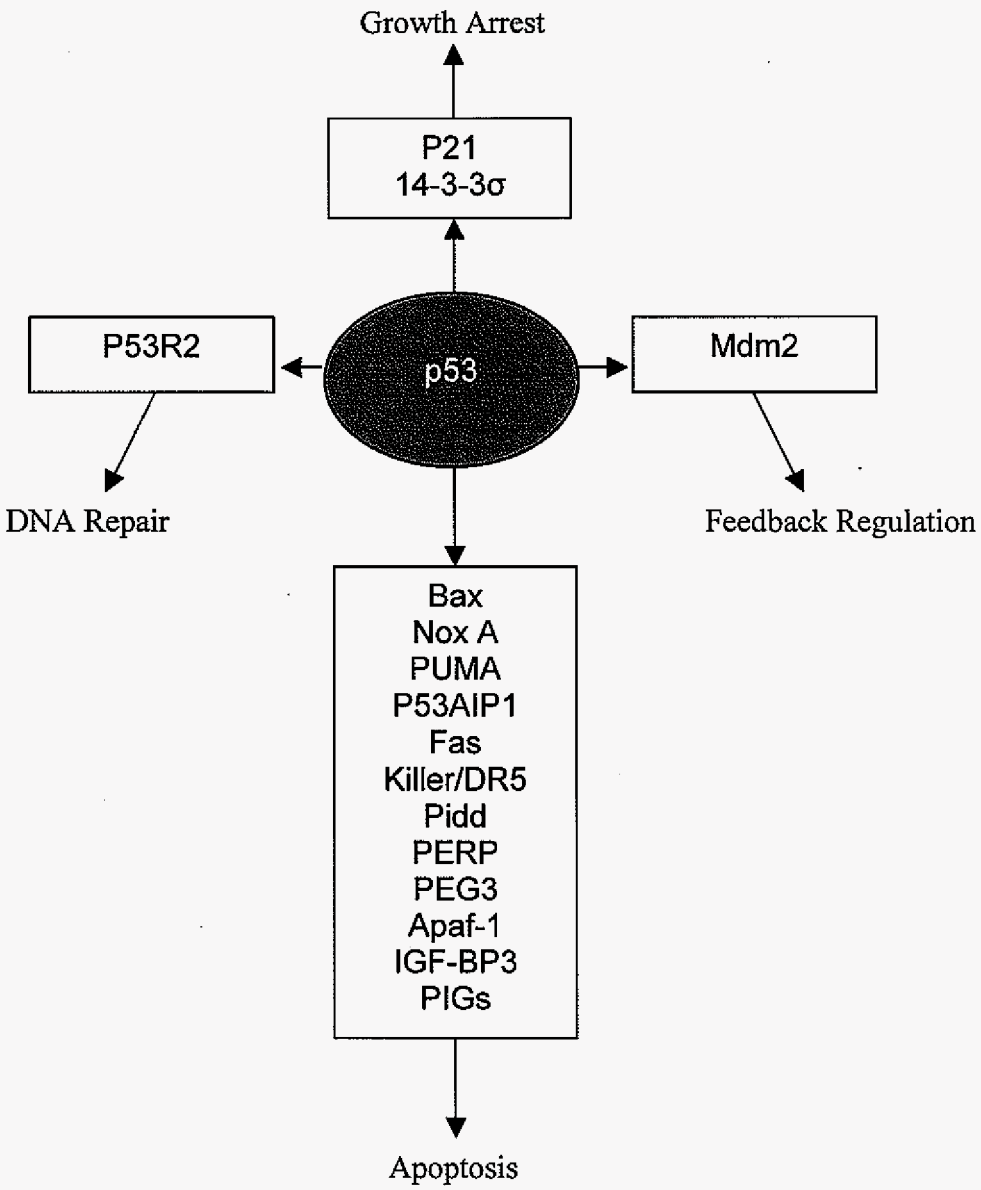

Figure 2.3 Target genes in cellular responses from p53. Each of the listed genes have been shown to contain p53 binding sites within their regulatory region. Signaling combinations result in noted cellular response. Adapted from Bargonetti and Manfredi [53].

To date, the most well documented resultant activity of such stress signals is p53 phosphorylation. Depending on the site of the phosphorylation, the outcome can be enhanced protein stability and eventual growth arrest and apoptosis or further binding to signalosomes that tag the protein for degradation [82]. Alternatively, target genes activated selectively by p53 are shown in Figure 2.3, with the signal outcome listed for each target gene. From the figure, four possibilities can be seen for response to p53 signaling: growth arrest, DNA repair, apoptosis, and feedback regulation. Growth arrest is reversible and can occur at the G1/S or G2/M barrier; DNA repair has been mentioned previously; apoptosis involves further complicated mechanisms but is more than deserving of further mention.

Research involving p53-dependent apoptosis is controversial to say the least, as researchers have cited evidence suggesting target gene activation as unnecessary for apoptosis as a cellular response to p53 [83-94]. However research also exists demonstrating definitive links, and interestingly mitochondria play a large role in control of apoptosis, along with a family of proteins known as Bcl-2. The family consists of (to date) nine proapoptic members and seven anti-apoptic members; of relevance for this discussion are Bcl-2, Bcl-x_L, Bax, and Bak, the first three of which have been shown to form channels in synthetic lipid membranes [95-97]. Bcl-2 is normally membrane-bound in mitochondrial outer membranes, the endoplasmic reticulum, and nuclear membranes. Bcl-x_L and Bax can be found in the cytosol or membrane-bound; in response to p53 death signals, Bax and Bak translocation to the mitochondrial membrane has recently been reported [98-101]. Further, Bax and Bak have been found to associate with adenine nucleotide

translocator (ANT) and the voltage dependent anion selective channel (VDAC), members of the mitochondrial permeability transition pore (PTP) [102]. The association results in depletion of the mitochondrial membrane potential, with subsequent activation of the caspase cascade, involving release of cytochrome c [103] and Smac/DIABLO [104], ultimately resulting in full cellular destruction.

Lastly, the oncoprotein Mdm2 forms an autoregulatory feedback loop with p53 in which p53 positively regulates Mdm2 and Mdm2 negatively regulates p53 levels and activity. In the example of DNA damage by ultraviolet (UV) irradiation, Mdm2 levels decrease immediately following exposure, activating P53 to initiate cell cycle arrest. If the damage is slight, and after repair of DNA, Mdm2 levels once again rise and serve to shuttle p53 from the nucleus to the cytoplasm, where p53 is eventually degraded and cell balance is restored [105]. The result, however, is that a control is introduced by which p53 may be overridden and tumorigenesis may propagate, and the Mdm2 protein is currently being investigated in p53-independent carcinogenesis.

Having thoroughly covered the tumor suppressing protein p53, we turn our attention back to the SV40 antigen for the purpose of determining the relation between these two. At this point, a distinction must be made between two SV40 proteins: Large T antigen (TAg) and small T antigen (tAg). TAg is necessary but not sufficient for immortalization of a cell line, but TAg alone can significantly extend the lifespan of fibroblast and epithelial cells [106]. tAg alone, on the other hand, cannot cause cellular transformation but can provide an important mitogenic signal that assists with the transforming activity of TAg [107]. The current focus shall be

concerned only with TAg, as it is the type used to transfect our subject cell line. The link between TAg antigen and p53, then, is the fact that TAg antigen transfects and transforms cells by binding to and inactivating p53. Further, most forms of TAg display temperature sensitivity, and can be introduced into a cell at a permissive temperature (34°C), whereby the cell culture gains an extended life span, continuing to proliferate without the natural growth controls resulting in apoptosis of the entire culture. The inherent temperature sensitivity allows a controlled release of the culture back to normal conditions, as a shift in temperature to 39°C results in TAg function becoming inactivated [106].

As alluded to previously, two other protein groups are involved with cellular manipulation by SV40 TAg. The retinoblastoma (namely, pRB and closely related p107 and p103/pRB2) and the transcriptional co-activators p300 and CBP are also targets of TAg binding [107]. No less important than p53, these proteins deserve brief mention of their purpose and their interaction with TAg. Following this discussion, a synopsis and model of the entire SV40 TAg – cell transformation as it is currently known will be presented.

The pRB protein and closely related p107 and p130 are critical for maintaining control over cell cycle progression, and were the first described tumor suppressors [108-110]. Regulation is accomplished through their binding to specific members of the transcription family E2F (designated E2F-1 through E2F-5). DP-1 and DP-2, protein components of the E2F transcription factor, further form heterodimers with any of the E2F proteins. These dimers in turn bind to specific DNA sequences in the promoter region of genes required for entry into S phase

[111-113]. E2F-DP dimers then serve to promote transcription or suppress it, with the latter case being accomplished by further interaction with pRB proteins. For cells transitioning from G1 to S, pRB is converted from a hypo- to a hyper-phosphorylated state. The latter portion of this transition also includes phosphorylation of p107 and p300. Phosphorylation is accomplished by the cyclin-dependent kinases cyclin D1/cdk4 and cyclin E/cdk2. The purpose of these phosphorylations is believed to be promotion of the dissociation of pRB proteins from E2F proteins, thereby relieving the pRB-induced suppression of E2F mediated transcription. SV40 TAg preferentially binds to the hypophosphorylated form of pRB, thus removing the control on E2F-initiated cell cycle progression and sending the cell into uncontrolled proliferation [107].

Lastly, numerous studies have shown that neither p53 binding alone, Rb family binding, nor the combination binding of both sets is enough to cause TAg-mediated transformation [114-121]. A third set of proteins, the p300 and CBP families, function as coactivators of transcription, forming associations with p53 and contributing to p53-mediated transcriptional activation of genes (Mdm2, p21 and Bax) which are involved in DNA damage response, ultimately contributing to G1 cell cycle arrest and apoptosis [122-124]. Seemingly in contradiction, p300/CBP interacts independently with Mdm2 and facilitates Mdm2-mediated degradation of p53 [125]. However, activity in both transcriptional activation and p53 degradation may be the result of p300/CBP operating in different states of the cell cycle. Low p53 levels trigger p300/CBP to facilitate transactivation, but sudden increases in p53 levels cause a switch to Mdm2 collaboration for p53 degradation [107]. As in the

case with pRb protein, phosphorylation plays a major part in the control of p300/CBP binding activity, and similarly, TAg shows preferential binding of p300/CBP in the hypophosphorylated form [126], targeting a similar process by which growth controls are checked. Relatively little more is known about p300/CBP, however, and it remains to be shown that p300 binding is involved in transformation by TAg [127].

Putting everything together, Figure 2.4 shows a flowchart in which all of the aforementioned TAg-protein associations are shown. As with most processes in biology, this is a snapshot of present day understanding and will undoubtedly change with time as research progresses. The most well known processes have been detailed here for the purpose of showing the complexity of the systems involved and also the level of knowledge that exists today in deciphering cellular respiration/proliferation processes. Furthermore, with relevance to our subject cell lines, we now have a detailed picture of the possible differences that exist between them in terms of mitochondrial respiration/structure and a complete understanding of the validity of the comparison between these two cell lines. Two of the objectives set out at the beginning of this thesis have been met, and in the next chapter, the means by which to meet our third objective will be introduced with background principles for the technique of NPHB imaging.

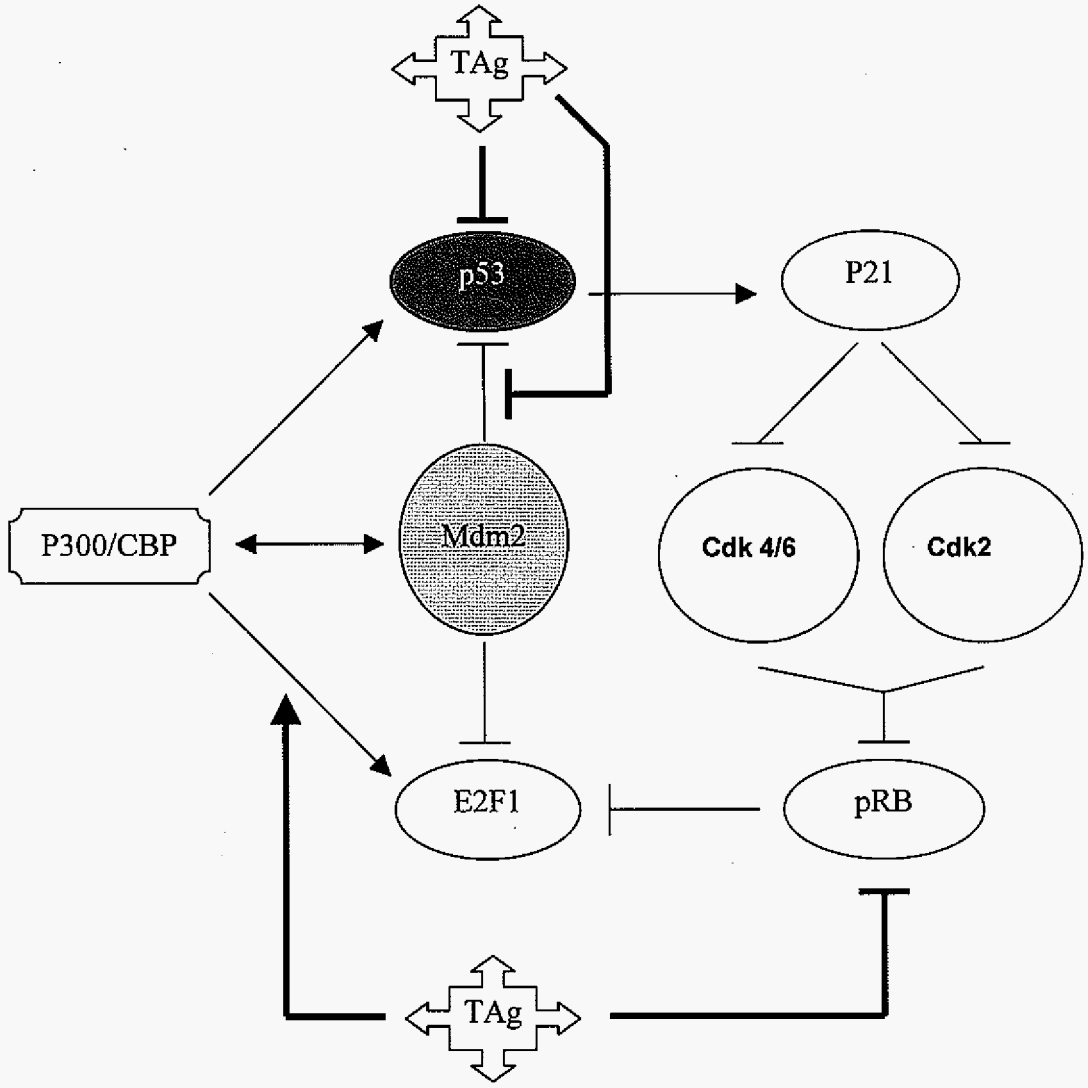

Figure 2.4. Model for p53, p300/CBP, and pRB binding and disruption by TAg. TAg binds to p53, pRB, and p300/CBP, directly influencing E2F1 as well as Mdm2 through various routes, disrupting controls on cell proliferation. Adapted from Ali and DeCaprio [107].

References

1. Bereiter-Hahn, J. Behavior of Mitochondria in the Living Cell. In *International Review of Cytology / A Survey of Cell Biology*; Jeon, K. W., Friedlander, M., Ed.; Academic Press, Inc.: San Diego, **1990**; Vol. 122; pp 1.

2. Whittaker, P. A., Danks, Susan M. *Mitochondria: structure, function and assembly*; Longman Inc.: New York, **1978**.

3. Altmann, R. *Die Elementarorganismen und ihre Beziehungen zu den Zellen*; Veit: Leipzig, **1890**.

4. Benda, C., *Arch. Anat. Physiol.* **1898**, 393.

5. Michaelis, L., *Arch. Mikr. Anat.* **1899**, *55*, 558.

6. Lewis, M. R., Lewis, W. H., *Amer. J. Anat.* **1915**, *17*, 339.

7. Palade, G. E., *Anat. Rec.* **1952**, *114*, 427.

8. Palade, G. E., *J. Histochem. Cytochem.* **1953**, *1*, 188.

9. Palade, G. E. In *Enzymes: units of biological structure and function*; Gaebler, O. H., Ed.; Academic: New York, **1956**; pp 185.

10. Sjorstrand, F. S., *Nature* **1953**, *171*, 30.

11. Sjorstrand, F. S., *J. Cell. Comp. Physiol.* **1953**, *42*, 15.

12. Tyler, D. *The mitochondrion in health and disease*; VCH Publishers, Inc.: New York, **1992**.

13. Scheffler, I. E. *Mitochondria*; Wiley-Liss, Inc.: New York, **1999**.

14. Chen, L. B., Rivers, E. N. Mitochondria in cancer cells. In *Genes and cancer*; Carney, D., Sikora, K., Ed.; John Wiley & Sons, Inc.: New York, **1990**; pp 127.

15. Summerhayes, I. C.; Lampidis, T. J.; Bernal, S. D.; Nadakavukaren, J. J.; Nadakavukaren, K. K.; Shepherd, E. L.; Chen, L. B., *Proc. Natl. Acad. Sci. U S A* **1982**, *79*, 5292.

16. Modica-Napolitano, J. S., Aprille, J. R., *Adv. Drug Deliv. Rev.* **2001**, *49*, 63.

17. Nadakavukaren, K. K.; Nadakavukaren, J. J.; Chen, L. B., *Cancer Res.* **1985**, *45*, 6093.

18. Papa, S.; Capuano, F.; Capitanio, N.; Lorusso, M.; Galeotti, T., *Cancer Res.* **1983**, *43*, 834.

19. Christman, J. E.; Miller, D. S.; Coward, P.; Smith, L. H.; Teng, N. N., *Gynecol. Oncol.* **1990**, *39*, 72.

20. Ara, G.; Aprille, J. R.; Malis, C. D.; Kane, S. B.; Cincotta, L.; Foley, J.; Bonventre, J. V.; Oseroff, A. R., *Cancer Res.* **1987**, *47*, 6580.

21. Mitchell, P., *Biol. Rev.* **1966**, *41*, 445.

22. Mitchell, P., *Nature* **1961**, *191*, 423.

23. Fliss, M. S., Usadel, H., Caballero, O. L., Wu, L., Buta, M. R., Eleff, S. M., Jen, J., Sidransky, D., *Science* **2000**, *287*, 2017.

24. Finkel, E., *Science* **2001**, *292*, 624.

25. Bereiter-Hahn, J., Voth, M., *Microsc. Res. Tech.* **1994**, *27*, 198.

26. Yaffe, M. P., *Science* **1999**, *283*, 1493.

27. Wallace, D. C., *Science* **1999**, *283*, 1482.

28. Trimmer, P. A.; Swerdlow, R. H.; Parks, J. K.; Keeney, P.; Bennett, J. P., Jr.; Miller, S. W.; Davis, R. E.; Parker, W. D., Jr., *Exp. Neurol.* **2000**, *162*, 37.

29. Djaldetti, M., *Acta Haemat.* **1982**, *68*, 241.

30. Eapen, C. E.; Madesh, M.; Balasubramanian, K. A.; Pulimood, A.; Mathan, M.; Ramakrishna, B. S., *Scand. J. Gastroenterol.* **1998**, *33*, 975.

31. Chou, J. Y., *Mol. Endocrinol.* **1989**, *3*, 1511.

32. Conover, C. A.; Hartmann, L. C.; Bradley, S.; Stalboerger, P.; Klee, G. G.; Kalli, K. R.; Jenkins, R. B., *Exp. Cell Res.* **1998**, *238*, 439.

33. Kalli, K. R.; Chen, B.-K.; Bale, L. K.; Gernard, E.; Overgaard, M. T.; Oxvig, C.; Conover, C. A., Manuscript in progress.

34. Cullen, K. J.; Yee, D.; Rosen, N., *Cancer Invest.* **1991**, *9*, 443.

35. Daughaday, W. H., *Endocrinology* **1990**, *127*, 1.

36. Daughaday, W. H.; Deuel, T. F., *Endocrinol. Metab. Clin. North Am.* **1991**, *20*, 539.

37. Karas, M.; Kleinman, D.; Danilenko, M.; Roberts, C. T., Jr.; LeRoith, D.; Levy, J.; Sharoni, Y., *Prog. Growth Factor Res.* **1995**, *6*, 513.

38. Kleinman, D.; Karas, M.; Danilenko, M.; Arbell, A.; Roberts, C. T.; LeRoith, D.; Levy, J.; Sharoni, Y., *Endocrinology* **1996**, *137*, 1089.

39. Cullen, K. J.; Allison, A.; Martire, I.; Ellis, M.; Singer, C., *Breast Cancer Res. Treat.* **1992**, *22*, 21.

40. Cullen, K. J.; Smith, H. S.; Hill, S.; Rosen, N.; Lippman, M. E., *Cancer Res.* **1991**, *51*, 4978.

41. Yee, D.; Rosen, N.; Favoni, R. E.; Cullen, K. J., *Cancer Treat. Res.* **1991**, *53*, 93.

42. Bentel, J. M.; Lebwohl, D. E.; Cullen, K. J.; Rubin, M. S.; Rosen, N.; Mendelsohn, J.; Miller, W. H., Jr., *J. Cell. Physiol.* **1995**, *165*, 212.

43. Kleinman, D.; Karas, M.; Roberts, C. T., Jr.; LeRoith, D.; Phillip, M.; Segev, Y.; Levy, J.; Sharoni, Y., *Endocrinology* **1995**, *136*, 2531.

44. Kleinman, D.; Roberts, C. T., Jr.; LeRoith, D.; Schally, A. V.; Levy, J.; Sharoni, Y., *Regul. Pept.* **1993**, *48*, 91.

45. Hernandez-Sanchez, C.; Werner, H.; Roberts, C. T., Jr.; Woo, E. J.; Hum, D. W.; Rosenthal, S. M.; LeRoith, D., *J. Biol. Chem.* **1997**, *272*, 4663.

46. LeRoith, D.; Werner, H.; Beitner-Johnson, D.; Roberts, C. T., Jr., *Endocr. Rev.* **1995**, *16*, 143.

47. Baserga, R., *Cancer Res.* **1995**, *55*, 249.

48. Bruzzone, M.; Onetto, M.; Campora, E.; Chiara, S.; Oliva, C.; Guido, T.; Merlini, L.; Parodi, S.; Bentivoglio, G.; Ventrella, W.; et al., *Anticancer Res.* **1990**, *10*, 1353.

49. Onetto, M.; Bruzzone, M.; Conte, P. F.; Ruvolo, M.; Conio, A.; Chiara, S.; Falcone, A.; Bentivoglio, G.; Serra, G. E.; Paganuzzi, M., *Oncology* **1989**, *46*, 117.

50. Maines Bandiera Sarah, L.; Kruk Patricia, A.; Auersperg, N., *Am. J. Obst. Gynecol.* **1992**, *167*, 729.

51. Nitta, M.; Katabuchi, H.; Ohtake, H.; Tashiro, H.; Yamaizumi, M.; Okamura, H., *Gynecol. Oncol.* **2001**, *81*, 10.

52. Hayflick, L., *Exp. Cell Res.* **1965**, *37*, 614.

53. Bargonetti, J.; Manfredi, J. J., *Curr. Opin. Oncol.* **2002**, *14*, 86.

54. Sweet, B. H., Hilleman, M. R., *Proc. Soc. Exp. Biol. Med.* **1960**, *105*, 420.

55. Butel, J. S., Tevethia, S. S., Melnick, J. L., *Adv. Cancer Res.* **1972**, *15*, 1.

56. Eddy, B. E., Borman, G. S., Grubbs G. E., Young, R. D., *Virol.* **1962**, *17*, 65.

57. Fraumeni, J. F., Ederer, F., Miller, R. W., *JAMA* **1963**, *185*, 713.

58. Girardi, A. J., Sweet, B. H., Slotnick, V. B., Hilleman, M. R., *Proc. Soc. Exp. Biol. Med.* **1962**, *109*, 649.

59. Shein, H. M., Enders, J. F., *Proc. Nat. Acad. Sci. USA* **1962**, *48*, 1164.

60. Matker, C. M.; Rizzo, P.; Pass, H. I.; Di Resta, I.; Powers, A.; Mutti, L.; Kast, W. M.; Carbone, M., *Monaldi Arch. Chest. Dis.* **1998**, *53*, 193.

61. Vilchez, R. A.; Lednicky, J. A.; Halvorson, S. J.; White, Z. S.; Kozinetz, C. A.; Butel, J. S., *J. Acquir. Immune Defic. Syndr.* **2002**, *29*, 109.

62. Lednicky, J. A.; Butel, J. S., *Front. Biosci.* **1999**, *4*, D153.

63. Carroll-Pankhurst, C.; Engels, E. A.; Strickler, H. D.; Goedert, J. J.; Wagner, J.; Mortimer, E. A., Jr., *Br. J. Cancer* **2001**, *85*, 1295.

64. Butel, J. S.; Jafar, S.; Stewart, A. R.; Lednicky, J. A., *Dev. Biol. Stand.* **1998**, *94*, 23.

65. Butel, J. S.; Arrington, A. S.; Wong, C.; Lednicky, J. A.; Finegold, M. J., *J. Infect. Dis.* **1999**, *180*, 884.

66. Butel, J. S.; Lednicky, J. A., *J. Natl. Cancer Inst.* **1999**, *91*, 119.

67. Horowitz, L. G., *Med. Hypotheses* **2001**, *56*, 677.

68. Tognon, M.; Martini, F.; Iaccheri, L.; Cultrera, R.; Contini, C., *J. Med. Microbiol.* **2001**, *50*, 165.

69. Cole, C. N. *Polyomavirinae*: the viruses and their replication. In *Fields virology*; 3rd ed.; Fields, B. N., Knipe, D. M., Howley, P. M., Chanock, R. M., Melnick, J. L., Monath, T. P., Ed.; Lippincott-Raven: Philadelphia, **1996**; Vol. 2; pp 1997.

70. Raptis, L., Ed.; *SV40 Protocols*, Humana Press, Inc.: Totowa, NJ, **2001**; Vol. 165, pp 310.

71. Snapka, R. M., Ed.; *The SV40 replicon model for analysis of anticancer drugs*, R. G. Landes Company: Austin, TX, **1996**, pp 193.

72. Lane, D. P., *Nature* **1992**, *358*, 15.

73. Wahl, G. M.; Carr, A. M., *Nat. Cell Biol.* **2001**, *3*, E277.

74. Szumiel, I., *Radiat. Res.* **1998**, *150*, S92.

75. Shen, Y.; White, E., *Adv. Cancer Res.* **2001**, *82*, 55.

76. Janus, F.; Albrechtsen, N.; Dornreiter, I.; Wiesmuller, L.; Grosse, F.; Deppert, W., *Cell. Mol. Life Sci.* **1999**, *55*, 12.

77. Attardi, L. D.; Jacks, T., *Cell. Mol. Life Sci.* **1999**, *55*, 48.

78. Jayaraman, L.; Prives, C., *Cell. Mol. Life Sci.* **1999**, *55*, 76.

79. Hupp, T. R., *Cell. Mol. Life Sci.* **1999**, *55*, 88.

80. Oren, M., Rotter, V., *Cell. Mol. Life Sci.* **1999**, *55*, 9.

81. Choi, J.; Donehower, L. A., *Cell Mol. Life Sci.* **1999**, *55*, 38.

82. Buschmann, T.; Potapova, O.; Bar-Shira, A.; Ivanov, V. N.; Fuchs, S. Y.; Henderson, S.; Fried, V. A.; Minamoto, T.; Alarcon-Vargas, D.; Pincus, M. R.; Gaarde, W. A.; Holbrook, N. J.; Shiloh, Y.; Ronai, Z., *Mol. Cell Biol.* **2001**, *21*, 2743.

83. Kao, S. Y.; Lemoine, F. J.; Marriott, S. J., *Virology* **2001**, *291*, 292.

84. Yarbrough, W. G.; Bessho, M.; Zanation, A.; Bisi, J. E.; Xiong, Y., *Cancer Res.* **2002**, *62*, 1171.

85. Tang, D.; Wu, D.; Hirao, A.; Lahti, J. M.; Liu, L.; Mazza, B.; Kidd, V. J.; Mak, T. W.; Ingram, A. J., *J. Biol. Chem.* **2002**.

86. Yu, Q.; He, M.; Lee, N. H.; Liu, E. T., *J. Biol. Chem.* **2002**.

87. Shi, Y. Q.; Wuergler, F. E.; Blattmann, H.; Crompton, N. E., *Radiat. Environ. Biophys.* **2001**, *40*, 301.

88. Yonezawa, M.; Otsuka, T.; Kato, T.; Moriyama, A.; Kato, K. H.; Asai, K.; Matsui, N., *J. Orthop. Sci.* **2002**, *7*, 117.

89. Chopin, V.; Toillon, R. A.; Jouy, N.; Le Bourhis, X., *Br. J. Pharmacol.* **2002**, *135*, 79.

90. Backus, H. H.; Wouters, D.; van der Wilt, C. L.; Kuiper, C. M.; van Groeningen, C. J.; Pinedo, H. M.; Peters, G. J., *Adv. Exp. Med. Biol.* **2000**, *486*, 303.

91. Takahashi, H.; Ishida-Yamamoto, A.; Iizuka, H., *J. Investig. Dermatol. Symp. Proc.* **2001**, *6*, 64.

92. Peng, D. F.; Sugihara, H.; Hattori, T., *Pathobiology* **2001**, *69*, 77.

93. Mahyar-Roemer, M.; Katsen, A.; Mestres, P.; Roemer, K., *Int. J. Cancer* **2001**, *94*, 615.

94. Brodowicz, T.; Kandioler, D.; Tomek, S.; Ludwig, C.; Rudas, M.; Kunstfeld, R.; Koestler, W.; Hejna, M.; Budinsky, A.; Wiltschke, C.; Zielinski, C. C., *Br. J. Cancer* **2001**, *85*, 1764.

95. Antonsson, B.; Montessuit, S.; Lauper, S.; Eskes, R.; Martinou, J. C., *Biochem. J.* **2000**, *345 Pt 2*, 271.

96. Minn, A. J.; Velez, P.; Schendel, S. L.; Liang, H.; Muchmore, S. W.; Fesik, S. W.; Fill, M.; Thompson, C. B., *Nature* **1997**, *385*, 353.

97. Schendel, S. L.; Xie, Z.; Montal, M. O.; Matsuyama, S.; Montal, M.; Reed, J. C., *Proc. Natl. Acad. Sci. USA* **1997**, *94*, 5113.

98. Tremblais, K.; Oliver, L.; Juin, P.; Le Cabellec, T. M.; Meflah, K.; Vallette, F. M., *Biochem. Biophys. Res. Commun.* **1999**, *260*, 582.

99. Khaled, A. R.; Kim, K.; Hofmeister, R.; Muegge, K.; Durum, S. K., *Proc. Natl. Acad. Sci. USA* **1999**, *96*, 14476.

100. Nomura, M.; Shimizu, S.; Ito, T.; Narita, M.; Matsuda, H.; Tsujimoto, Y., *Cancer Res.* **1999**, *59*, 5542.

101. Griffiths, G. J.; Dubrez, L.; Morgan, C. P.; Jones, N. A.; Whitehouse, J.; Corfe, B. M.; Dive, C.; Hickman, J. A., *J. Cell. Biol.* **1999**, *144*, 903.

102. Gross, A.; McDonnell, J. M.; Korsmeyer, S. J., *Genes Dev.* **1999**, *13*, 1899.

103. Liu, X.; Kim, C. N.; Yang, J.; Jemmerson, R.; Wang, X., *Cell* **1996**, *86*, 147.

104. Verhagen, A. M.; Ekert, P. G.; Pakusch, M.; Silke, J.; Connolly, L. M.; Reid, G. E.; Moritz, R. L.; Simpson, R. J.; Vaux, D. L., *Cell* **2000**, *102*, 43.

105. Freedman, D. A.; Wu, L.; Levine, A. J., *Cell. Mol. Life Sci.* **1999**, *55*, 96.

106. Jha, K. K., Banga, S., Palejwala, V., Ozer, H. L., *Exp. Cell. Res.* **1998**, *245*, 1.

107. Ali, S. H.; DeCaprio, J. A., *Semin. Cancer Biol.* **2001**, *11*, 15.

108. Dyson, N.; Buchkovich, K.; Whyte, P.; Harlow, E., *Princess Takamatsu Symp.* **1989**, *20*, 191.

109. Dyson, N.; Buchkovich, K.; Whyte, P.; Harlow, E., *Cell* **1989**, *58*, 249.

110. Stiegler, P.; Kasten, M.; Giordano, A., *J. Cell. Biochem. Suppl.* **1998**, *30-31*, 30.

111. Blake, M. C.; Azizkhan, J. C., *Mol. Cell Biol.* **1989**, *9*, 4994.

112. DeGregori, J.; Kowalik, T.; Nevins, J. R., *Mol. Cell. Biol.* **1995**, *15*, 4215.

113. Johnson, D. G.; Schwarz, J. K.; Cress, W. D.; Nevins, J. R., *Nature* **1993**, *365*, 349.

114. Zhu, J.; Rice, P. W.; Gorsch, L.; Abate, M.; Cole, C. N., *J. Virol.* **1992**, *66*, 2780.

115. Cavender, J. F.; Conn, A.; Epler, M.; Lacko, H.; Tevethia, M. J., *J. Virol.* **1995**; *69*, 923.

116. Conzen, S. D.; Cole, C. N., *Oncogene* **1995**, *11*, 2295.

117. Dickmanns, A.; Zeitvogel, A.; Simmersbach, F.; Weber, R.; Arthur, A. K.; Dehde, S.; Wildeman, A. G.; Fanning, E., *J. Virol.* **1994**, *68*, 5496.

118. Dobbelstein, M.; Arthur, A. K.; Dehde, S.; van Zee, K.; Dickmanns, A.; Fanning, E., *Oncogene* **1992**, *7*, 837.

119. Manfredi, J. J.; Prives, C., *J. Virol.* **1993**, *67*, 4750.

120. Tevethia, M. J.; Lacko, H. A.; Kierstead, T. D.; Thompson, D. L., *J. Virol.* **1997**, *71*, 1888.

121. Thompson, D. L.; Kalderon, D.; Smith, A. E.; Tevethia, M. J., *Virology* **1990**, *178*, 15.

122. Lill, N. L.; Grossman, S. R.; Ginsberg, D.; DeCaprio, J.; Livingston, D. M., *Nature* **1997**, *387*, 823.

123. Gu, W.; Shi, X. L.; Roeder, R. G., *Nature* **1997**, *387*, 819.

124. Avantaggiati, M. L.; Ogryzko, V.; Gardner, K.; Giordano, A.; Levine, A. S.; Kelly, K., *Cell* **1997**, *89*, 1175.

125. Kaelin, W. G., Jr.; Ewen, M. E.; Livingston, D. M., *Mol. Cell. Biol.* **1990**, *10*, 3761.

126. Avantaggiati, M. L.; Carbone, M.; Graessmann, A.; Nakatani, Y.; Howard, B.; Levine, A. S., *Embo. J.* **1996**, *15*, 2236.

127. Simmons, D. T. SV40 Large T antigen functions in DNA replication and transformation. In *Advances in virus research*; Maramorosch, K., Murphy, F. A., Shatkin, A. J., Ed.; Academic Press: San Diego, **2000**; Vol. 55; pp 75.

CHAPTER 3. NONPHOTOCHEMICAL HOLE BURNING FOR INVESTIGATION OF BIOLOGICAL STRUCTURE

Biological systems are comprised mainly of similar components and can consist of any given combination of lipids, connective proteins, functional proteins, and nucleic acids. Order and structure of these components are dominating characteristics of all flora and fauna, and nowhere is this truer than in the more highly evolved species of our world. Combinations of these various components are organized into classifiable cell types, which in turn organize and facilitate classification into tissues that are highly specialized conglomerations of cells. Ultimately, these tissues perform dedicated functions for an organism, and their operation is (usually) critical for survival.

Cancer, however, is an anomaly by comparison, and characteristics prevalent in normal, functioning tissue become distorted as cells earmarked for tumorigenicity begin to proliferate rapidly resulting in extreme deviation from normal structural controls and order. A diagnostic system based upon observing this distortion, it would appear, could be an extreme benefit, depending on the scale of the detection, with single cell structural anomaly detection being the ultimate in sensitivity. The basis for just such a diagnostic system is found within the solid-state molecular probing technique of Hole Burning Imaging (HBI).

Mechanistically, three different types of HBI are possible: photochemical (PHB), transient or population bottleneck hole burning (THB), and nonphotochemical (NPHB), but only NPHB is utilized in this work. For fundamentals and reviews of the two former, the reader is referred to ref. [1-6] for PHB and ref. [7-9] for THB. NPHB

was first experimentally reported by Kharlamov et al. [10] in 1974, with the standard tunneling model mechanism for NPHB being proposed in 1978 by Hayes and Small [11]. Before discussing this model, however, an understanding of basic principles related to low temperature spectroscopic techniques is imperative. From there, requirements for observing spectral holes will be covered, with subsequently discussion of the mechanism of NPHB as it is understood today. Dispersive hole growth kinetics and the Stark effect, two types of measurements utilizing NPHB, will be discussed, and finally the marriage of NPHB with biological systems for the detection of anomalies will complete this chapter.

3.1 Homogeneous versus Inhomogeneous Broadening

Solid-state systems typically provide characteristically simpler optical spectra relative to those of molecules in liquid or gaseous form. This is due mainly to the restricted freedom of movement (rotational and translational) inherent to solid state systems, and consequently spectral line broadening is mainly composed of two factors: homogeneous (Γ_{hom}) and inhomogeneous (Γ_{inh}) [12]. Γ_{hom} is an inherent factor of any transition line as it is inversely proportional to the excited state lifetime, τ:

$$\Gamma_{hom}=(2\pi\tau)^{-1} \tag{3.1}$$

as dictated by the uncertainty principle. With increases in temperature, Γ_{hom} increases as well due to thermally induced dephasing processes:

$$\Gamma_{hom}=(2\pi\tau)^{-1} + (\pi T_2^*)^{-1} \tag{3.2}$$

where T_2^* is the pure dephasing time of the transition and results from phonons that are excited by thermal motion, hence the temperature dependence. Additionally, T_2^*

can be considered to be attributable to the single site transition frequency modulations resulting from the interaction of the excited state of the chromophore and the host matrix. T_2^* is always a component of Γ_{hom}, but at temperatures $T \geq 10$ K, T_2^* is much greater than that of lifetime broadening (the first term of eq. 3.2), and therefore dictates that low-temperatures are required for maximum achievable resolution of absorption/excitation line spectra. As an illustration, we can consider a chromophore in an amorphous solid at room temperature (298 K). Γ_{hom} from T_2^* is typically in hundreds of wavenumbers. At the boiling point of helium, (4.2 K) however, the T_2^* contribution to Γ_{hom} is ≤ 0.1 cm^{-1}.

Until now this discussion has neglected Γ_{inh}, however its effect on optical spectra is best illustrated in Figure 3.1. From the figure, examples of both Γ_{hom} and Γ_{inh} can be seen. For chromophores embedded in matrixes of perfect crystalline order (Fig. 3.1A), all chromophores encounter identical interactions with the host matrix and therefore exhibit identical absorption frequencies. Depicted on the right side of Fig. 3.1A is the spectrum of electronic transitions (the absorption profile) of the molecule embedded in the crystal matrix on the left. However for randomly arrayed matrixes (amorphous glasses) such as polymers, organic glasses, or more importantly, biological matrixes, interactions differ markedly, distributing the Γ_{hom} absorption lines for various absorption frequencies (ω_1, ω_2, ω_3) and create inhomogeneous broadening, as depicted in Fig 3.1B.

All is not lost for this type of sample, however: from under a broad inhomogeneous band, information on homogeneous linewidth can be obtained by line narrowing techniques such as hole-burning and fluorescence line-narrowing

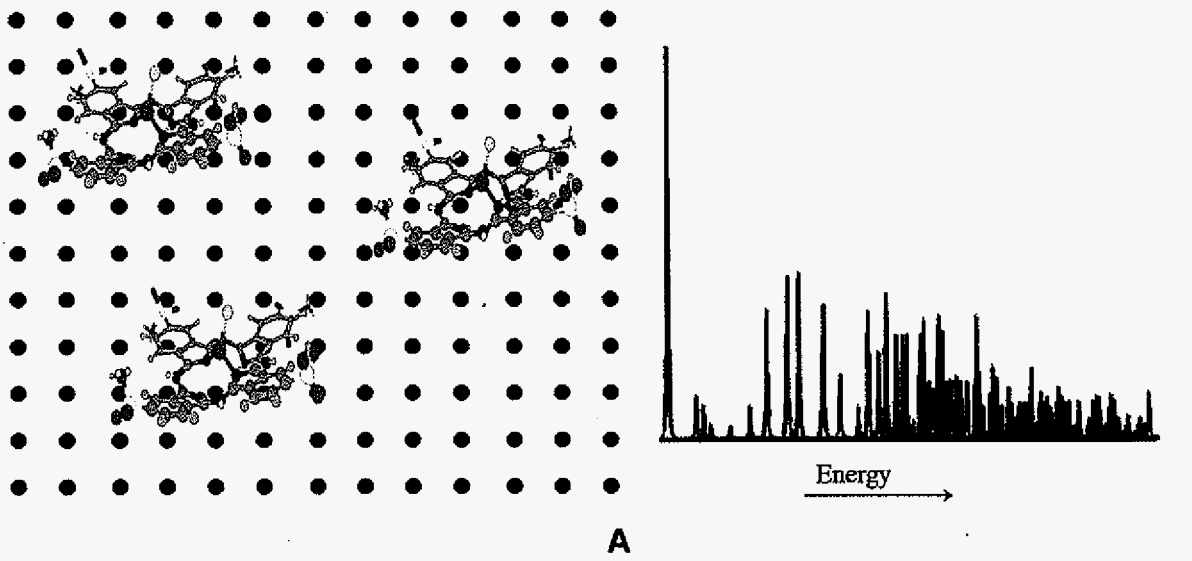

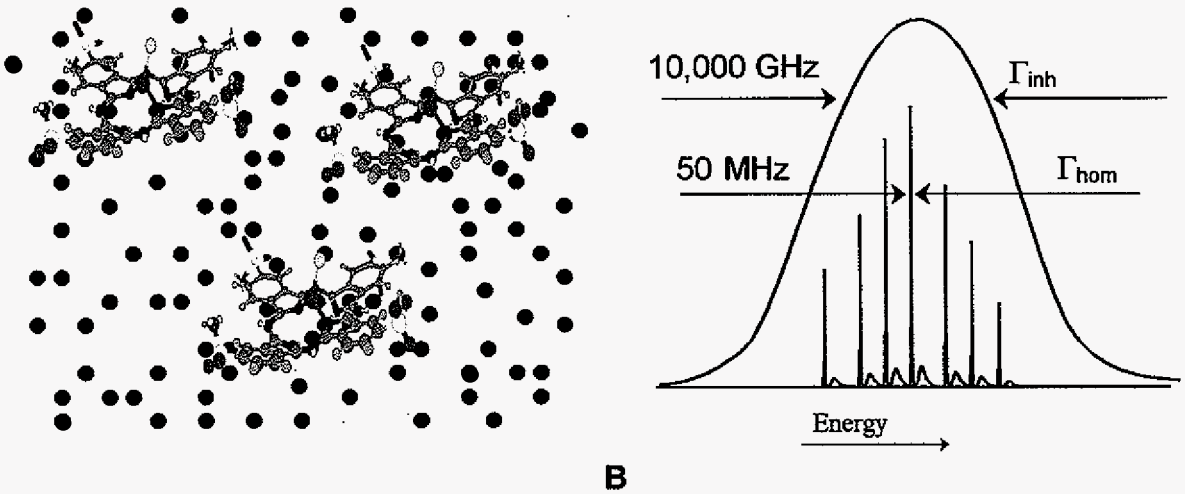

Figure 3.1 (A) Homogeneous broadening of a chromophore located in an ordered matrix. (B) Inhomogeneous broadening of a chromophore in a disordered matrix.

spectroscopy (FLNS). FLNS utilizes selective excitation of energetically narrow subsets of chromophores followed by narrow band emission to obtain spectral information normally hidden in inhomogeneous bands [13-15]. However, unlike FLNS, hole-burning allows for transitioning guest chromophores to a different state such that the product absorbs at a different frequency, creating a "hole" in the original absorption band. The mechanism by which this occurs is extremely dependent on the environment (vide infra). Consequently, this is the basis for utilizing NPHB to elucidate differences in biological structures.

3.2. Zero-Phonon Lines and Phonon Sidebands

As briefly mentioned previously, host matrix phonons are coupled to electronic transitions of guest chromophores, which gives rise to a phonon band. As seen in Figure 3.2, absorption by a single site consists of two parts: a Lorentzian shaped zero phonon line (ZPL), which refers to an electronic transition of a guest chromophore with no net change in the number of phonons in the host matrix; and a higher frequency ZPL phonon wing or phonon sideband (PSB), which occurs due to phototransitions in the guest chromophore with the creation or destruction of matrix phonons [16]. It follows that the low temperature single site absorption spectra is composed of two parts:

$$L(\omega_i - \omega) = L_{ZPL}(\omega_i - \omega)e^{-S} + L_{PSB}(\omega_i + \omega_m - \omega)(1 - e^{-S}) \qquad (3.3)$$

where S is the Huang-Rhys factor due to low frequency phonons centered at ω_m. L_{ZPL} is the Lorentzian line shape function of the ZPL with a FWHM of γ and exp(-S) is its Franck-Condon factor. The PSB contribution is contained within the second part of eq. 3.3, and the factor [1-exp(-S)] is the Franck-Condon factor for a one-phonon

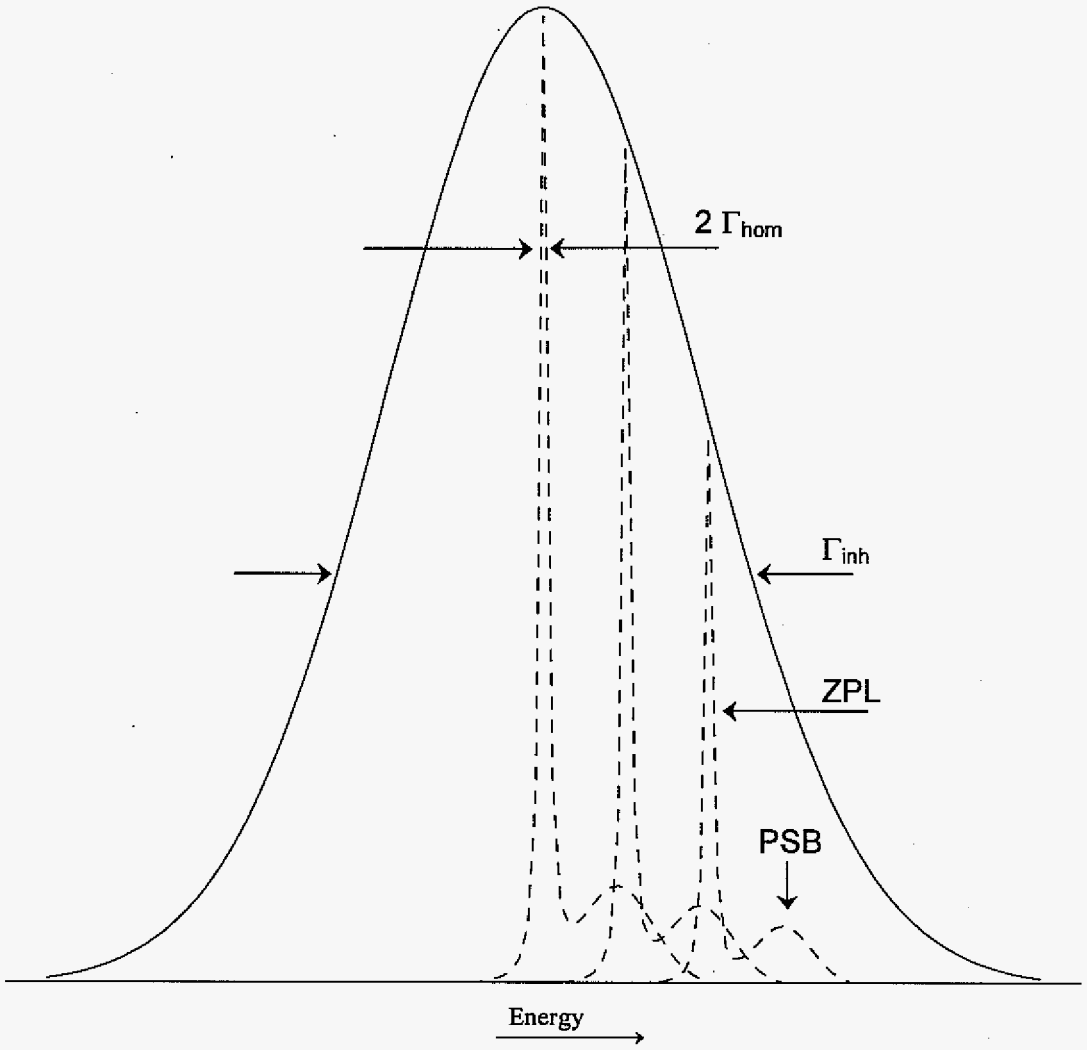

Figure 3.2 Schematic illustration of an inhomogeneously broadened Γ_{inh} fluorescence excitation band (solid line). The sharper, more intense portion of the dashed lines represent the zero phonon lines (ZPL) and the smaller, broader contributions to higher energy represent the phonon side bands (PSB).

profile. It should be noted that eq. 3.3 is for valid for the case of weak electron-phonon coupling ($S \leq 1$), which is the assumed case for the probe molecule of chapters 4 and 5 due to the observation of single, sharp ZPH with fluences producing hole depths up to 30%. In reality, however, the *S*-factor may be slightly larger than 1, but this is deemed to have minor ramifications.

3.3. Zero Phonon Holes and Phonon Sideband Holes

The laser excitation source is generally considered to be a narrow-band relative to the ZPL ($\Gamma_L \leq 20$ MHz), so that ZPH width contribution from the laser can be neglected. For a hole burning experiment, the hole created represents a negative replica of the homogeneous spectral transition, and can be characterized as a zero phonon hole (ZPH). The measured hole is a convolution of a burning step and a probing step, resulting in [12]:

$$\Gamma_{hole} = 2\Gamma_{hom} \tag{3.4}$$

Concurrent with and higher in energy to the ZPH is a phonon-sideband hole (PSBH), equivalent to a PSB accompanying a ZPL. A typical ZPH-PSBH spectrum for a "deep" burn is shown in Figure 3.3. Frequently, however, the PSBH is not observed with holes analyzed in an experiment, for the following reason: the area contained within a ZPH is directly proportional to the area contained within the PSBH. For example, for the molecule used in the research presented in chapters 4 and 5, the Huang-Rhys factor *S* yields that ZPL and PSB areas are approximately equal. But their widths, which can be measured experimentally, are 1.5 GHz and 30 cm^{-1} (~1000 GHz). This implies that the PSB amplitude must be ~1000× smaller than that of the ZPL, and therefore cannot be observed within the typical signal to noise

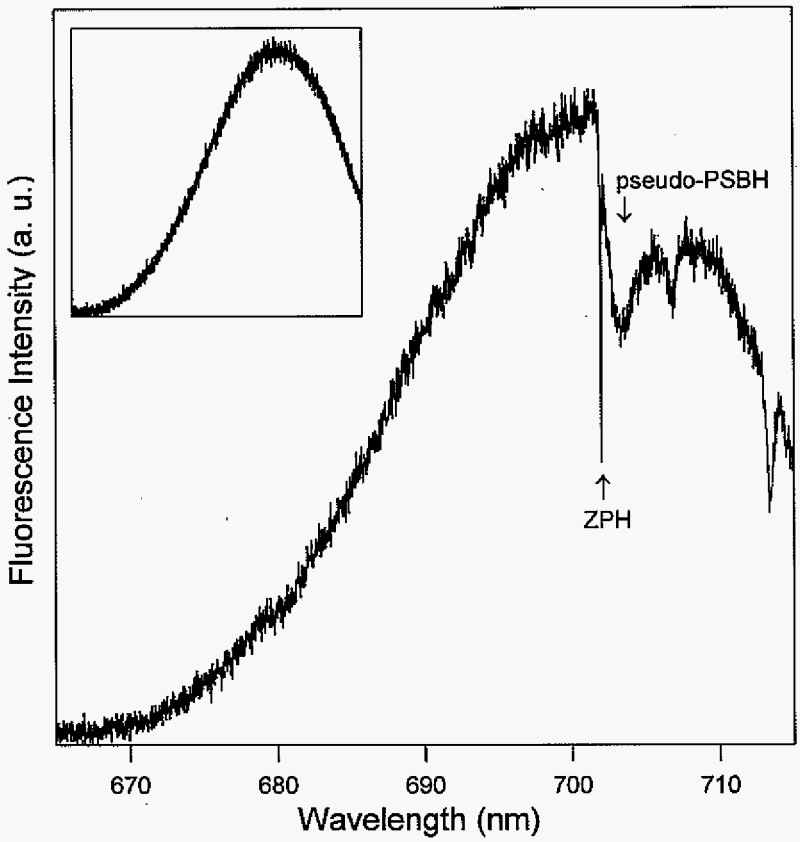

Figure 3.3 Fluorescence excitation pre- (inset) and post-burn spectra profiles for OV167 carcinoma cells incubated with MitoFluor Far Red 680. Note the formation of a zero phonon hole (ZPH) and the pseudo-phonon side band hole (PSBH) 30 cm^{-1} lower than the ZPH. The two holes to lower energy of the PSBH are vibronic satellite holes due to vibrations of 95 and 227 cm^{-1}.

ratio. Additionally, an antihole product is formed on the same side as the PSBH, further masking its intensity.

As depicted in Figure 3.3, there is a PSBH on the lower energy side of the ZPH, however, and this can be explained by considering the following events. The laser is exciting a set of molecules in different environments, which can absorb at a frequency ν_L via two pathways: purely electronic $\omega(S_0 \rightarrow S_1)$ or vibronic $\omega(S_0 \rightarrow S_1) + \omega_{vibration}$. Vibrational relaxation occurs on the picosecond timescale, whereas the hole burning event leading to frequency change is several orders of magnitude slower. Therefore, before the hole-burning event can take place, fast vibrational relaxation occurs, resulting in phonons being dissipated into the glass. Because of energy conservation, burning takes place at lower energies, relative to ν_L, and the PSBH is observed on the lower energy side of the ZPH. It should be noted that since the PSBH and ZPH intensities are not linked according to eq. 3.3, and given sufficient fluence, this PSBH intensity can be comparable (or greater than) to the ZPH intensity. As such, this PSBH is often referred to as a pseudo-PSBH.

In general, the single site absorption profile, L, with a ZPL at ν can be written as [17,18]:

$$L(\Omega-\nu)=\prod_{j=1}^{N}\sum_{r_j=0}^{\infty}\frac{e^{-S_j}S_j^{r_j}}{r_j!}\ell\left(\Omega-\nu-r_j\omega_j\right) \tag{3.5}$$

where *j* accounts for the discreet pseudolocalized or localized phonons and intramolecular modes. S_j is the Huang-Rhys factor, a measure of the strength of electron-*j*th phonon interactions. ω_j is the frequency for the *j*th mode; ω_m is the center frequency (referenced to the ZPL) of the one-phonon profile. The summation over *r* represents the contribution from the continuous distribution of low frequency

phonons of the amorphous solid and, with the Huang-Rhys factor S, ℓ is the lineshape function. In the case of $r_j = 0$, ℓ describes the ZPL associated with the total zero-point level of the excited electronic state whereby the ZPL is a Lorentzian with the ZPH homogeneous width, Γ_{hole}. Each phonon contribution to the absorption corresponds to nonzero values of r_j, with sequential values corresponding to one-, two-, three-,... phonon profiles (for $r_j = 1, 2, 3,...$ respectively) obtained from the convolution of the one-phonon profile with itself r_j times. An expression for the inhomogeneously broadened absorption spectrum is obtained by convolving the single site absorption profile, $L(\Omega-\nu)$, with a Gaussian zero-phonon site excitation distribution function, $N(\nu-\nu_m)$, having a center at ν_m and a FWHM of Γ_I:

$$A_o(\Omega) = \int d\nu N_0(\nu - \nu_m) L(\Omega - \nu). \tag{3.6}$$

Finally, summary conclusions may be drawn as to the requirements for observing ZPHs. First, the host matrix and guest chromophore must exhibit an inhomogeneously broadened absorption band, as the result of interactions between the guest and an amorphous glassy host. Second, a frequency change mechanism for the guest chromophore absorption must be present (this shall be covered in the next section, 3.4). Last, a method of detecting ZPHs is necessary, most easily accomplished through the use of high-resolution lasers and typical photon detection devices (e.g. a photomultiplier tube, or PMT).

3.4. The Extrinsic Two-Level-System Model: The Mechanism of NPHB

A persistent frequency change mechanism requires two stable potential energy minima. Traditionally, such systems are called Two-Level-Systems (TLS). Figure 3.4 shows one such TLS in the inset, where W represents the tunneling

frequency, Δ represents the zero-point energy difference, and *q* allows for numerous distinctly different TLS coordinates. The factor $\lambda = d(2mV)^{1/2}$ is the tunnel parameter, with *d* representing the displacement between the two potential energy minima, *m* is the effective mass of the tunneling element, and *V* is barrier height. The main portion of the figure illustrates the Hayes-Small TLS mechanism [11], representing a glass system containing a distribution of asymmetric intermolecular double-well potentials. The TLS structural model was first proposed independently by Anderson et al. [19] and Phillips [20] for the purpose of explaining the anomalous T-dependence of the specific heat and thermal conductivity of inorganic glasses at low temperatures ($T \leq 10$ K). The Hayes-Small model was developed without knowledge of these models, but provided modifications such that hole formation is due to a *subset* of the TLS, called extrinsic TLS (TLS_{ext}) localized at impurity molecules. At the burn temperature T_B, TLS_{ext} have the following two properties [21]: 1) ground state relaxation between minima by phonon assisted tunneling or thermal activation is relatively slow (i.e. hours) and 2) relaxation between the excited extrinsic TLS (TLS^{e}_{ext}) minima is competitive with the normal decay processes of the excited electronic state of the impurity. From Fig. 3.4, hole burning occurs in the excited state via phonon-assisted tunneling between two minima of potential energy wells. Since competition in the excited state occurs between relaxation rates and tunneling rates, a hole-burning quantum yield can be defined:

$$\phi(R) = \frac{R_{HB}}{R_{HB} + R_{Relax}} = \frac{\Omega \exp(-2\lambda)}{\Omega \exp(-2\lambda) + \tau^{-1}} \tag{3.7}$$

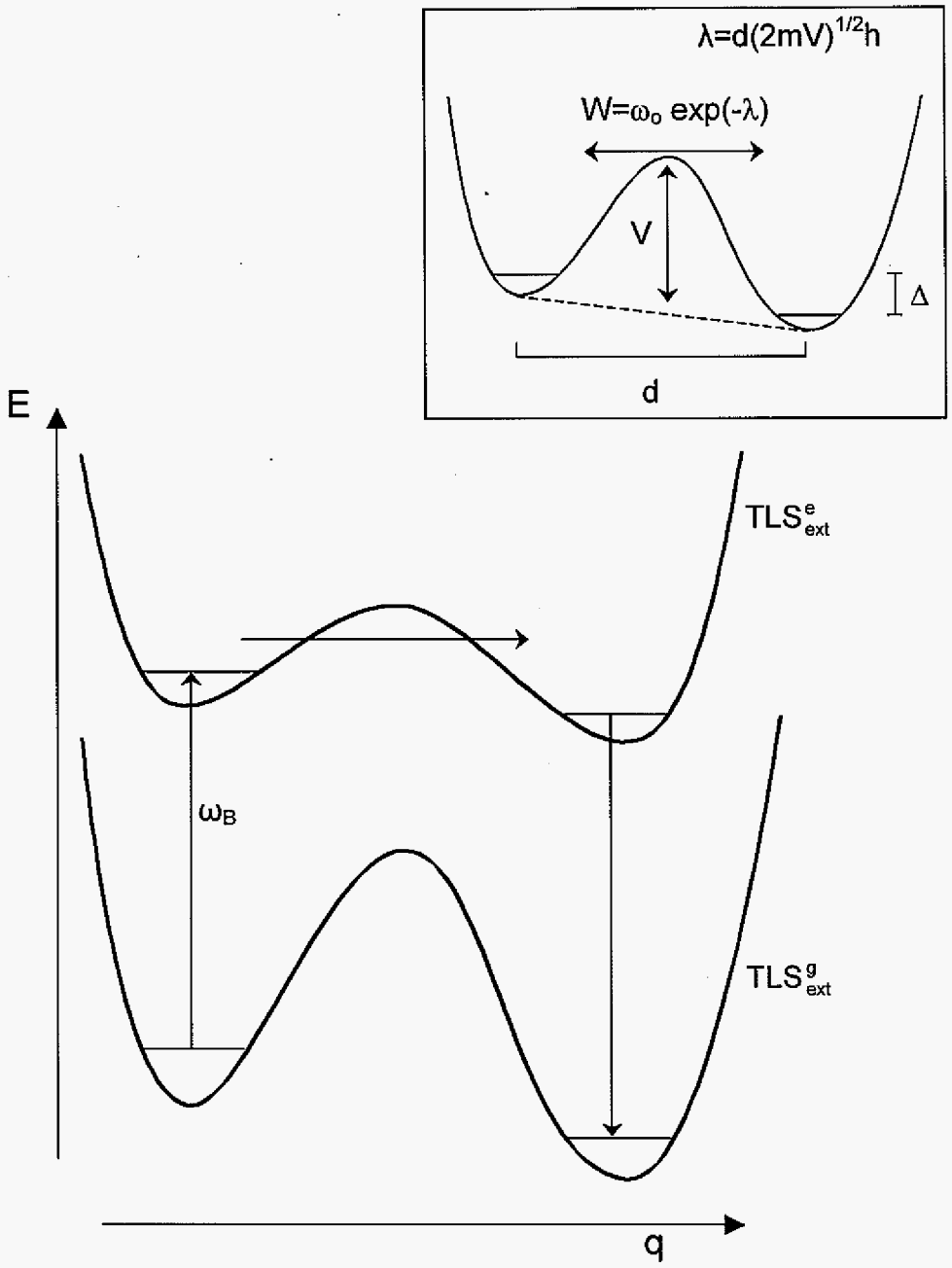

Figure 3.4 Schematic illustration of the extrinsic Two Level Systems (TLS_{ext}). Indices e and g denote ground and excited states, respectively. ω_B is the burn frequency of the laser. The inset defines the TLS parameters. W is the tunneling frequency, which is a function of λ. Within λ, m is the tunneling mass, d is the displacement between the two potential energy minima, and h is Planck's constant.

where τ^{-1} is the excited state lifetime, and $\Omega\exp(-2\lambda)$ represents the phonon-assisted tunneling relaxation rate Ω is set to 7.6×10^{12} s^{-1}(comparable to ω), and a quantum mechanical expression for Ω is given in ref. [22]. For the majority of TLS_{ext},

$$\phi(R) = \frac{R_{HB}}{R_{HB} + R_{Relax}} \approx \frac{R_{HB}}{R_{Relax}} << 1. \quad (3.8)$$

Further modifications in 1981 by Hayes et al. [23] concluded NPHB to be intimately associated with the static distribution of TLS_{ext}, whereas a second TLS_{int} process is necessary to account for fast relaxation events of pure dephasing and spectral diffusion. As a result, TLS_{int} are associated with spatially extended motions of the host matrix and influence the holewidth. Hole-burning studies of dye molecules suspended in hydrogen-bonding glasses composed of ethanol, glycerol, and poly(vinyl alcohol) polymers (among others) resulted in further development of the model [24-26]. In these alcoholic solvents, the TLS_{int} was determined to be spatially extended hydrogen-bonded networks that undergo small amplitude motion of the H atoms. Alternatively, the TLS_{ext} involves H atoms that undergo large amplitude motion, resulting in large rearrangements of the hydrogen-bonding network in close proximity to the guest [24]. Shu and Small [27] concluded further in 1992 that NPHB cannot be understood in terms of a static distribution of TLS_{ext}. From these experiments, an "outside-in" series of steps was postulated, with the requirement that excess free volume exist for NPHB to occur. The Shu-Small model predicted that NPHB would cease in a crystalline matrix, since excess free volume is absent by definition. Experiments by Kim et al. [28] with Aluminum Phthalocyanine Tetrasulfonate (APT) in hyperquenched glassy water (HGW) validated this prediction, observing a cessation of NPHB after annealing at 150 K, the point of

formation of cubic ice. In keeping with numerous published studies [29,30], the model also predicted PHB would not cease in a crystalline matrix. Recently the TLS model has been expanded to a multilevel system model to take into account high fluence hole burning phenomena [31], however it has been agreed upon that for moderate and low fluence hole burning, the TLS model is sufficient.

3.5. Dispersive Nonphotochemical Hole Growth Kinetics

The working model of NPHB as a manifestation of tunneling between different glass-chromophore configurations is currently widely accepted. The classification as dispersive stems from the mechanism: the amorphous matrix of a glass creates a distribution of phonon-assisted relaxation rates, R, associated with TLS_{ext}^{e}, and cannot be described by a single rate constant. Hence, burn kinetics are dispersive.

To examine dispersive NPHB, a theory was developed by Kenney et al. [24] utilizing a Gaussian distribution function [32] for the TLS_{ext}^{e} tunneling parameter, λ (section III.c). The ZPH fractional hole depth, 1-$D(t)$, could be fit according to the following:

$$D(t) = (2\pi)^{-1/2} \int_{-\infty}^{\infty} dx \exp\left(-x^2/2\right) \exp\left[-\Sigma_o \xi(x) t\right] \tag{3.9}$$

where $\Sigma_o \equiv P\sigma\Omega_o/\tau$ (P is the burn photon flux, τ is the excited state lifetime, and σ the peak absorption cross section), $x = (\lambda - \lambda_o)/\sigma_\lambda$, and $\xi(x) = \exp\left[-2(\lambda_o - \sigma_2 x)\right]$. For simplicity, the theory neglects the contribution of intrinsic dispersion from photoselection due to the polarization of the burn laser (α, which is designated as the angle between the laser polarization and the transition dipole). Also neglected is the absorption of off-resonant laser excitation by the ZPL (ω). Even so, theoretical

fits from this model matched well with experimental data, and afforded determination of λ_0 and variance σ_λ, whose importance shall be mentioned briefly, *vide infra*.

The simplifications made by Kenney et al. were introduced to an expanded equation (the "master equation") due to inadequate computing power at the time. Recently, it has been shown by Reinot and Small [33] that it is now possible to work with the complete master equation [34], as fits can be accomplished in a reasonable amount of time. NPHB kinetic curves can be obtained using

$$D(\omega_p,t) = \int d\omega L(\omega_p-\omega)G(\omega)\int d\lambda f(\lambda)\int d\alpha \sin\alpha\cos^2\alpha e^{-P\sigma\phi\,(\lambda)L(\omega_B-\omega)\cos^2(\alpha)t} \qquad (3.10)$$

which is the fractional hole depth probed at frequency ω_P following a burn time t. P is the total photon flux with units of number of photons cm^{-2} s^{-1}, α and λ are the same as previous and $f(\lambda)$ is the Gaussian distribution function of tunneling parameter λ centered at λ_0 with variance σ_λ. It should be noted that NPHB quantum yield, Φ, is assumed to be the same as that given in eq. 3.8, and the L term of equation 3.10 was already given in eq. 3.3. The ZPL frequency is given by ω, and $G(\omega)$ is its Gaussian distribution of ZPL frequencies. Although the probe chromophore used in chapters 4 and 5 is different from that used in ref. [33], a similar method was used to determine that $G(\omega)$ for the chromophore has a FWHM of 600 cm^{-1}, with all burn frequencies located on the lower energy side of the absorption profiles obtained for the dye *in vivo*.

It is important to mention that the parameters λ and α each define a distribution of hole burning rates that leads to dispersive kinetics, with the λ distribution being the dominant factor [33] and accounting well for the first 80% of a burn. Because of this, equation 3.10 is typically used in a more simplified form:

$$D(\omega_B,t)=\int d\lambda f(\lambda)\int d\alpha \sin\alpha\cos^2\alpha e^{-P\sigma\Phi_{LT}\phi(\lambda)\cos^2(\alpha)t}. \quad 3.11$$

All parameters are identical to those defined for equation 3.10.

Most importantly, the parameters obtained from fitting the kinetics curves are informative as to the matrix organization: λ_o provides a measurement of the mean distribution of tunneling rates, and σ_λ provides the variance of this measurement. The latter parameter, σ_λ, is informative as to the structural heterogeneity of the host matrix: values obtained from fitting can be used to draw conclusions regarding the relative order of any given system, possibly allowing comparisons to be made between different cellular matrixes. Based on the work presented by Milanovich [35], a dye probe placed in a cell is expected to provide quantifiable NPHB information regarding the assembly of that cell's matrix. In the present case, this will allow for a comparison between *in vitro* carcinoma cells and normal analogs based on specific staining of *in vivo* mitochondria, which have previously been discussed (see section 2.1.) and determined to be structurally anomalous for mitochondria derived from cancerous tissue.

3.6. Effects of an External Applied Electric Field (the Stark Effect)

The typical NPHB experiment involves two steps for the production and detection of spectral holes, assuming the chromophore burns efficiently, the sample is an amorphous glassy matrix, and the temperature of the sample is ≤ 10 K. The first is the application of a narrow-band laser of sufficient fluence to cause burning, with the excitation intensity usually able to be monitored. Second, the hole is read by lowering the fluence to a point where the sample will not burn at a significant rate (to avoid alteration of the hole), lowering the frequency of the laser,

and then scanning across the ZPH with resolution sufficient to detect the hole while measuring either laser transmission or fluorescence. For the latter, this can easily be accomplished by increasing the laser frequency in steps of ~1% of the anticipated hole FWHM; i.e. for a hole with FWHM of 5 GHz, the step size should be 0.05 GHz, well within the limit of high resolution laser systems. For experiments where NPHB dispersive kinetics are desired, only the first step need be taken.

A further experiment that can be conducted involves the Stark effect. An external electric field ($\leq$ 40 kV/cm^2) is applied while re-scanning the ZPH to measure the effect of the electric field. Information gained from such an experiment pertains to the magnitude of the permanent dipole moment difference vector $|\Delta\vec{\mu}_{mol}|$. From a biological point of view the measurement of $\Delta\vec{\mu}_{mol}$ yields structural as well as functional information. As an example, recent advances in the understanding of photosynthetic electron transfer processes have been made possible by Stark hole-burning spectroscopy [36-39], where measured $f\Delta\mu$ (f is the local field correction factor) values were used to identify excitonic states associated with closely spaced chlorophylls whose strong coupling is significantly contributed to by electron exchange. In turn, electron exchange interactions lead to charge-transfer states whose mixing with neutral Q_y states endows them with charge-transfer character.

At the laboratory scale, the Stark effect involves the measurement of frequency shifts caused by external electric fields. As absorption and emission frequencies are determined by the energy differences between the ground and excited state, an electric field-induced shift can only occur if the field shifts the ground state and the excited state differently [40]. For an isolated chromophore in a

matrix, the Stark shift of the optical transition frequency of the absorber is given by [41]

$$\Delta\omega = -\hbar^{-1}\left[\left(\Delta\mu_{mol} + \Delta\alpha \boldsymbol{E}_{\text{int}}\right) f\boldsymbol{E}_{St} + 1/2\,(f\boldsymbol{E}_{St})\Delta\alpha\left(f\boldsymbol{E}_{St}\right)\right] \tag{3.12}$$

where the local field correction factor f is taken to be a scalar, $\Delta\mu_{mol}$ is the molecular dipole moment change, and $\boldsymbol{E}_{St}$ is the external applied field. $\boldsymbol{E}_{\text{int}}$ is the matrix field experienced by the absorber and $\Delta\alpha\boldsymbol{E}_{\text{int}} = \Delta\mu_{ind}$, with $\Delta\mu_{ind}$ the dipole moment change induced by the matrix field. $\Delta\alpha$ is the molecular polarizability difference tensor. As discussed in ref. [36], the first term in the brackets represents the linear Stark effect, and the second represents the quadratic effect. When $\Delta\mu_{mol}$ is small relative to $\Delta\mu_{ind}$, both depend linearly on $\Delta\alpha$. In this case the condition for observation of the quadratic Stark effect is

$$\boldsymbol{E}_{\text{int}} \leq 1/2 f\boldsymbol{E}_{St} \tag{3.13}$$

which for $\boldsymbol{E}_{\text{int}}$ = 10^6 V cm^{-1} requires $\boldsymbol{E}_{St}$ = 10^6 V cm^{-1} (for f~1.5), which is two orders of magnitude greater than the largest Stark field used in experiments presented in chapters 4 and 5. Further, Stark broadening of holes is consistent with $\Delta\mu_{mol} < \Delta\mu_{ind}$, and only broadening (not splitting) is observed with the research presented in this thesis.

It is interesting to note, using an illustration of the Stark effect, the causes of broadening or splitting of holes in an external applied electric field based on analysis of dipole moment interactions. Figure 3.5 provides a vectorial representation of the Stark effect for four different extremes of the angle ϑ between the transition dipole

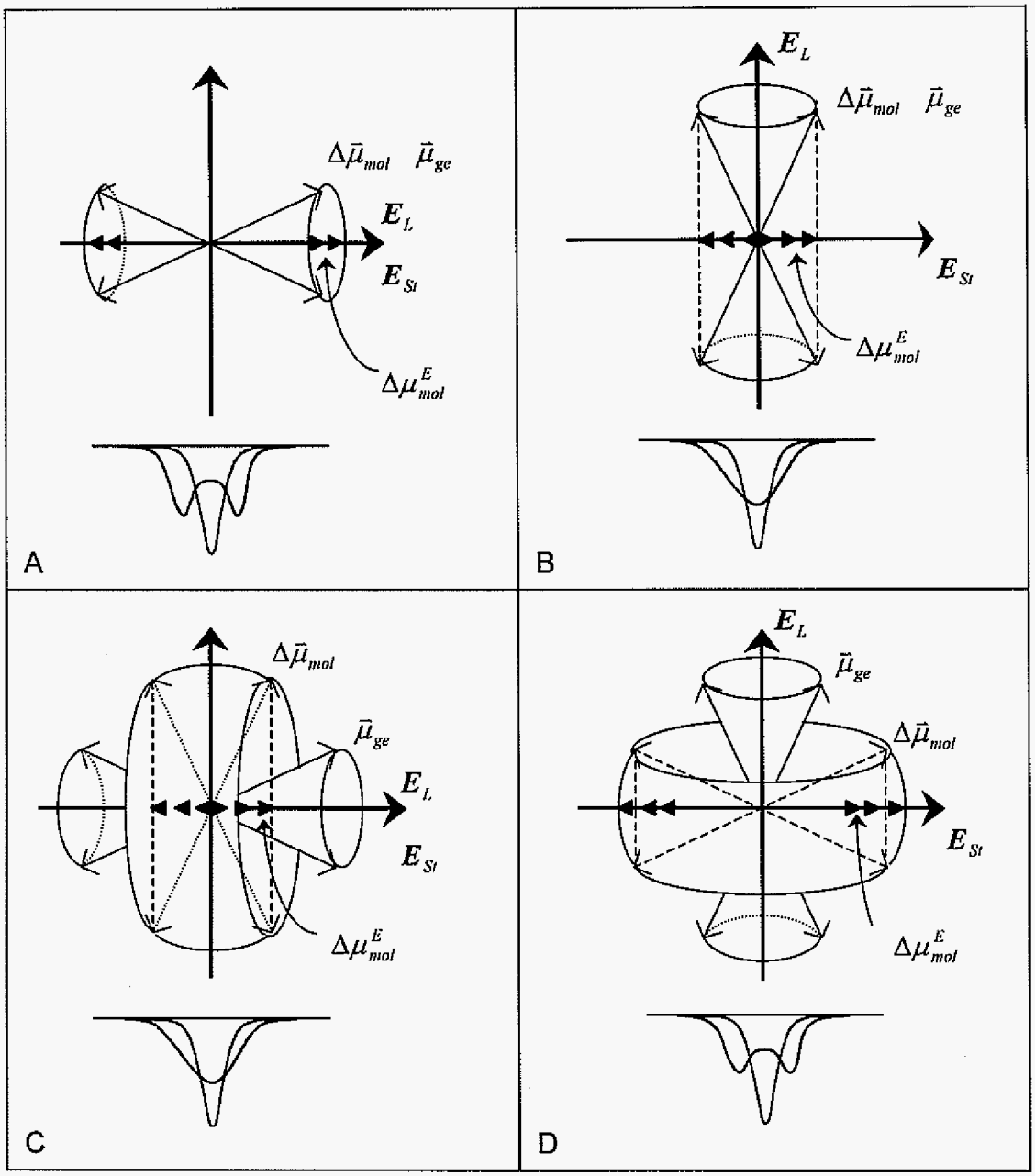

Figure 3.5 Vectorial representation of the Stark effect illustrating hole splitting/broadening. Adapted from [40].

moment and the dipole moment difference, either at 0° or at 90°. In the first case, Fig. 3.5A, $\vartheta = 0°$ and $\boldsymbol{E}_L \parallel \boldsymbol{E}_{St}$. If γ is considered to be the angle between the transition dipole moment and the laser polarization, then the distribution about $\cos^2\gamma$ of the ground and excited transition dipole moments ($\vec{\mu}_{ge}$) around the laser polarization $\boldsymbol{E}_L$ is represented by $\vec{\mu}_{ge}$ vectors deviating about 30° from the maxima of their angular distributions. Denoted by $\Delta\mu^E_{mol}$, the black triangles represent the projections of the products of the dipole moment differences $\Delta\vec{\mu}_{mol}$ and $\boldsymbol{E}_{St}$. As notable from the figure, strongly positive and strongly negative projections prevail, and thus hole splitting is observed. For the cases in Fig. 3.5B and C, $\vartheta = 0°$, $\boldsymbol{E}_L \perp \boldsymbol{E}_{St}$, and $\vartheta = 90°$, $\boldsymbol{E}_L \parallel \boldsymbol{E}_{St}$, respectively. By similar arguments, the projections show that no splitting occurs, only broadening. Finally, in the case of Fig. 3.5D, ϑ = 90° and $\boldsymbol{E}_L \perp \boldsymbol{E}_{St}$, the hole splits but not as distinctly as in the first case.

As mentioned previously, only broadening is observed for the research presented in chapters 4 and 5, and thus hole broadening in response to an applied electric field becomes the basis of our measurement. In 1987 Kador et al. [42] presented a relation between $\boldsymbol{E}_{St}$ and measured hole width:

$$\Gamma_{hole}(F) = 2\left(\gamma' + \gamma'_d\right)\left(1 + F^2\right)^{1/2} \tag{3.14}$$

where

$$F = \frac{2f\Delta\mu\boldsymbol{E}_{St}}{\hbar\left(\gamma' + \gamma'_d\right)} \tag{3.15}$$

and the sum $\left(\gamma' + \gamma'_d\right)$ represents the hole width at zero field, where γ' is the homogeneous width of the zero-phonon line and γ'_d is the additional width associated with artifacts such as saturation broadening. This parameter is measured in both ground and excited states, and can be broken into two parts: an

intrinsic molecular dipole ($\Delta\vec{\mu}_{mol}$) and a matrix induced dipole ($\Delta\vec{\mu}_{ind}$). The latter of these two parameters is the more important of the two, for the reason that it can be further split into two contributors, the first of which is a matrix induced dipole moment fixed in the frame of the chromophore caused by the average structural organization of the matrix ($\Delta\vec{\mu}_{ind,ff}$), and a second matrix induced dipole moment difference which is not fixed in the frame of the chromophore and which is caused by a random distribution of the atoms around the average matrix structure ($\Delta\vec{\mu}_{ind,nff}$). The $\Delta\vec{\mu}_{ind,nff}$ is the factor which gives rise to different frequency shifts for each single chromophore molecule [40]. This entire scheme of interactions is illustrated in Figure 3.6. Most importantly, we have once again obtained a measurement system sensitive to the structural makeup of any given sample, and which, based on the work of Milanovich et al. [43], should afford resolution of mitochondrial structural and/or membrane potential differences between carcinoma and normal cell lines.

3.7. The Marriage of NPHB with Biological Anomaly Detection

The preceding discussions have served the purpose of demonstrating the utility of NPHB for discerning differences in the structures of biological specimens. Although the first such work of this nature was presented by Milanovich [35], it has been through continued refinements and molecular biological exploration that this technique has met with expanded success. Although not every possible question has been addressed in this thesis, it may very well be impossible to do so. However it is my hope that the preceding chapters have presented you, the reader, with a thorough background of the reasoning behind the research to be presented in chapters 4 and 5.

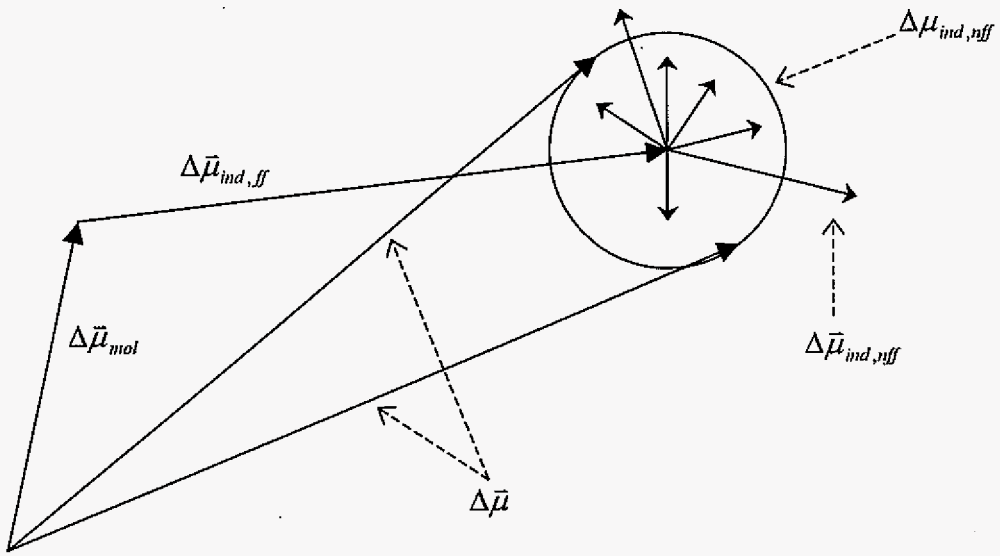

Figure 3.6 Contributions to entire dipole moment difference. The entire dipole moment difference ($\Delta\vec{\mu}$) is composed of two parts: the intrinsic dipole moment difference ($\Delta\vec{\mu}_{mol}$) and the induced dipole moment difference, which can further be divided into two contributors, fixed frame ($\Delta\vec{\mu}_{ind,ff}$) and non fixed frame ($\Delta\vec{\mu}_{ind,nff}$) interactions. Adapted from [40].

By now, we have met with (ideological) success behind our objectives: the objective to find and target structural differences between normal and carcinoma cells has been met with the discussion of mitochondrial anomalies; the objective to utilize relevant, valid normal and carcinoma cell lines has been met with the introduction of the two cell lines OV167 and OSE(tsT)-14; and the objective to present the ability of NPHB imaging for resolving and quantifying those structural differences has been covered in a fundamental sense. The time has come to assemble all of the aforementioned, and move on to the presentation of research results.

References

1. Gorokhovskii, A. A.; Kaarli, R. K.; A., R. L., *Opt. Commun.* **1976**, *16*, 282.
2. Gorokhovskii, A. A.; Kaarli, R. K.; A., R. L., *J. Exp. Theor. Phys. Lett.* **1974**, *20*, 216.
3. De Vries, H.; Wiersma, D. A., *Phys. Rev. Lett.* **1976**, *36*, 91.
4. Völker, S.; Macfarlane, R. M.; Genack, A. Z.; Trommsdorff, H. P.; Van der Waals, J. H., *J. Chem. Phys.* **1977**, *67*, 1759.
5. Völker, S.; Van der Waals, J. H., *Mol. Phys.* **1976**, *32*, 1703.
6. Moerner, W. E., Ed.; *Persistent spectral hole-burning: science and applications*, Springer-Verlag: Berlin, Germany, **1988**; Vol. 44.
7. Szabo, A., *Phys. Rev. B* **1975**, *11*, 4512.
8. Shelby, R. M.; Macfarlane, R. M., *Chem. Phys. Lett.* **1979**, *64*, 545.
9. Dicker, A. I. M.; Johnson, L. W.; Völker, S.; Van der Waals, J. H., *Chem. Phys. Lett.* **1983**, *100*, 8.

10. Kharlamov, B. M.; Personov, R. I.; Bykovskaya, L. A., *Opt. Commun.* **1974**, *12*, 191.

11. Hayes, J. M.; Small, G. J., *Chem. Phys.* **1978**, *27*, 151.

12. Völker, S. High-resolution spectroscopy of organic solids: hole-burning in molecular crystals and amorphous systems at low temperature. In *Excited-state spectroscopy in solids: Varenna on Lake Como, Villa Monastero, 9-19 July 1985*; Grassano, U. M., Terzi, N., Ed.; North-Holland: Amsterdam, **1987**; pp 363.

13. Riesberg, L. A., *Phys. Rev. A* **1973**, *7*, 671.

14. Personov, R. I.; Al'Shits, E. I.; Bykovskaya, L. A., *Opt. Commun.* **1972**, *6*, 169.

15. Szabo, A., *Phys. Rev. Lett.* **1970**, *25*, 924.

16. Personov, R. I. Site selection spectroscopy of complex molecules in solutions and its applications. In *Spectroscopy and excitation dynamics of condensed molecular systems*; Agranovich, V. M., Hochstrasser, R. M., Ed.; North-Holland: Amsterdam, **1983**; Vol. 4; pp 555.

17. Jankowiak, R.; Hayes, J. M.; Small, G. J., *Chem. Rev.* **1993**, *93*, 1471.

18. Lyle, P. Ph.D., Iowa State University, **1993**.

19. Anderson, P. W.; Halperin, G. I.; Varma, C. M., *Philos. Mag.* **1972**, *25*, 1.

20. Phillips, W. A., *J. Low Temp. Phys.* **1972**, *7*, 351.

21. Small, G. J. Persistent nonphotochemical hole burning and the dephasing of impurity electronic transitions in organic glasses. In *Spectroscopy and excitation dynamics of condensed molecular systems*; Agranovich, V. M., Hochstrasser, R. M., Ed.; North-Holland: Amsterdam, **1983**; Vol. 4; pp 515.

22. Kim, W. H.; Reinot, T.; Hayes, J. M.; Small, G. J., *J. Chem. Phys.* **1996**, *104*, 6415.

23. Hayes, J. M.; Stout, R. P.; Small, G. J., *J. Chem. Phys.* **1981**, *74*, 4266.

24. Kenney, M. J.; Jankowiak, R.; Small, G. J., *Chem. Phys.* **1990**, *146*, 47.

25. Kokai, F.; Tanaka, H.; Braumann, J. I.; Fayer, M. D., *Chem. Phys. Lett.* **1988**, *143*, 1.

26. Narasimhan, L. R.; Littau, K. A.; Pack, D. W.; Bai, Y. S.; Elschner, A.; Fayer, M. D., *Chem. Rev.* **1990**, *90*, 439.

27. Shu, L.; Small, G. J., *J. Opt. Soc. Am. B* **1992**, *9*, 724.

28. Kim, W. H.; Reinot, T.; Hayes, J. M.; Small, G. J., *J. Phys. Chem.* **1995**, *99*, 7300.

29. Macfarlane, R. M.; Shelby, R. M. Persistent spectral hole-burning in inorganic materials. In *Persistent spectral hole-burning: science and applications*; Moerner, W. E., Ed.; Springer-Verlag: Berlin, Germany, **1988**; Vol. 44; pp 127.

30. Reinot, T.; C., D. N.; Small, G. J., *J. Lumin.* **In press**.

31. Reinot, T.; Small, G. J., *J. Chem. Phys.* **2001**, *114*, 9105.

32. Jankowiak, R.; Richert, R.; Bässler, H., *J. Phys. Chem.* **1985**, *89*, 4569.

33. Reinot, T.; Small, G. J., *J. Chem. Phys.* **2000**, *113*, 10207.

34. Elschner, A.; Bässler, H., *Chem. Phys.* **1988**, *123*, 305.

35. Milanovich, N. Application of Spectral Hole Burning to the Study of In Vitro Cellular Systems. Ph. D., Iowa State University, **1999**.

36. Rätsep, M.; Wu, H. M.; Hayes, J. M.; Small, G. J., *Spectrochim. Acta, Part A* **1998**, *54A*, 1279.

37. Rätsep, M.; Johnson, T. W.; Chitnis, P. R.; Small, G. J., *J. Phys. Chem. B* **2000**, *104*, 836.

38. Rätsep, M.; Wu, H. M.; Hayes, J. M.; Blankenship, R. E.; Cogdell, R. J.; Small, G. J., *J. Phys. Chem. B* **1998**, *102*, 4035.

39. Wu, H. M.; Rätsep, M.; Young, C. S.; Jankowiak, R.; Blankenship, R. E.; Small, G. J., *Biophys J* **2000**, *79*, 1561.

40. Köhler, M.; Friedrich, J.; Fidy, J., *Biochim. Biophys. Acta* **1998**, *1386*, 255.

41. Meixner, A. J.; Renn, A.; Bucher, S. E.; Wild, U. P., *J. Phys. Chem.* **1986**, *90*, 6777.

42. Kador, L.; Haarer, D.; Personov, R., *J. Chem. Phys.* **1987**, *86*, 5300.

43. Milanovich, N.; Rätsep, M.; Reinot, T.; Hayes, J. M.; Small, G. J., *J. Phys. Chem. B* **1998**, *102*, 4265.

CHAPTER 4. NONPHOTOCHEMICAL HOLE BURNING SPECTROSCOPY OF A MITOCHONDRIAL SELECTIVE RHODAMINE DYE MOLECULE IN NORMAL AND CANCEROUS OVARIAN SURFACE EPITHELIAL CELLS

A paper accepted by the Journal of Luminescence, *In Press*

R. J. Walsh, T. Reinot, J. M. Hayes, K. R. Kalli, L. C. Hartmann, and G. J. Small

4.1 Abstract

Results are presented of nonphotochemical hole burning experiments on the mitochondrial dye rhodamine 800 (MitoFluor Far Red 680, Molecular Probes) incubated with two human ovarian surface epithelial cell lines: OSE(tsT)-14 normal cells and OV167 carcinoma (cancer) cells. This dye is believed to be selective for the plasma and inner membranes of the mitochondria. Importantly, the dispersive (distributed) growth kinetics of zero-phonon holes (ZPH) were found to be significantly different with the OV167 line exhibiting the higher burn efficiency. This may reflect greater structural heterogeneity of that line. Equally interesting is that the permanent dipole moment change ($\Delta\mu$) for the $S_0 \rightarrow S_1$ transition of the dye is markedly different for the two cell lines, the $\Delta\mu$ value for the carcinoma cell line being a factor of 1.5 higher. Discussion of this finding in terms of membrane potentials is given.

4.2. Introduction

Previous work by this group has explored hole burning imaging (HBI), a technique that seeks to exploit the inherent nano-environmental sensitivity of spectral nonphotochemical hole burning (NPHB), for detecting quantifiable differences between cancerous and non-cancerous cells.[1,2] That work focused on the establishment of the procedural feasibility of HBI as a diagnostic tool, and was the first experiment to demonstrate that NPHB of intra-cellular dye molecules is possible.

Specifically, the above studies used two different cultured human breast epithelial cell lines: MCF-7 (cancerous) and MCF-10F (normal) cells, both stained with aluminum phthalocyanine tetrasulfonate (APT). The two cell lines could not be distinguished on the basis of the optical dephasing time (T_2), dispersive growth kinetics of the zero-phonon holes (ZPH), the linear pressure shift rate of the ZPH, or the linear electron-phonon coupling of APT [3]. However, a distinction between the two cell lines was possible on the basis of the Stark (St) effect (dependence of the width of the ZPH on an applied electric field (E_{St}) with laser excitation (E_L) either parallel or perpendicular to E_{St}). This dependence yielded the permanent dipole moment change ($f\Delta\mu$) associated with the $S_0 \rightarrow S_1$ optical transition of APT, where f is the local field correction factor. The APT molecules sensitive to the Stark effect were argued to be located in the cell membrane. However, the difference between the $f\Delta\mu$ values for the two cell lines was small, ~0.1 D. For this reason, it was decided that APT does not provide enough sensitivity to be useful for distinguishing between normal and cancerous cells.

In order to build upon these results, it was necessary to search for a different dye molecule, one that could provide improvements over APT, especially in the area of staining specificity. A listing of the compartments of the cell gives many potential target organelles and structures, however several factors must be taken into account when determining suitability of both the dye molecule and the target cellular component. It is desirable for the dye molecule to absorb strongly in the red region, to avoid auto fluorescence, and to have a high fluorescence quantum yield. The dye molecule must exhibit efficient NPHB. It should be soluble in a non-toxic solvent, preferably water or DMSO. Lastly, the target component of the cell should confer some degree of differentiation in a cell transformed from its normal state.

Taking these factors into account, mitochondria became the organelle of choice for reasons discussed here. Recent research on mitochondria has shown that the mitochondria of carcinoma cells [4] and cancerous tissues [5] exhibit numerous differences from normal tissues, among them a difference in the membrane potential ($\Delta\Psi_m$) generated by mitochondria and also morphological differences in shape and size [6,7], which could be the result of structural differentiation. Further, cationic dye molecules in the rhodamine family have been found to concentrate preferentially in mitochondria [8-10], which is attributable to mitochondrial composition (mostly lipids, with a negative $\Delta\Psi_m$ relative to the cytoplasm). Rhodamines also tend to have red/far red excitation and emission bands, respectively. Of the aforementioned criteria, the last parameter for consideration is NPHB efficiency. Despite being difficult to predict for any given molecule in a given host, previous work by this group on ionic dye molecules [11],

similar to the rhodamine family of dyes, predicted a favorable outcome for this requirement.

Research presented here, then, is a continuation, refinement, and expansion of work presented previously. Specifically, we present spectral hole burning results for a rhodamine dye (Molecular Probes MitoFluor Far Red 680 (MF680), commonly known as rhodamine 800) that is known to be specific for *in vivo* mitochondria. MF680 was incubated with two different cultured cell lines of human ovarian surface epithelial cells, one cancerous and one analogously normal. With regard to ZPH widths and temperature dependent ZPH widths, no significant differences were detected. Differences in electron-phonon coupling were too slight to be useful. Nevertheless, advances were made with significant differences measured in the areas of burn kinetics and the Stark effect, allowing us to further our attempts to use NPHB as an imaging technique for subcellular anomalies.

4.3. Experimental

4.3.1. Cell Culture

The choice of model cell cultures in the present study is a topic of a future paper by the authors [12]. Only pertinent details are given here.

Ovarian surface epithelial carcinoma cells (OV167) [13] were grown in Alpha MEM Earle's salts with nucleosides (Irvine Scientific; Santa Ana, CA), supplemented with 20% Fetal Bovine Serum (FBS), Penicillin/Streptomycin (100 U/ml and 100 μg/ml, respectively) and L-Glutamine (2mM final concentration, re-supplemented every two weeks). For each hole burning experiment, cells were

cultured for 6-7 days (medium re-supplementation on day 3) before staining and cryopreservation. Cells were incubated at 37°C and 5.5% CO_2 atmosphere.

For analogously normal cells, short-term normal ovarian surface epithelial (OSE) cell cultures were infected with pZipSVtsA58, a retrovirus encoding a temperature-sensitive mutant of the SV40 large T antigen; for simplicity, we will refer to them as OSE(tsT)-14. OSE(tsT)-14 cells were cultured in a 1:1 mixture of Medium 199 and MCDB105 medium mix, supplemented with 15% FBS, Penicillin/Streptomycin (100 U/ml and 100 μg/ml, respectively) and L-Glutamine(2mM final concentration, re-supplemented every two weeks). Cells were expanded at the permissive temperature of 34°C, 5.5% CO_2 for 6-7 days (medium re-supplementation on day 3) and cultured at 39°C, 5.5% CO_2 for 12-18 hours (allowing degradation of the heat-sensitive large T antigen) prior to staining and cryopreservation.

Cells were stained using MF680 for 15 minutes at a concentration of 40 nM. MF680 was initially dissolved in DMSO. At concentrations used for staining (after diluting with phosphate buffered saline (PBS) and subsequently growth medium), the DMSO component of the staining medium was negligible (0.0002%). OV167 cells were removed from the culture flask using trypsin/EDTA (2.5 g/L / 1 mM) solution. OSE(tsT)-14 were removed with a trypsin (2.5 g/L) solution.

Cryopreservation of both cell lines was carried out by suspending the cells in a 95%/5% (v/v) solution of respective medium/DMSO and frozen to –70°C overnight in a Nalgene Cryo 1°C freezing container. Cells were determined to be well preserved by this method, as viability was tested and found to be ≥ 90% after

freezing, thawing, and culturing (data not presented). Gelatin capsules were used to contain the suspension; capsules were mounted and rapidly plunged into helium for all hole burning studies.

Unless otherwise noted, all chemicals were purchased from Sigma, St. Louis, MO.

4.3.2. Laser System

The fluorescence excitation apparatus has been previously described [1], with the exception of a few minor modifications. In brief, a ring dye laser using LD 688 (Exciton; Dayton, OH) was pumped by a Coherent Innova 90-6 argon ion laser (Coherent; Santa Clara, CA). The laser system provided 100-500 mW power over a wavelength region of 660-720 nm. Laser intensity was stabilized by an LS100 laser power stabilizer (Cambridge Research and Instrumentation; Cambridge, MA) and the laser beam spot was expanded with a telescope. Two scanning modes were also utilized: broad-range scanning without intercavity etalons (scanning ranges and linewidths of 1000 cm^{-1} and 0.1 cm^{-1}, respectively) and short-range scanning with intercavity etalons (scanning ranges and linewidths <1.5 cm^{-1} and <0.0003 cm^{-1} (<10 MHz), respectively). When necessary, laser polarization was controlled with a polarizer.

Laser fluence for hole burning (typically ~5 mJ/cm^2) was varied with the use of a series of neutral density absorption filters. Scanning fluence was chosen so as to avoid alteration of the hole burned spectra. Burn kinetics were collected with rapid sampling at 0.1 s per channel for the first 30 s allowed for detailed fluorescence signal collection, as the signal tends to show the greatest decrease in this time. After 30 s, channel collection time was increased to 1 s.

Fluorescence intensity was collected with a Hamamatsu model R2949 GaAs photomultiplier tube (PMT) and photon counter (Model #SR-400, Stanford Research; Sunnyvale, CA). A 720 nm longpass filter (Model #720ALP, Omega Optical; Brattleboro, VT) was used to block excitation frequencies from reaching the PMT. Laser scanning and data collection were done with a PC, controlled by in house software.

4.3.3. Cryostat and Thermal Spray Chamber

The apparatus used to create hyperquenched glassy films of a water/DMSO (99.9%/0.1%, v/v) mixture containing MF680 at a concentration of ~1.0×10^{-5} M for an initial investigation of MF680's hole burning characteristics was recently described in detail in [14].

Gelatin capsules containing cell suspension samples were mounted in a Janis cryostat (Model 10DT, Janis Research; Wilmington, MA) pre-cooled to liquid helium temperature (4.2 K). Burn kinetics and Stark effect experiments were conducted with the sample mounted in a previously described [2] manner: between two copper plates, separated by 5 mm. All studies of burn kinetics and Stark effect were done in triplicate; when relevant, representative data are presented.

4.4. Results and Discussion

Broad scan fluorescence excitation spectra for MF680 presented in Fig. 4.1 show large shifts in the peak intensity signal depending on the host matrix. Although the exact cause of these shifts was not a major focus of this study, it is interesting to note the possible sources of these shifts. The controlled environment

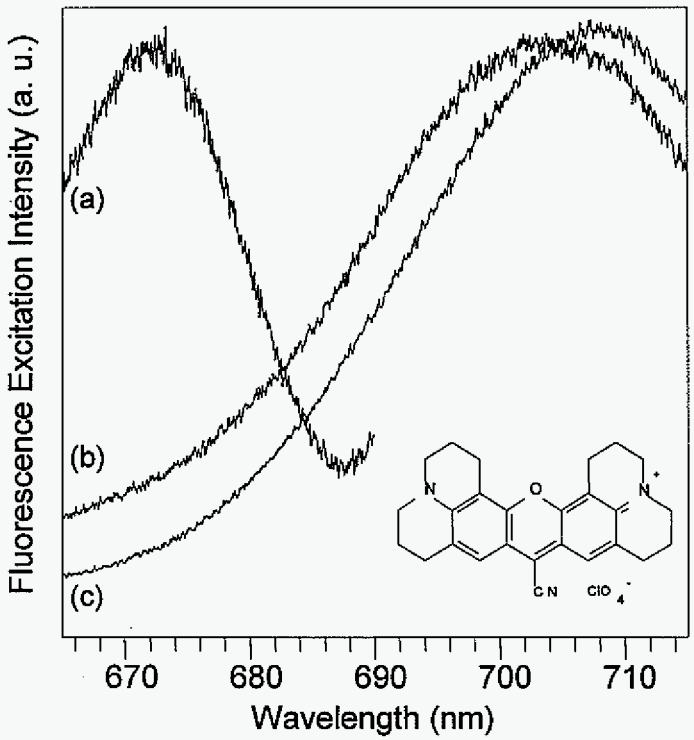

Fig. 4.1. Fluorescence excitation spectra of MF680 in three different environments: (a) Water/DMSO (99.9%/0.1%, v/v) thermal spray sample; (b) OSE(tsT)-14 cells; and (c) OV167 cells. Inset molecular structure is that of MF680.

of (a) has no lipid nature whatsoever; in each cell line, however, the dye molecule is located in a lipid-rich environment common to mitochondria. Another factor was elucidated in the work presented by Sakanoue et al. [15] on isolated rat liver mitochondria, who found that the MF680 dye molecule displayed spectral changes dependent on $\Delta\Psi_m$. These authors also make no attempt to explain the shifts, but it is apparent that this molecule's fluorescence excitation is inherently sensitive to $\Delta\Psi_m$ and/or its host matrix composition. The possibility that the shift is the result of molecular modifications made to the dye *in vivo* can be discounted, as the rat liver mitochondria study presented data of reversibility of fluorescence changes based on perturbations of $\Delta\Psi_m$, which indicates the molecular structure is not being changed.

Dispersive hole growth kinetics presented in Fig. 4.2 show MF680 to burn more rapidly in the OV167 cell line relative to the OSE(tsT)-14 cell line. The difference is exaggerated in (a), where the burn wavelength (λ_b) is farther in the red (712 nm) than in (b), where λ_b is 705nm. In both cases, the OSE(tsT)-14 cell lines normalized fluorescence excitation results in about the same fractional hole depth of 0.23. The OV167 cell line, however, shows a difference in the fractional hole depth dependent on λ_b. For Fig. 4.2 (a), the burn is contained to the low energy side of the absorption maximum for both cell types, whereas for Fig. 4.2 (b), λ_b is on the high energy side of the absorption maximum for the OV167 cells but still on the low energy side of the absorption max for the OSE(tsT)-14 cells. We are currently in the process of analyzing the hole growth kinetics data applying the theory presented in [16] and to be included in [12].

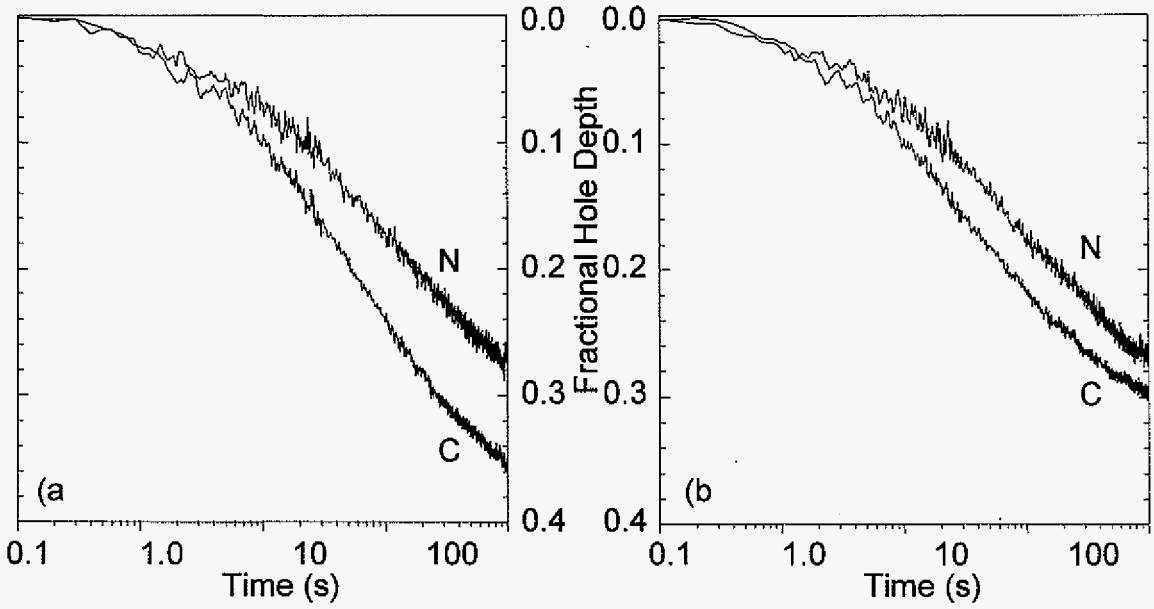

Fig. 4.2. Hole growth kinetics for MF680 in OSE(tsT)-14 normal cells (N) and OV167 cancerous cells (C) at (a) λ_b of 712nm and at (b) λ_b of 705 nm.

Overlaying hole growth profiles to take into account the shift in peak fluorescence excitation (calculated to be ~3 nm from fits applied to plots such as those presented in Fig. 4.1 (b) and (c)) was also attempted but not presented. These plots continued to exhibit different shapes. This is interpreted as evidence of the matrix surrounding the dye molecule affecting the hole growth. In effect, the dye molecule is in a distinct environment in each cell line, which is capable of being resolved by hole growth kinetics.

Interestingly, the typical FWHM of the ZPH (4-5 GHz) as a result of these burns showed little difference between the two cell lines; there was a slight tendency for the FWHM of normal cells to be narrower, but the difference was typically within 0.5 GHz and considered statistically insignificant (data not presented). A hole burning study was also conducted on each cell type at λ_b ~706 nm at six different temperatures in the range 1.4 – 11 K. The FWHM of the ZPH at each temperature (data not presented) was found not to vary significantly between the two cell lines. Results of experiments conducted utilizing the Stark effect are presented in Fig. 4.3 and Table 1. Representative fits for ZPH at λ_b = 711.6 and 711.8 nm with effects of a zero and 6.4 kV/cm E_{St} field applied parallel and perpendicular to E_L with C representing the OV167 (carcinoma) cell line and N representing the OSE(tsT)-14 (normal) cell line are given in Fig. 4.3 (a) and (b), respectively. From the fit overlays it is evident that both cell lines tend to have similar ZPH profiles at zero applied E_{St}; the maximum applied E_{St}, however, produces large differences between the two. As observed in our previous Stark hole burning experiment utilizing APT in normal and

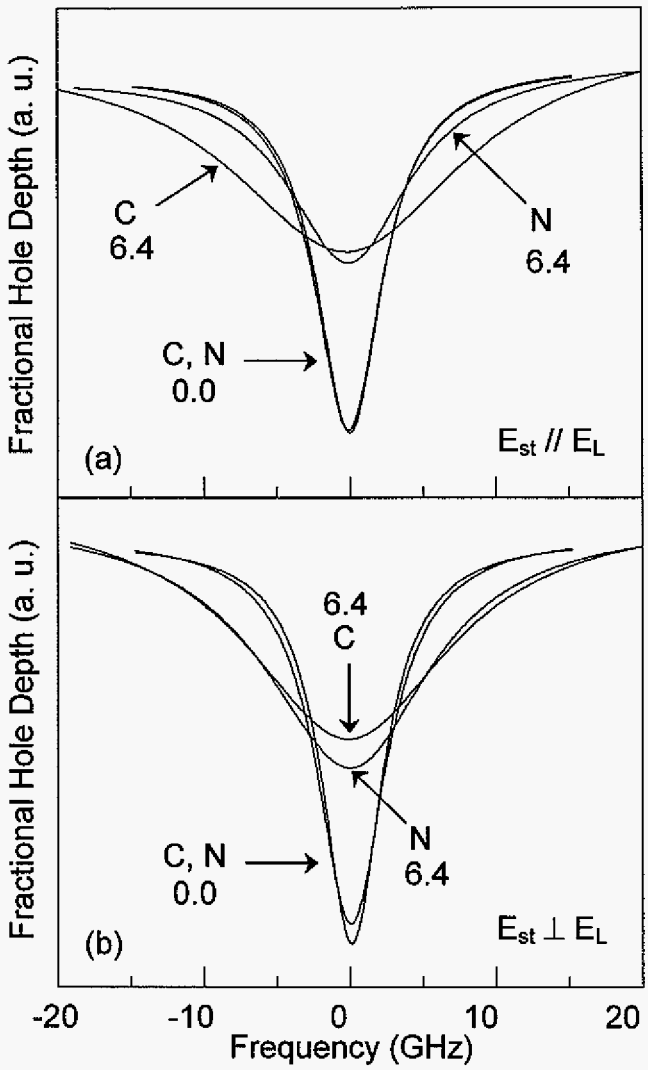

Fig. 4.3. Representative fits of ZPH at zero-field and 6.4 kV applied external field for MF680 in OSE(tsT)-14 cells (N) and OV167 cells (C). Panel (a) corresponds to burn and read laser polarization parallel to the Stark field, and panel (b) corresponds to burn and read laser polarization perpendicular to the Stark field. Units for all numbers given in figure are kV/cm.

cancerous breast epithelial cells [2], no splitting of the ZPH is observed for either orientation of E_{St} relative to E_L; only broadening is observed. Quantitative comparisons between the two cell lines based on $f\Delta\mu$ values are given in Table 4.1. Calculations to obtain these values were performed according to Kador et al. [17] and were determined by fitting a plot of hole width as a function of applied E_{St}. Clearly, differences in the values of $f\Delta\mu$ exist between the two cell lines tested; within experimental error, the values also do not exhibit a dependency on the polarization of E_{St}. Of particular interest is the determination that $f\Delta\mu$ for the normal cell line is lower in value than the carcinoma cell line, most likely a result of the lowered $\Delta\psi_m$ in normal cultured cells, *vide infra*. Also of interest in Table 1 is the observed standard deviation for $f\Delta\mu$ between each cell line differs by a factor of about two. A reasonable explanation for this is attributed to variance in the cell growth stages for each cell line. Although every precaution was taken with the culturing of these cell lines to eliminate the possibility of variance (replenishing growth medium at regular intervals, staining and harvesting after the same number of days in culture, etc.), it is difficult to replicate cell cultures that are in identical growth stages. Future planned studies will elucidate with more certainty growth stage variability effects on HBI measurements, as preparations are being made to include flow cytometry measurements.

Relating to our previous Stark study [2], we can also draw conclusions for understanding the results presented in Table 1. In the present case only broadening of the ZPH is observed for each cell line, which is indicative of two key points. However, it must be noted beforehand that overall $\Delta\mu$ is composed of two parts, the

change in intrinsic permanent dipole moment of the ground and excited electronic states ($\Delta\mu_o$), and the matrix-induced dipole moment change ($\Delta\mu_{ind}$). The first key

Table 4.1: Permanent dipole moment changes for MF680 in OV167 (carcinoma) and OSE(tsT)-14 (normal)

Cell Line	$f\Delta\mu$ (D)	Laser Polarization	λ_b (nm)
OSE(tsT)-14	1.64 ± 0.24	$E_{St} \perp E_L$	711.8
OV167	2.47 ± 0.10		711.8
OSE(tsT)-14	1.68 ± 0.32	$E_{St} // E_L$	711.6
OV167	2.51 ± 0.12		711.6
OSE(tsT)-14	1.73 ± 0.28	$E_{St} // E_L$	707.1
OV167	2.38 ± 0.17		707.1
OSE(tsT)-14	1.92 ± 0.33	$E_{St} \perp E_L$	706.9
OV167	2.43 ± 0.08		706.9

point, then, is the absence of splitting indicates that $\Delta\mu_{ind} >> \Delta\mu_o$. Second, $\Delta\mu_{ind}$, which itself is composed of a random ($\Delta\mu_r$) and nonrandom ($\Delta\mu_{nr}$) component, varies in random fashion. This is consistent with the observation that $\Delta\mu_\perp \cong \Delta\mu_{//}$ within each cell line. Most importantly, these observations conclude that overall $\Delta\mu$ in the present case is due to matrix-induced factors, and our observations are explained by the *in vivo* interaction of the dye molecule with the mitochondrial matrix.

A parameter we have not elaborated on to this point is $\Delta\Psi_m$. It has been observed in previous studies by others [10,18-21] to be greater in magnitude in carcinoma cells relative to normal epithelial cells. Although the reported values differ ($100 \text{ mV} \leq \Delta\Psi_m \geq 200 \text{ mV}$), there is an approximate 60-90 mV range difference between reported comparative carcinoma and normal cell cultures. A ratio based on this difference gives a value of ~1.5; similarly, the ratio between $f\Delta\mu$ values for λ_b of 711.8 and 711.6 nm gives a value of ~1.5. Although further experimentation is

necessary to expand on the correlation, it is interesting to note the apparent relation between the two.

In summary, we are encouraged by our findings of significant differences in the zero-phonon hole growth kinetics between the OV167 (carcinoma) and OSE(tsT)-14 (normal) cell lines and the differences between the two cell lines found in the series of experiments utilizing the Stark effect. We anticipate additional studies targeting *in vivo* mitochondria will allow us to expand these findings.

4.5. Acknowledgement

Ames Laboratory is operated for the U. S. Department of Energy by Iowa State University under Contract W-7405-Eng-82. This work was supported by the Office of Health and Environmental Research. T. Reinot was supported by the Solid State Chemistry and Polymers Program of the National Science Foundation.

References

1. Milanovich, N.; Reinot, T.; Hayes, J. M.; Small, G. J., *Biophys. J.* **1998**, *74*, 2680.
2. Milanovich, N.; Rätsep, M.; Reinot, T.; Hayes, J. M.; Small, G. J., *J. Phys. Chem. B* **1998**, *102*, 4265.
3. Milanovich, N. Application of Spectral Hole Burning to the Study of In Vitro Cellular Systems. Ph. D., Iowa State University, **1999**.
4. Modica-Napolitano, J. S.; Aprille, J. R., *Adv. Drug Deliv. Rev.* 2001, *49*, 63.
5. Yaffe, M. P., *Science* **1999**, *283*, 1493.
6. Eapen, C. E.; Madesh, M.; Balasubramanian, K. A.; Pulimood, A.; Mathan, M.; Ramakrishna, B. S., *Scand. J. Gastroenterol.* **1998**, *33*, 975.
7. Djaldetti, M., *Acta Haematol.* **1982**, *68*, 241.

8. Chen, L. B.; Summerhayes, I. C.; Johnson, L. V.; Walsh, M. L.; Bernal, S. D.; Lampidis, T. J., *Cold Spring Harb. Symp. Quant. Biol.* **1982**, *46 Pt 1*, 141.

9. Chen, L. B., *Methods Cell Biol.* **1989**, *29*, 103.

10. Johnson, L. V.; Walsh, M. L.; Chen, L. B., *Proc. Natl. Acad. Sci. USA* **1980**, *77*, 990.

11. Feary, B. L.; Carter, T. P.; Small, G. J., *J. Phys. Chem.* **1983**, *87*, 3590.

12. Walsh, R. J., Nonphotochemical hole-burning imaging studies of *in vitro* carcinoma and normal cells utilizing a mitochondrial specific dye, Ph. D., Iowa State University, **2002**.

13. Conover, C. A.; Hartmann, L. C.; Bradley, S.; Stalboerger, P.; Klee, G. G.; Kalli, K. R.; Jenkins, R. B., *Exp. Cell. Res.* **1998**, *238*, 439.

14. Reinot, T.; Small, G. J., *J. Chem. Phys.* **2001**, *114*, 9105.

15. Sakanoue, J.; Ichikawa, K.; Nomura, Y.; Tamura, M., *J. Biochem. (Tokyo)* **1997**, *121*, 29.

16. Reinot, T.; Small, G. J., *J. Chem. Phys.* **2000**, *113*, 10207.

17. Kador, L.; Haarer, D.; Personov, R., *J. Chem. Phys.* **1987**, *86*, 5300.

18. Summerhayes, I. C.; Lampidis, T. J.; Bernal, S. D.; Nadakavukaren, J. J.; Nadakavukaren, K. K.; Shepherd, E. L.; Chen, L. B., *Proc. Natl. Acad. Sci. USA* **1982**, *79*, 5292.

19. Modica-Napolitano, J. S.; Aprille, J. R., *Cancer Res* **1987**, *47*, 4361.

20. Davis, S.; Weiss, M. J.; Wong, J. R.; Lampidis, T. J.; Chen, L. B., *J Biol Chem* 1985, *260*, 13844.

21. Dairkee, S. H.; Hackett, A. J., *Breast Cancer Res Treat* **1991**, *18*, 57.

CHAPTER 5. CARCINOMA AND SV40-TRANSFECTED NORMAL OVARIAN SURFACE EPITHELIAL CELL COMPARISON BY NONPHOTOCHEMICAL HOLE-BURNING IMAGING

A paper to be submitted to Biophysical Journal

R. J. Walsh, T. Reinot, J. M. Hayes, K. R. Kalli, L. C. Hartmann, and G. J. Small

5.1. Abstract

Results are presented of nonphotochemical hole burning experiments on the mitochondrial specific dye rhodamine 800 (MitoFluor Far Red 680, Molecular Probes) incubated with two human ovarian surface epithelial cell lines: OSE(tsT)-14 normal cells and OV167 carcinoma cells. This dye is selective for the plasma and inner membranes of the mitochondria, exhibited in confocal microscopy images. Dispersive hole growth kinetics (HGK) of zero-phonon holes (ZPH) are analyzed with theoretical fits, facilitating the conclusion that subcellular structural heterogeneity of the carcinoma cell line is lower relative to the analogous normal cell line. Permanent dipole moment change ($\Delta\mu$) for the $S_0 \rightarrow S_1$ transition of the dye is markedly different for the two cell lines, the $\Delta\mu$ value for the carcinoma cell line being a factor of 1.5 higher. Flow cytometry results are presented to determine the possible correlation between increases in mitochondrial membrane potentials and increases in permanent dipole moment changes for the carcinoma cell line.

5.2. Introduction

Proof-of-principle experiments by this group have established that persistent nonphotochemical hole burning (NPHB) spectroscopy of probe molecules in cells is facile [1,2]. NPHB is a high-resolution frequency domain technique which facilitates resolution of the inhomogeneously broadened absorption spectra of chromophores in glasses and other complex condensed media such as proteins and polymers. It provides an increase in spectral resolution by several orders of magnitude (10^4-10^5) over conventional (non line-narrowed) absorption techniques. NPHB has been instrumental for fundamental studies of many systems, from spectral dynamics in glasses and polymers [3-10] to elucidation of electron and excitation energy transfer processes in photosynthetic reaction centers and antenna complexes [11-15].

Notably, NPHB is a technique that can provide an "image" of the structural domain of a chromophore in a given amorphous matrix, and can thus be referred to as hole-burning imaging (HBI). In this sense, HBI is analogous to magnetic resonance imaging (MRI), in that MRI is based on proton T_1 relaxation times and the spatial or spectral resolution of HBI is based in part on the T_2 optical relaxation time of the probe molecule which governs hole width. The high resolution of NPHB allows accurate measurements to be made of spectral parameters such as electron-phonon coupling and vibrational frequencies, as well as spectral shifts due to external applied electric fields (the Stark effect), or spectral shifts due to applied pressure. For a given chromophore, narrow-line excitation at low temperatures can lead to the development of narrow zero-phonon holes (ZPH) burned into an inhomogeneously broadened electronic absorption band of a chromophore.

Although photochemical [16] and transient hole burning mechanisms are also possible, in the present case we are concerned only with NPHB, as its mechanism, described below, is inherently sensitive to the nanoenvironment surrounding a chromophore.

HBI is seen as a possible addition to disease detection methods available today, namely radiography, Computed Axial Tomography (CAT), and MRI, with resolution at the subcellular level. Past studies by this group have focused on demonstrating HBI as a cellular analog of MRI. HBI was used to detect structural differences between two cultured human breast epithelial cell lines, one (MCF7) characterized as a carcinoma line, and the other (MCF10F) an analogous normal line [1]. This work demonstrated the possibilities of NPHB in cultured cells by introducing the fluorescent probe molecule aluminum phthalocyanine tetrasulfonate (APT) to the cells and subsequently hole burning the molecule *in situ*. The characteristics of APT hole burning in aqueous structurally disordered (amorphous) glassy systems are well documented [17], so that an accurate comparison could be made for APT hole burning in cells. The basis for the use of NPHB in this type of application is contained within the mechanism of NPHB (vide infra). It is noteworthy that NPHB is a line-narrowing technique that eliminates inhomogeneous broadening, and recent review articles should be consulted [18,19] for further information.

A model for the mechanism by which NPHB occurs was presented by Hayes and Small [20,21]. A schematic of the model is given in Figure 5.1. The Hayes-Small mechanism is based on a persistent frequency change mechanism requiring

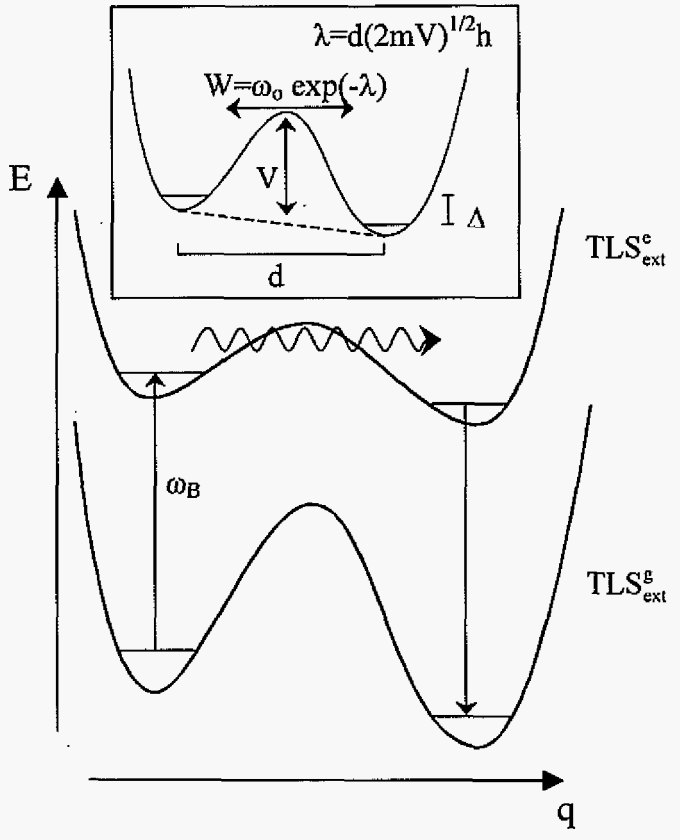

Figure 5.1. Schematic illustration of the extrinsic Two Level Systems (TLS_{ext}). Indices e and g denote ground and excited states, respectively. ω_B is the burn frequency of the laser. The inset defines the TLS parameters. W is the tunneling frequency, which is a function of λ. Within λ, m is the effective mass of the tunneling entity, d is the displacement between the two potential energy minima, and h is Planck's constant.

two stable potential energy minima, referred to as Two-Level-Systems (TLS). TLS are thought to be universally present in disordered matrices, and can be subdivided into those intrinsic to the glass (TLS_{int}) and those due to the presence of an impurity (extrinsic TLS, or TLS_{ext}). According to the model, a chromophore and surrounding inner shell solvent molecules associated with TLS_{ext} (TLS^{g}_{ext} and TLS^{e}_{ext}, where g and e denote the ground and excited states of the chromophore) are responsible for NPHB. Phonon-assisted tunneling in the excited state follows narrow band laser excitation of the chromophore, and results in a decrease in the absorption frequency of the chromophore (i.e. a spectral hole). This process results in persistent holes when TLS^{g}_{ext} tunneling can be neglected, which is a reasonable assumption for the experimental time scale. In the Hayes-Small model, the tunneling was proposed to occur between the two wells of the TLS^{e}_{ext}, with the assumption that there was a static distribution of TLS^{e}_{ext} with different values of the tunneling parameter (λ, vide infra). Further modifications by Shu and Small [22] concluded that NPHB cannot be understood in terms of a static distribution of TLS_{ext}, however. From these experiments, an "outside-in" series of steps was postulated: NPHB occurs due to a hierarchy of tunneling events triggered by optical excitation that begins with the faster relaxing intrinsic TLS (TLS_{int}) in the outer shell and terminates in the inner shell, where the rate determining step of NPHB takes place. Importantly, the Shu-Small model connected the migration of excess free volume with TLS_{int} "flipping", or concurrent configuration tunneling and further predicted that NPHB would cease in a crystalline matrix, since excess free volume is absent by definition. This prediction was later proven correct by studies using APT in hyperquenched glassy water,

where it was shown that samples annealed to 158 K (the temperature at which cubic ice forms) ceased to hole-burn [23]. A complete review of the present understanding of TLS relevant to NPHB has recently been given [24]. A complete description of the model is contained in this reference and references therein.

In the present case, cultured cells are expected to be disordered amorphous structures when frozen to liquid helium temperatures. Based on the work presented by Milanovich [25], an efficient hole-burnable fluorescent dye probe placed in a cellular matrix is expected to provide quantifiable information regarding the assembly of that matrix by using NPHB, assuming controls can be placed on the specific location of the probe. As described above, NPHB is modeled to include interactions dependent on an amorphous glassy matrix with excess free volume, resulting in a host matrix rearrangement around the chromophore. This rearrangement is therefore inherently linked to the structural configuration of the host matrix, and provides the basis for expecting hole burning parameters of a chromophore, e.g. the rate of hole formation (hole growth kinetics) or the response to the Stark effect, to differ in dissimilar cells. For our purposes, it is envisioned that NPHB can provide a tool for detecting cellular anomalies, as the aforementioned kinetics measurements are highly matrix dependent. Structural differences anticipated between the model cell lines may thus provide discernable hole burning characteristics.

Although the results of the experiments with cultured breast epithelial cells (MCF7 and MCF10F) were able to show a small difference in dipole moment change between the two cell lines based upon the Stark effect response of APT, the

results were acknowledged to suffer from the inability of APT to localize in specific areas of the cells, thereby inhibiting the ability of NPHB to exploit the sensitivity of discerning cellular ultrastructural differences. Further, the model cell lines used for this study had undesirable qualities, such as the normal analogs being immortalized, an adverse quality for a cell line that is to be the reference for a concurrently immortalized carcinoma cell line.

Fortunately, techniques have been developed to facilitate the culturing of cell lines [26-29] that exhibit extended proliferation capabilities without undergoing transformation or immortalization. These lines are intended to provide model cell lines for general understanding of cellular biological processes as well as for use in the development of cellular anomaly diagnostic techniques and treatments. Most importantly, these cell culture techniques have allowed multidisciplinary approaches to be realized, as in the present case.

The focus of the work presented here is to expand upon NPHB application to biological systems. In a recent study [30], we reported promising NPHB results obtained with a mitochondrial specific dye molecule passively internalized by the cell. Mitochondria were targeted because they are reported to undergo radical changes in both their membrane potential ($\Delta\psi_m$) and morphology in cancerous cells [31,32], thus becoming a strong candidate to be a specific target for fluorescent probe staining and subsequent hole burning. Also for this work, new cell lines were chosen that would present improved comparative carcinoma and normal analogues, both of which are characterized and in the case of the normal analogues have not undergone immortalization. The means by which the latter was accomplished was

to use the common technique of transfecting the cell line with a strain of a temperature sensitive Large T Antigen Simian Virus 40 (SV40), providing an internal control by which the transfection could be eliminated. It is documented [33] that this method allows the cells to proliferate without the added disadvantage of causing large genetic and/or morphological changes in the cells typically brought about by increased passaging of cell cultures obtained from normal tissue. A further advantage is the ability to controllably return the cell culture to conditions nearly identical to their state prior to transfection by denaturing the SV40 antigen by simply increasing the temperature of the culture for a short period (12-18 hours).

The cell lines utilized were of human ovarian surface epithelial origin, with the carcinoma cell line (OV167) having been characterized previously by Conover et al. [34] and the temperature sensitive SV40 normal analogs (OSE(tsT)-14) to be characterized Kalli et al. [35]. Ovarian surface epithelial cells are thought to be involved heavily in the onset of ovarian cancer, as it has been documented [36] that ~90% of ovarian cancers have their origin in this cell type. Based on this fact, we have determined this to be an ideal model cell line for use in our studies to probe for the development of sub cellular anomalies that lead to a normal cell transforming into a cancerous cell.

In choosing a probe dye molecule, a commercially available dye from the rhodamine family of dyes, commonly known as Rhodamine 800 (Molecular Probes' MitoFluor Far Red 680, hereafter referred to as MF680) has proven useful for numerous reasons. Specifically, the hydrophobic, carbocationic dye localizes preferentially in mitochondrial membranes of live cells due to favorable conditions:

mitochondria are composed heavily of lipids and generate a large $\Delta\psi_m$. The dye enters the cells passively and does not disrupt normal cellular processes (to the best of our knowledge), so that staining and cryofixation of the cells can be done rather easily on live, non-fixed cells. Also, the dye's absorption maximum of 680nm (red-shifted once inside the cell) results in minimal background signal intrusion due to auto-fluorescence.

Work presented here includes a hole-burning study of dispersive hole-growth kinetics (HGK) that exhibits significant differences between the two ovarian surface epithelial cell lines, along with expanded results of measurements of permanent dipole moment changes due to the Stark effect. Results from studies with confocal microscopy are introduced to reinforce the claim of MF680 exhibiting mitochondrial specificity. To investigate the possible correlation of mitochondrial membrane potentials effect on Stark spectroscopy results, the results of membrane potential measurements by flow cytometry are presented in an attempt to determine if differences in reported permanent dipole moment change values between the two cell lines are indeed attributable to a large difference in $\Delta\psi_m$.

5.3. Experimental

5.3.1. Cell Culture

Two lines of Ovarian Surface Epithelial Cells were cultured for the model cell lines: OV167 (cancerous) and short-term normal ovarian surface epithelial (OSE) cell cultures infected with pZipSVtsA58, a retrovirus encoding a temperature-sensitive mutant of the SV40 large T antigen. For simplicity, we will refer to the latter as OSE(tsT)-14. OV167 cells were cultured in Alpha MEM with nucleosides

(Irvine Scientific; Santa Ana, CA), supplemented with 20% Fetal Bovine Serum (FBS), Penicillin/Streptomycin (100 U/ml and 100 μg/ml, respectively) and L-Glutamine (2mM final concentration, re-supplemented every two weeks). OSE(tsT)-14 cells were cultured in a 1:1 mixture of Medium 199 and MCDB105 medium mix, supplemented with 15% FBS, Penicillin/Streptomycin (100 U/ml and 100 μg/ml, respectively) and L-Glutamine(2mM final concentration, re-supplemented every two weeks). Both cell lines were cultured to sub-confluent populations, harvested, and then cryopreserved in 1 mL aliquots with 5% Dimethyl Sulfoxide (DMSO). For each hole burning experiment, an aliquot of cells was cultured for 6-7 days (non-confluent samples) or 12 days (confluent samples) before staining and cryopreservation. OV167 cells were grown at 37°C and 5% CO_2 atmosphere. OSE(tsT)-14 cells were grown at the permissible temperature of 34°C, 5% CO_2 for SV40 Large T antigen (LT). For cells in which it was desirable to keep the antigen present (ltOSE(tsT)-14), cells were stained and cryopreserved at the desired coverage conditions. For cells in which the SV40 LT antigen was desired to be denatured (htOSE(tsT)-14), cells were cultured to desired coverage conditions and subsequently incubated for 12-18 hours at 39°C and 5% CO_2 prior to staining and cryopreservation. Unless otherwise noted, all chemicals were purchased from Sigma-Aldrich (St. Louis, MO).

5.3.2. Staining

Staining of the culture was accomplished by dissolving the MF680 (Molecular Probes; Eugene, OR) initially in DMSO, then diluting into 1× Phosphate Buffered Saline (PBS) to the desired concentration for final staining concentration. Incubations were carried out under normal culture growth conditions, and cells were

rinsed three times with PBS prior to cryopreservation. Hole burning experiments were conducted with cells stained with MF680 at a concentration of 40 nM for 15 minutes; confocal experiments were conducted as noted.

5.3.3. Cryopreservation

Cells were cryopreserved by suspending in 130 μL of their respective medium with 5% DMSO and subsequent placement in a gelatin capsule. Because the capsules tended to soften and dissolve prior to freezing, two sizes were used (#4 and #5), with the smaller #5 being placed inside the larger #4. The entire suspension was placed in a Nalgene Cryo 1°C freezing container (Nalgene Products; Rochester, NY) and frozen to –70°C undisturbed for at least 4 hours. Capsules were then plunged directly into liquid helium for hole burning studies. Cells were also tested for post-staining and freezing viability by rapidly thawing and returning the cells to their respective medium.

5.3.4. Confocal Microscopy

All confocal and time-lapse imaging was performed at the Roy J. Carver Laboratory for Ultra-high Resolution Biological Microscopy (Iowa State University; Ames, IA). The microscope utilized for both imaging methods was a Nikon Eclipse TE200 with an inverted 60X oil-immersion lens (NA: 1.40; Theoretical Resolution at 632.8nm: 0.276 μm). The confocal/video instrumentation was manufactured by Prairie Technologies, LLC (Middleton, WI). Confocal imaging was performed with He-Ne (632.8 nm) and Ar^+ (514 nm) ion lasers laser for excitation, with PMT detection, and a variable pinhole size (set to 100 μm). All software to control the hardware was by Prairie Technologies utilizing National Instruments LabView 5.1.

Cells were grown and imaged on poly-L-Lysine (Sigma; St. Louis, MO) treated coverglass (25 × 75 mm). To facilitate multiple stainings without removing the sample from the microscope, an in-house silicone culture well (vol. ~0.5 mL) was created and affixed to the glass. Cultures were transferred 24-48 hours prior to use, and were incubated under normal conditions. All images were collected within one hour of preparation. Cells cultured for use in confocal microscopy studies were not passage restrained, however were within one passage of those used for hole burning studies.

5.3.3. Flow Cytometry

Flow cytometric measurements were performed on a Beckman Coulter EPICS Altra (Miami, FL), utilizing Beckman Coulter's Expo32 software for Windows, version 1.2. The procedure followed for the measurement of $\Delta\psi_m$ was that of Rottenberg and Wu,[37] with minor adjustments. Briefly, measurements were performed by aliquoting samples of cells into populations of ~10^6, staining 20 minutes with 4 nM MF680 (the concentration determined to be the threshold for detectability), washing 2 × with PBS, and taking fluorescence measurements using a He-Ne laser (633 nm) for excitation. Samples were then incubated for 20 minutes with 0.5 mM carbonyl cyanide *m*-chlorophenyl-hydrazone (CCCP) to collapse the membrane potential, and remeasured. Calibration for the Nernst equation relation to calculate $\Delta\psi_m$ was performed utilizing KCl concentrations of 0.1, 1.0, 30, 60, 120, and 240mM, 3μM valinomycin, 4 nM MF680, and 0.5 mM CCCP to collapse $\Delta\psi_m$.

5.3.5. Laser/Cryostat System for Hole Burning

The fluorescence excitation system has been previously described [2], with the exception of a few modifications. In brief, a ring dye laser using LD 688 (Exciton; Dayton, OH) was pumped by a Coherent Innova 90-6 argon ion laser (Coherent; Santa Clara, CA). The laser system provided 100-500 mW power over a wavelength region of 660-720 nm. Laser intensity was stabilized by an LS100 laser power stabilizer (Cambridge Research and Instrumentation; Cambridge, MA) and the laser beam spot was expanded with a telescope. Two scanning modes were utilized: broad-range scanning without intercavity etalons (scanning ranges and linewidths of 1000 cm^{-1} and 0.1 cm^{-1}, respectively) and short-range scanning with intercavity etalons (scanning ranges and linewidths <1.5 cm^{-1} and <0.0003 cm^{-1} (<10 MHz), respectively). When necessary, laser polarization was controlled with a polarizer.

Laser intensity for hole burning and scanning was varied with the use of a series of neutral density absorption filters. Scanning fluences were chosen to avoid alteration of spectra. Burn kinetics were collected so that rapid sampling at 0.1 s per channel for the first 30 s allowed for detailed fluorescence signal collection, as the signal tends to show the greatest decrease in this time. After 30 s, channel collection time was increased to 1 s.

Fluorescence intensity was collected with a Hamamatsu model R2949 GaAs photomultiplier tube (PMT) and photon counter (Model #SR-400, Stanford Research; Sunnyvale, CA). A 720 nm low pass filter (Model #720ALP, Omega Optical; Brattleboro, VT) was used to block excitation frequencies from reaching the

PMT. Laser scanning and data collection were done with a PC running in-house software.

For the cells and the glycerol-water mixture, hole burning was performed with the sample mounted in a Janis cryostat (Janis Research; Wilmington, MA). Both kinetics and Stark experiments were done using a sample holder described previously [1]; briefly, for the Stark experiments two Teflon walls separated by 11 mm and positioned parallel to the cryostat walls hold two copper electrodes positioned perpendicular to the cryostat walls and separated by 4.95 mm. The hole burning apparatus for the hyperquenched glassy water (HGW) system has been described previously [38], and was performed by thermospraying an aqueous MF680 (10^{-5} M) solution onto a copper block under vacuum and at ~5 K.

5.4. Results

5.4.1. Confocal and Microscope Studies

Confocal Microscopy images of the two cell lines OV167 and OSE(tsT)-14 are presented in Figure 5.2. A noteworthy feature of the images for the OV167cells in 2B and the OSE(tsT)-14 cells in 2D is the observation of the dye in a specific, structured organelle, which most closely resembles mitochondria when referenced to other studies staining for *in situ* mitochondria [39]. To rule out the possibility that the MF680 dye was locating preferentially elsewhere than the mitochondria in either cell line, two tests were conducted. The first was to add a small amount of sodium azide to the culture while imaging on the microscope; within several seconds, the fluorescence intensity of the cells was observed to diminish (data not presented). Sodium azide is a toxin targeted to enzyme complex IV in the mitochondria electron

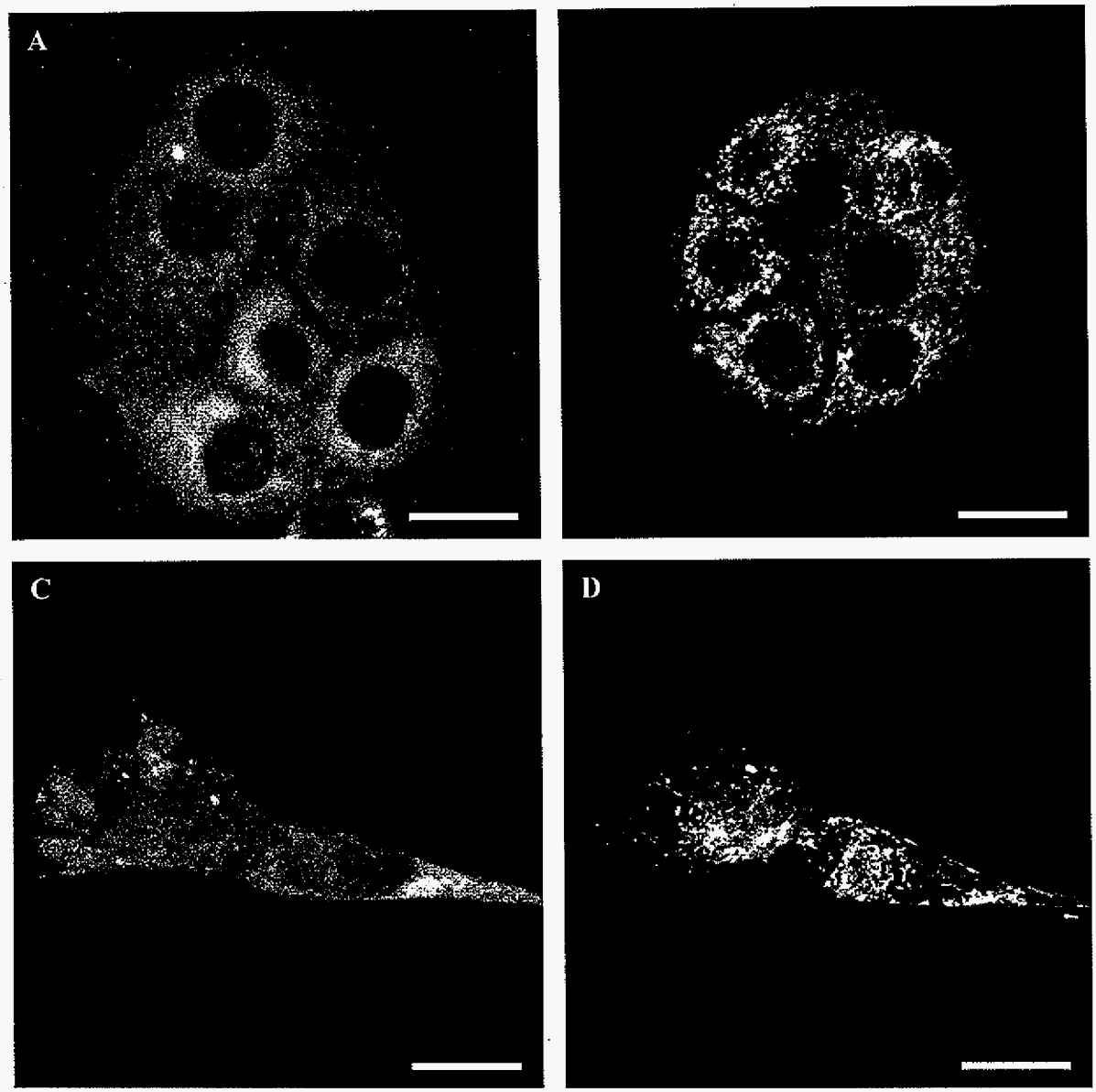

Figure 5.2. Confocal images of OV167 (carcinoma) cells (A, B) and OSE(tsT)-14 (normal analog) cells (C, D). Images in A and C were stained with Brefeldin-A BODIPY, specific for the endoplasmic reticulum. Images in B and D were stained with MF680, specific for mitochondria. The white bar represents 20 μm.

transport chain, resulting in deterioration of the mitochondrial membrane potential. Since the MF680 dye is cationic and requires the membrane potential to maintain its position within mitochondrial membranes, this observation was the direct result of the MF680 being released by the mitochondria to levels below detection due to the insult by the sodium azide. The second test conducted was to target and stain the endoplasmic reticulum, suspected as a possible alternative repository for the MF680 molecule due to similarities to mitochondria in maintaining a membrane potential and having a lipid structure. This was accomplished by using a second dye, Molecular Probes' BODIPY conjugated to Brefeldin-A (with a non-interfering absorbance and fluorescence relative to MF680), added to a culture in growth medium and mounted on the microscope. After a short incubation and collection of confocal images where the BODIPY dye is the source of the fluorescence signal, MF680 was added and subsequently allowed to incubate for a short period and then imaged. The results are presented in Fig. 5.2A and 5.2C, where the two cell lines are presented for comparison of staining localization. It is apparent from an inspection of the structures stained by each dye that their positions and morphology differ, and hence provides further evidence of MF680's preferentiality for mitochondrial membranes.

5.4.2. Dispersive Hole Growth Kinetics of MF680

Figure 5.3 exhibits fluorescence excitation spectra for three types of samples, one formed by hyperquenching a solution of MF680 dissolved in water and two samples with intracellular MF680. The HGW sample was prepared for a preliminary investigation of MF680 to determine if the molecule could be hole-burned. Fig. 5.3A

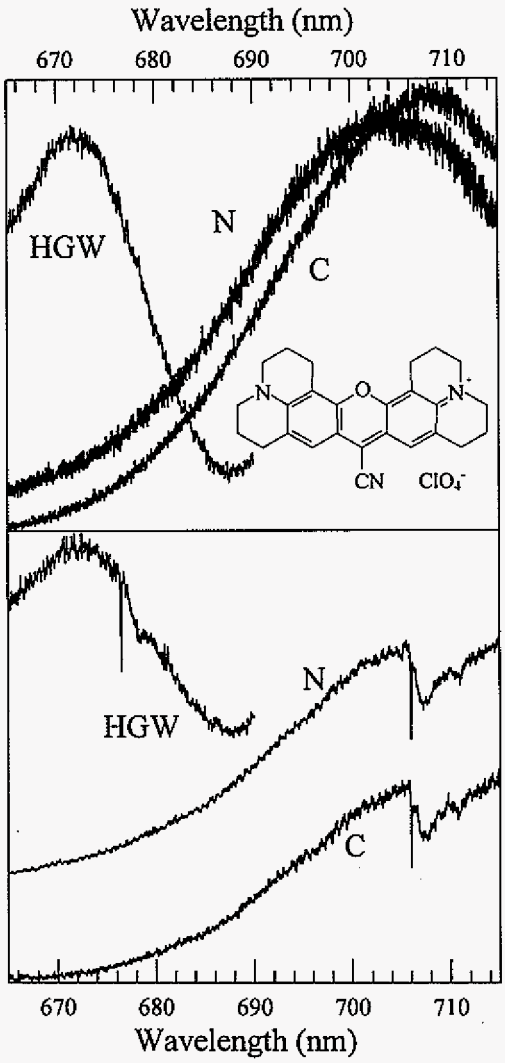

Figure 5.3. Fluorescence excitation spectra (A) of MF680 in hyperquenched glassy water (HGW), OSE(tsT)-14 normal cells (N) and OV167 carcinoma cells (C). The inset in A is the dye molecule MF680. The spectra in B are post-burn spectra, exhibiting the ZPH and the pseudo-phonon side band (PSB) for each type of sample. Fluences for each type of sample are 33 mJ/cm^2 and 1.4 J/cm^2 for the HGW and each cell line, respectively.

and 5.3B present the pre- and post-burn fluorescence excitation spectrum obtained from this sample, respectively, and it is evident that the molecule is capable of being spectrally hole-burned. A sample created with MF680 in glycerol:water (1:1) and frozen in a gelcap produced a fluorescence excitation profile (data not shown for clarity) similar to those presented in Fig. 5.3, except with peak excitation centered at 685 nm.

Noteworthy from Fig. 5.3A, there is a large red shift in the MF680 *in vivo* excitation maxima relative to the HGW sample, with the OV167 carcinoma (C) cell line being further red shifted than the OSE(tsT)-14 normal (N) cells by ~3 nm. Apparent from Fig. 5.3B are representative "deep" burns, created with fluences for the intracellular samples at 1.4 J/cm^2 and for the HGW sample at 33 mJ/cm^2. From the figure, the pseudo-phonon side band hole (PSBH) is observed to be 30 ± 3 cm^{-1} for the HGW and normal cells and 28 ± 3 cm^{-1} for the carcinoma cells. Although not significantly different between the two cell lines, the large separation between the ZPH and the PSBH translates into favorable conditions for observing hole growth kinetics (HGK) for the formation of ZPHs with little or no formation of the PSBH. A representative comparison of the burn kinetics for each of the two cell lines is presented in Figure 5.4. Fits obtained from the data are superimposed to show the agreement of fits with actual data. It is apparent from the figure that the carcinoma cells burn to a deeper fractional hole depth with respect to the normal cells in the same amount of time for the same fluence. Experimentally obtained NPHB kinetics curves were fit using [40]

$$D(\omega_B,t) = \int d\lambda f(\lambda) \int d\alpha \sin\alpha \cos^2\alpha e^{-P\sigma_{LT}^{P}\phi(\lambda)\cos^2(\alpha)t} \qquad (5.1)$$

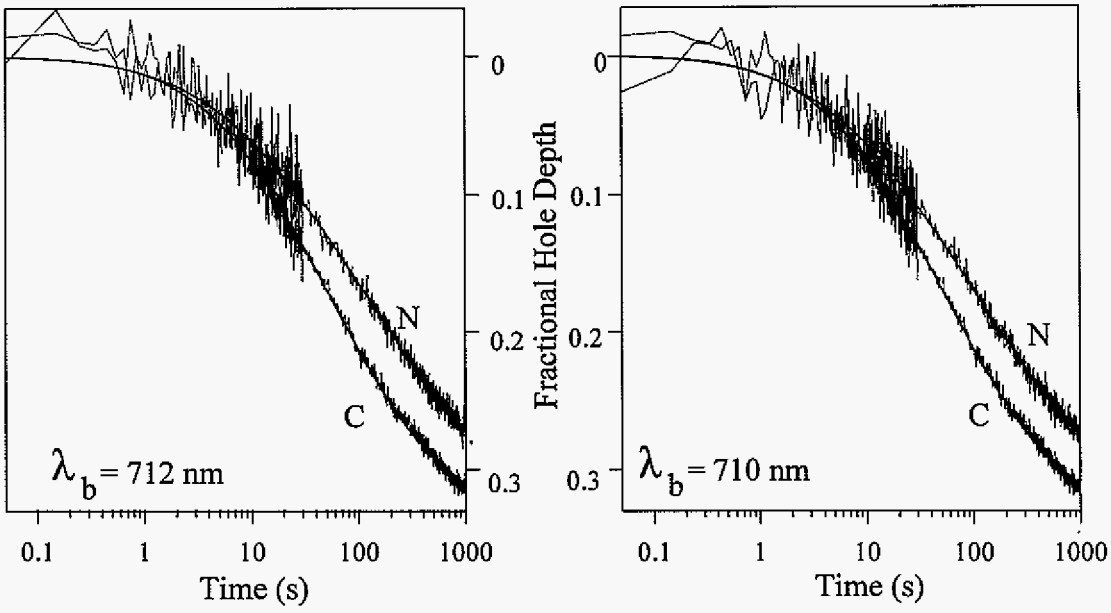

Figure 5.4. Representative hole growth kinetics (HGK) curves for each cell type, with (N) the OSE(tsT)-14 normal cells and (C) the OV167 carcinoma cells. Fits are superimposed to show agreement of theoretical fit to actual data.

which is the fractional hole depth following a burn for time t at a burn frequency ω_B. P is the total photon flux with units of number of photons cm^{-2} s^{-1}, α is the angle between the laser polarization and the transition dipole of the laser, and $f(\lambda)$ is the Gaussian distribution function of tunneling parameter λ centered at λ_0 with variance σ_λ. The parameter σ_{LT}^{p} is the peak absorption cross section (2.8×10^{-12} cm^2). The NPHB quantum yield, ϕ, is given by

$$\phi(\lambda) = \frac{\Omega \exp(-2\lambda)}{\Omega \exp(-2\lambda) + \tau^{-1}} = \frac{R_{HB}}{R_{HB} + R_{Relax}} \approx \frac{R_{HB}}{R_{Relax}} << 1 \qquad (5.2)$$

where $\Omega\exp(-2\lambda)$ represents the phonon-assisted tunneling relaxation rate, Ω is set to 7.6×10^{12} s^{-1} [41] and τ, the fluorescence lifetime, was determined to be 1.8 ns at 77 K. A quantum mechanical expression for Ω can be found in ref. [42]. Note that the parameters λ and α each cause a distribution of hole burning rates that leads to dispersive kinetics, and it has been shown [40] that the λ distribution is the dominant factor. When fitting kinetics data, it is necessary to know the Huang-Rhys (S) factor, which determines the maximum depth of the saturated ZPH. For the data fits presented, S was set equal to 1.1, based on independent measurements of saturated hole depths (data not shown). For the data presented in Table 5.1, several different sets of samples were generated, with the values for λ_o and σ_λ generated by fits with eq. 1. Figure 5.5 presents the case where an attempt was made to account for the observed shift in fluorescence excitation profiles. By comparing burn wavelengths that are offset by about 2 nm, we have attempted to determine if the observed shift would alter the hole growth kinetics, so that both samples would display similar hole growth rates. The HGK curve for the normal

Table 5.1. Dispersive Hole Growth Kinetics Fit Parameters

λ_B (nm)	OV167 $\bar{\lambda}_o$	OSE(tsT)-14 $\bar{\lambda}_o$	OV167 $\bar{\sigma}_\lambda$	OSE(tsT)-14 $\bar{\sigma}_\lambda$
712	7.84 ± 0.10	8.36 ± 0.10	0.68 ± 0.10	1.15 ± 0.08
710	7.78 ± 0.13	8.36 ± 0.12	0.85 ± 0.10	1.10 ± 0.09
707	7.80 ± 0.11	8.41 ± 0.10	1.07 ± 0.10	1.19 ± 0.08
705	7.76 ± 0.12	8.61 ± 0.12	1.05 ± 0.10	1.22 ± 0.10

cells was burned at 710 nm, and the carcinoma line was burned at 712 nm. However, as can be seen in the curves, burn rate differences are still observed for each cell line.

5.4.3. Application of Stark Fields

Representative results for the application of external electric fields ($\mathbf{E}_{St}$) to MF680 in a water-glycerol mixture (1:1) and in OV167 cells are presented in Figure 5.6. From the figure, typical signal to noise ratios can be observed, exhibiting an unfortunate drawback of MF680: the observed decrease in fluorescence quantum efficiency once the molecule is located inside the mitochondrial membrane [43], however this did not present an insurmountable handicap. Only one of the cell lines is displayed, as data for both cell lines appears similar at the resolution shown. Superimposed on the curves are representative Lorentzian fits to the data, exhibiting the general agreement between the two. Using the theory of Kador et al. [44] and the ZPH fits, ZPH full widths at half maximum (Γ) are plotted against $\mathbf{E}_{St}$ according to the following relation:

$$\Gamma(F) = 2(\gamma' + \gamma_d')(1 + F^2)^{1/2} \tag{5.3}$$

where γ' is the homogeneous width of the zero-phonon line and γ_d' is the additional

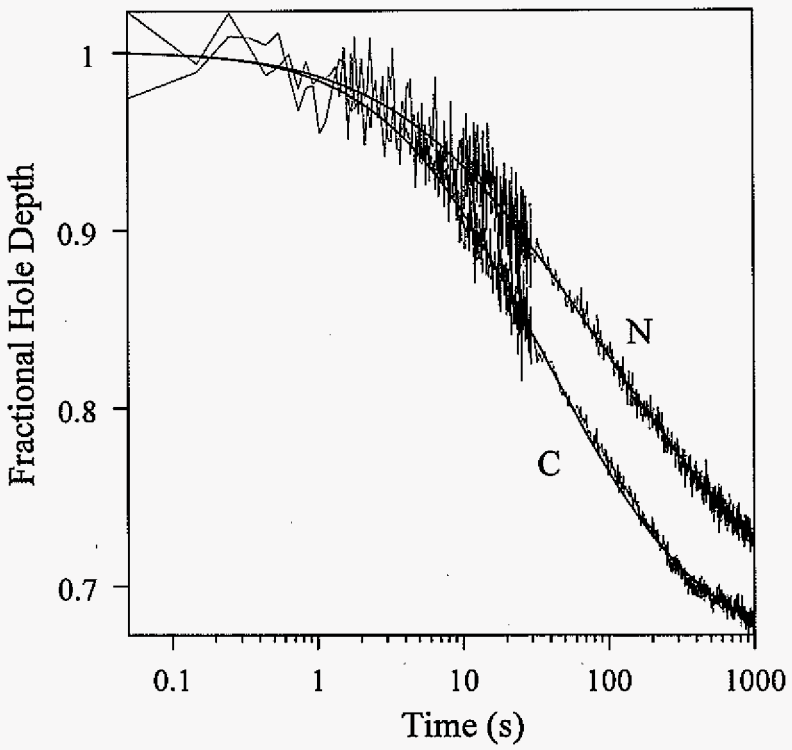

Figure 5.5. Hole growth kinetics (HGK) curves for each cell type, with (N) the OSE(tsT)-14 normal cells and (C) the OV167 carcinoma cells. Fits are superposed to show agreement of theoretical fit to actual data. The curve for C was burned at 712 nm, and the curve for N was burned at 710 nm, in an attempt to account for burn differences based on the observed fluorescence excitation shift between the two cell lines.

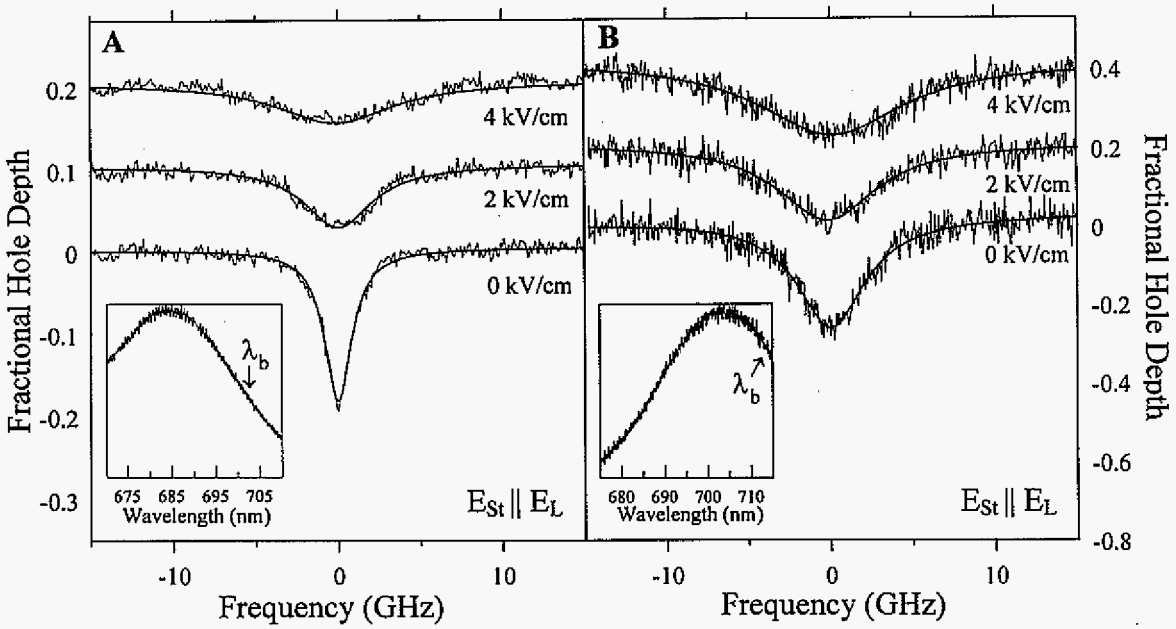

Figure 5.6. Representative Stark broadening curves for MF680 in 1:1 water:glycerol (A) and in OSE(tsT)-14 normal cells (B). The inset in both A and B shows the fluorescence excitation profile and the burn location. Only parallel orientations of E_{St} to E_L is shown, as splitting occurred in the perpendicular orientation of A and observed broadening in B was similar to the parallel orientation.

width associated with such artifacts as saturation broadening. F is defined by:

$$F = \frac{2f\Delta\mu E_{St}}{\hbar\left(\gamma' + \gamma_d'\right)} \tag{5.4}$$

where the denominator sum $\left(\gamma' + \gamma_d'\right)$ is the width at zero field. The parameter f is the local field correction factor and is taken to be a scalar. Most importantly, eq. 3 provides a relation by which $\Delta\mu$, the change in permanent molecular dipole moment, can be determined in relation to ZPH width at an applied $\mathbf{E}_{St}$. This parameter can be written as $\Delta\mu = \Delta\mu_{mol} + \Delta\mu_{ind}$, where $\Delta\mu_{mol}$ is the intrinsic molecular dipole moment change and $\Delta\mu_{ind}$ is the matrix-induced dipole moment change. In cases where $\Delta\mu_{mol} >> \Delta\mu_{ind}$, splitting of holes can be observed due to the angle between $\Delta\mu_{mol}$ and the laser polarization, $\mathbf{E}_L$, being well defined (the photoselection phenomenon). In the present case, however, only broadening of holes is observed, an observation when $\Delta\mu_{ind} >> \Delta\mu_{mol}$, due to the randomness of orientations of $\Delta\mu_{ind}$ relative to $\mathbf{E}_{St}$ and D, the transition dipole vector. Further discussions of the significance of dipole moment measurements with regard to cellular ultrastructure will be given later. In Figure 5.7, the solid curves are representative theoretical fits to data using eq. 5.3 illustrating the dependence of hole width on $\mathbf{E}_{St}$. It is noteworthy that eq. 5.3 has been simplified considerably by identifying $F \leq 3.5$, which is valid for our experiments. Also, only the linear Stark effect is observed in this case, which is valid when the internal electric field surrounding the chromophore is considered to be much larger than $\mathbf{E}_{St}$ [11].

Measurements of $\Delta\mu$ for MF680 in several types of samples are presented in Table 5.2. Contained within the table are some previously reported values for the sake of comparison. The $\Delta\mu$ values for MF680 in a 1:1 mixture of water-glycerol

exhibits values extremely close to those for the dye in OSE(tsT)-14 cells. Only one orientation of $\mathbf{E}_L$ to $\mathbf{E}_{St}$ is presented (the parallel case), as the case in which $\mathbf{E}_L \perp \mathbf{E}_{St}$ exhibited Stark splitting. Splitting was not observed in either cell line, however, a result of inter-cellular dye molecule orientations being random (vide infra).

Table 5.2. Permanent dipole moment changes for MF680 and APT in aqueous and in *in vivo*

Cell Line	$f\Delta\mu$ (D)	Laser Polarization	λ_b (nm)
htOSE(tsT)-14	1.64 ± 0.24[a]	$\mathbf{E}_{St} \perp \mathbf{E}_L$	711.8
OV167	2.47 ± 0.10[a]		711.8
ltOSE(tsT)-14	2.72 ± 0.20		711.8
htOSE(tsT)-14	1.68 ± 0.32[a]	$\mathbf{E}_{St} \parallel \mathbf{E}_L$	711.6
OV167	2.51 ± 0.12[a]		711.6
ltOSE(tsT)-14	2.86 ± 0.22		711.6
Water-glycerol	1.65 ± 0.05		704.0
MCF-7	0.20 ± 0.01[b]	$\mathbf{E}_{St} \parallel \mathbf{E}_L$	678.0
MCF-10F	0.27 ± 0.01[b]		677.5
MCF-7	0.21 ± 0.01[b]	$\mathbf{E}_{St} \perp \mathbf{E}_L$	677.5
MCF-10F	0.22 ± 0.01[b]		678.0

[a] From Ref. [30]; [b] From Ref. [1]

Notably, the $\Delta\mu$ values presented here roughly show a 1.5-fold increase in the carcinoma cells over the normal analogs. OSE(tsT)-14 cells were also stained without high temperature incubation treatment to test for any effect the SV40 virus might have on the cell. The normal analogs with the SV40 antigen still present (ltOSE(tsT)-14) exhibit an intriguing result, in that the measured $\Delta\mu$ changes roughly align with those of the OV167 carcinoma line. This is explained considering the mechanism of SV40 transfection: the still present antigen preferentially binds to the p53, pRb, and p300 proteins, all of which are involved in cell proliferation control [33,45].

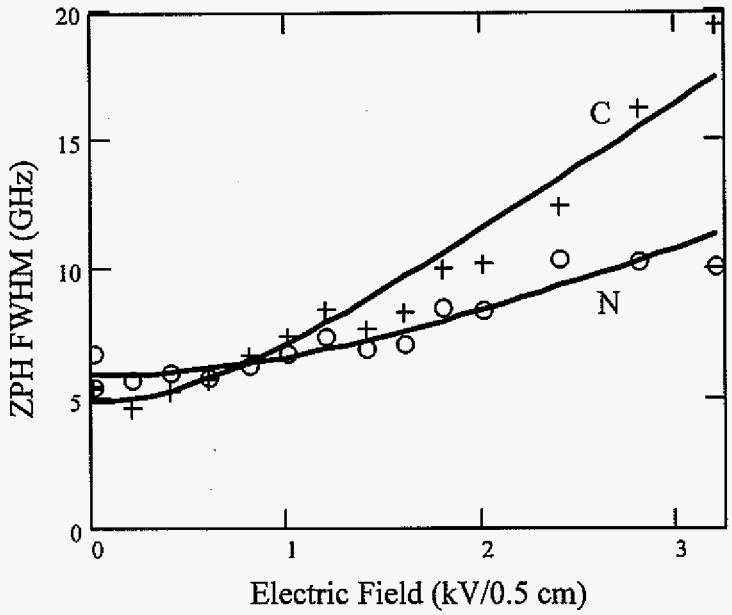

Figure 5.7. Representative fits of Stark effect broadening to the Kador equation. N represents the OSE(tsT)-14 normal cell line, and C the OV167 carcinoma cell line.

5.4.4. Measuring $\Delta\psi_m$

Measurements to determine $\Delta\psi_m$ for each cell line were performed using flow cytometry. The procedure for measuring $\Delta\psi_m$ documented by Rottenburg and Wu [37] was utilized based on staining similarities in the present situation. This study also utilized a lipophilic, cationic dye, and was performed using flow cytometry. This was deemed a favorable method of measurement, as large numbers (10^4-10^5) of cells were analyzed, thus dampening effects of inhomogeneities in cell phases. Membrane potential values were measured using the equation:

$$\Delta\psi_m = \log(F / F_{CCCP}) / 0.0031 \text{ mV} \qquad (5.5)$$

where F and F_{CCCP} are the initial fluorescence intensity after incubation with MF680 only and the fluorescence measurement after incubating 20 minutes with 0.5 mM CCCP, respectively. The value of 0.0031 mV was determined experimentally by manipulating $\Delta\psi_m$ values with KCl concentrations (0.1, 1, 30, 60, 120, 240 mM). In the presence of high concentrations of valinomycin (3μM), increasing the K^+ concentration results in increased cytosolic K^+ and therefore collapses $\Delta\psi_m$. The resulting plot of F/F_{CCCP} values versus [KCl] produced a line with slope of .0031. The values measured for each cell line - carcinoma, temperature treated, and non-temperature treated cells - were measured to be 168 mV, 143 mV, and 149 mV, respectively, with deviation of about 5% of these values for each cell type. Only slightly elevated values of $\Delta\psi_m$ were measured in the carcinoma cell line. The membrane potential ratio of carcinoma to normal did not approach the 1.5-fold increase previously reported [46-49] for different carcinoma cell lines.

5.5. Discussion

Differences in the fluorescence excitation spectrum, hole growth kinetics, and hole-burning Stark shifts are clearly seen in the data presented, demonstrating that NPHB has the capability to resolve differences between the model cell lines used. The success of these findings is based in large part on the ability of the probe dye MF680 to locate specifically in *in situ* cellular mitochondria which are documented to have undergone ultrastructural alterations due to carcinogenesis.

From the data presented in Fig. 5.3, it is evident that the MF680 probe molecule is located in a non-aqueous environment. MF680 excitation profiles show a large red shift in the dye located in either cell line relative to the dye being located in water (HGW or a glycerol-water glass). The dye molecule is composed mainly of aromatic hydrocarbons and is cationic, thus preferentially locates in the lipid-based, negatively charged mitochondrial matrix. Although there is a shift in the fluorescence excitation profile between the two cell lines, the spectral shift is small relative to the profile width, and would not be accurate as a diagnostic due to uncertainties in measurements that would accompany large-scale sampling techniques. Furthermore, these shifts would not be evident in heterogeneous mixtures of samples, whereas hole-burning characterization has the potential for resolving differences in such samples (vide infra).

Interpretation of the above results concerning HGK provide intriguing insight into model cell line ultrastructures. Recalling that the λ-distribution is dominant in eq. 5.1, fitting kinetics curves yields σ_λ, a parameter which directly reflects the order of an amorphous matrix (structural heterogeneity). For the two types of cell lines

presented, the carcinoma cells display lower values for λ_o (the mean distribution of tunneling rates) and σ_λ (distribution variance). Notably, the σ_λ value is directly related to the degree of structural heterogeneity of a guest suspended in a structurally disordered host, and in the present case is interpreted to mean that carcinoma mitochondrial ultrastructures are more ordered relative to the normal cell line. Reasoning behind this observation in HGK differences is limited to speculation at this point, but may be due to structural differences noticed in confocal microscopy studies. From these studies, it was observed that the OV167 cell line exhibits small, more cobblestone-like shapes for the majority of the cells. Experiments were also conducted with higher magnification (100×) than presented in Fig. 5.2 (60×), with the further finding that the mitochondria observed within the OV167 cells are shorter, more highly aggregated structures relative to the OSE(tsT)-14 normal cells, possibly due to the rapid proliferation rate of the carcinoma cell line. It is conceivable that these smaller structures are more uniform in ultrastructure as a consequence of the increased rate of cellular reproduction, and this would dictate that long networks of mitochondria were not formed within the time frame used in these experiments. Such networks were observed in the normal cells, as these cells had a tendency to grow into long structures, similar in shape to fibroblasts.

A point of importance from this data is the consideration of the ease with which dispersive HGK can be measured. The only necessity is the measurement of fluorescence intensity (vs. time) with application of a narrow band laser at cryogenic temperatures, which can potentially be accomplished with an inexpensive diode laser. Further, detection methods could be varied as well, and work to develop a

detection system based on optical microscopy (with CCD detection) is proceeding [50], with potential for use in analysis of cell smears and tissue samples. ZPH FWHMs created by the aforementioned kinetics presented only slight differences between the two cell lines and therefore could not be used for an accurate assessment of differences (data not presented), thus negating the necessity for scanning resultant holes.

A final point of consideration regarding HGK is the observation that the σ_λ values for the carcinoma cells show a measurable burn frequency dependence (Fig. 5.6) for fitting parameters while the normal cells do not. This is most likely due to differences in the fluorescence excitation profile peaks observed between the two types of cells. For the shorter wavelength burns, the burning occurs at or very near the peak of the absorption, especially in the case of the OV167 cells. Accurate measurements of hole-burning parameters should always be performed on the red (lower-energy) side of absorption bands [18], however. As burning wavelengths approach the absorption peak, the likelihood increases that vibronic hole burning will occur, which will interfere with accurate measurements, and which is the most likely source of the wavelength dependence observed.

The Stark values presented in Table 5.1 show further evidence of unique interactions between the MF680 dye and the surrounding cellular matrix for each cell line. Our previous interpretation [30] of this data concluded that the 1.5-fold increase in permanent dipole moment changes for carcinoma cells were consistent with the observations of others who have measured $\Delta\psi_m$ to be ~1.5-fold higher in cancerous cells, and that this was the source of the increase for the $f\Delta\mu$ values

presented. Flow cytometric measurements were undertaken to verify this conclusion, however the data is not consistent with such a large difference. Although the procedure of ref. [37] to measure $\Delta\psi_m$ was followed as closely as possible, present measurements differed in that MF680 was utilized for staining the cells, whereas in ref. [37] the fluorescent probe used was 3, 3'-dihexylcarbocyanine iodide ($DiOC_6$). MF680 was used to be consistent with the hole-burning and Stark broadening results presented here, and because the similarities between MF680 and $DiOC_6$ (both are lipophilic, carbocationic dyes) seemed to justify its suitability for use in determining $\Delta\psi_m$. However, there may be unforeseen underlying factors which hindered our measurement of the true membrane potential, such as differences in binding affinities between the two dye molecules and the use of different cells (extracted spleen lymphocytes) by Rottenberg. Because of these uncertainties, the results regarding the influence of $\Delta\psi_m$ on Stark effect measurements remain inconclusive, and further analysis for accurate measurements of $\Delta\psi_m$ are to be performed, albeit with the $DiOC_6$ dye.

For reference, Stark data from the MCF7 and MCF10F cell lines are also presented in Table 5.1. With these cell lines, it was argued that the slight difference seen in the dipole moment changes between the MCF10F and MCF7 line for the case of $\mathbf{E}_{St} \parallel \mathbf{E}_L$ was attributable to $\Delta\mu_{ind}$ not being completely random, and that some degree of ordering existed within the MCF10F cells that did not exist within the cancer cells. For the present case, however, neither orientation of $\mathbf{E}_{St}$ with $\mathbf{E}_L$ dominates, indicating that interactions of the dipole moment with the laser are indeed due to random orientations of the dye in the cellular matrix.

Finally, an $f\Delta\mu$ comparison between the htOSE(tsT)-14 and that of water-glycerol exhibits no difference within experimental uncertainty. These cells were found to be viable after freezing, staining, and re-suspending in growth medium, and also exhibited the extreme fluorescence excitation profile red shift relative to MF680 in water-glycerol, so that cell death can be ruled out as a possible explanation for this observation.

5.6. Acknowledgements

Ames Laboratory is operated for the U. S. Department of Energy by Iowa State University under Contract W-7405-Eng-82. This work was supported by the Office of Health and Environmental Research. T. Reinot was supported by the Solid State Chemistry and Polymers Program of the National Science Foundation (Grant DMR-9908714).

Refereneces

1. Milanovich, N.; Raetsep, M.; Reinot, T.; Hayes, J. M.; Small, G. J., *J. Phys. Chem. B* **1998**, *102*, 4265.
2. Milanovich, N.; Reinot, T.; Hayes, J. M.; Small, G. J., *Biophys J* **1998**, *74*, 2680.
3. Van den Berg, R.; Voelker, S., *Chem. Phys.* **1988**, *128*, 257.
4. Reinot, T.; Hayes, J. M.; Small, G. J., *J. Chem. Phys.* **1997**, *106*, 457.
5. Reinot, T.; Kim, W. H.; Hayes, J. M.; Small, G. J., *J. Opt. Soc. Am. B* **1997**, *14*, 602.
6. Reinot, T.; Hayes, J. M.; Small, G. J., *J. Chem. Phys.* **1999**, *110*, 4820.
7. Silbey, R. J.; Koedijk, J. M. A.; Völker, S., *J. Chem. Phys.* **1996**, *105*, 901.

8. Walsh, C. A.; Berg, M.; Narasimhan, L. R.; Fayer, M. D., *J. Chem. Phys.* **1987**, *86*, 77.

9. Hayes, J. M.; Reinot, T.; Small, G. J., *Chem. Phys. Lett.* **1999**, *312*, 362.

10. Kador, L.; Personov, R.; Richter, W.; Sesselmann, T.; Haarer, D., *Polym. J. (Tokyo)* **1987**, *19*, 61.

11. Rätsep, M.; Wu, H. M.; Hayes, J. M.; Blankenship, R. E.; Cogdell, R. J.; Small, G. J., *J. Phys. Chem. B* **1998**, *102*, 4035.

12. Rätsep, M.; Wu, H. M.; Hayes, J. M.; Small, G. J., *Spectrochim. Acta, Part A* **1998**, *54A*, 1279.

13. Rätsep, M.; Johnson, T. W.; Chitnis, P. R.; Small, G. J., *J. Phys. Chem. B* **2000**, *104*, 836.

14. Wu, H. M.; Rätsep, M.; Young, C. S.; Jankowiak, R.; Blankenship, R. E.; Small, G. J., *Biophys. J.* **2000**, *79*, 1561.

15. Zazubovich, V.; Matsuzaki, S.; Johnson, T. W.; Hayes, J. M.; Chitnis, P. R.; Small, G. J., *Chem. Phys.* **2002**, *275*, 47.

16. Moerner, W. E., Ed.; *Persistent spectral hole-burning: science and applications*, Springer-Verlag: Berlin, Germany, **1988**; Vol. 44.

17. Reinot, T.; Hayes, J. M.; Small, G. J., *Photonics Science News* **2000**, *6*, 83.

18. Jankowiak, R.; Hayes, J. M.; Small, G. J., *Chem. Rev.* **1993**, *93*, 1471.

19. Jankowiak, R. Fundamental aspects of fluorescence line-narrowing spectrscopy. In *Shpol'skii spectroscopy and other site-selection methods*; Gooijer, C., Ariese, F., Hofstraat, J. W., Eds.; John Wilet & Sons: New York, N.Y., **2000**; pp 235.

20. Hayes, J. M.; Small, G. J., *Chem. Phys.* **1978**, *27*, 151.

21. Hayes, J. M.; Stout, R. P.; Small, G. J., *J. Chem. Phys.* **1981**, *74*, 4266.

22. Shu, L.; Small, G. J., *J. Opt. Soc. Am. B* **1992**, *9*, 724.

23. Kim, W. H.; Reinot, T.; Hayes, J. M.; Small, G. J., *J. Phys. Chem.* **1995**, *99*, 7300.

24. Reinot, T.; Zazubovich, V.; Hayes, J. M.; Small, G. J., *J. Phys. Chem. B* **2001**, *105*, 5083.

25. Milanovich, N. Application of Spectral Hole Burning to the Study of In Vitro Cellular Systems. Ph. D., Iowa State University, **1999**.

26. Maines-Bandiera, S. L.; Kruk, P. A.; Auersperg, N., *Am. J. Obstet. Gynecol.* **1992**, *167*, 729.

27. Nitta, M.; Katabuchi, H.; Ohtake, H.; Tashiro, H.; Yamaizumi, M.; Okamura, H., *Gynecol. Oncol.* **2001**, *81*, 10.

28. Chou, J. Y., *Mol Endocrinol* **1989**, *3*, 1511.

29. Jenkins, N., Ed.; *Animal cell biotechnology : methods and protocols*, Humana Press: Totowa, N.J., **1999**; Vol. 8.

30. Walsh, R. J.; Reinot, T. R.; Hayes, J. M.; Kalli, K. R.; Hartmann, L. C.; Small, G. J., *J. Lumin.* **2002**, *In Press*.

31. Djaldetti, M., *Acta Haemat.* **1982**, *68*, 241.

32. Eapen, C. E.; Madesh, M.; Balasubramanian, K. A.; Pulimood, A.; Mathan, M.; Ramakrishna, B. S., *Scand. J. Gastroenterol.* **1998**, *33*, 975.

33. Jha, K. K., Banga, S., Palejwala, V., Ozer, H. L., *Exp. Cell. Res.* **1998**, *245*, 1.

34. Conover, C. A.; Hartmann, L. C.; Bradley, S.; Stalboerger, P.; Klee, G. G.; Kalli, K. R.; Jenkins, R. B., *Exp. Cell. Res.* **1998**, *238*, 439.

35. Kalli, K. R.; Chen, B.-K.; Bale, L. K.; Gernard, E.; Overgaard, M. T.; Oxvig, C.; Conover, C. A., Manuscript in progress.

36. Scully, R. E., *Am. J. Pathol.* **1977**, *87*, 686.

37. Rottenberg, H.; Shaolong, W., *Biochim. Biophys. Acta* **1998**, *1404*, 393.

38. Reinot, T.; Small, G. J., *J. Chem. Phys.* **2001**, *114*, 9105.

39. Chen, L. B.; Summerhayes, I. C.; Johnson, L. V.; Walsh, M. L.; Bernal, S. D.; Lampidis, T. J., *Cold Spring Harb. Symp. Quant. Biol.* **1982**, *46 Pt 1*, 141.

40. Reinot, T.; Small, G. J., *J. Chem. Phys.* **2000**, *113*, 10207.

41. Kim, W. H.; Reinot, T.; Hayes, J. M.; Small, G. J., *J. Chem. Phys.* **1996**, *104*, 6415.

42. Kenney, M. J.; Jankowiak, R.; Small, G. J., *Chem. Phys.* **1990**, *146*, 47.

43. Sakanoue, J.; Ichikawa, K.; Nomura, Y.; Tamura, M., *J. Biochem. (Tokyo)* **1997**, *121*, 29.

44. Kador, L.; Haarer, D.; Personov, R., *J. Chem. Phys.* **1987**, *86*, 5300.

45. Ali, S. H.; DeCaprio, J. A., *Semin. Cancer. Biol.* **2001**, *11*, 15.

46. Modica-Napolitano, J. S.; Aprille, J. R., *Cancer Res.* **1987**, *47*, 4361.

47. Summerhayes, I. C.; Lampidis, T. J.; Bernal, S. D.; Nadakavukaren, J. J.; Nadakavukaren, K. K.; Shepherd, E. L.; Chen, L. B., *Proc. Natl. Acad. Sci. USA* **1982**, *79*, 5292.

48. Davis, S.; Weiss, M. J.; Wong, J. R.; Lampidis, T. J.; Chen, L. B., *J. Biol. Chem.* **1985**, *260*, 13844.

49. Dairkee, S. H.; Hackett, A. J., *Breast Cancer Res. Treat.* **1991**, *18*, 57.

50. Walsh, R. J., Nonphotochemical hole-burning imaging studies of *in vitro* carcinoma and normal cells utilizing a mitochondrial specific dye, Ph. D., Iowa State University, **2002**.

CHAPTER 6. CONCLUSION

This thesis has shown that Nonphotochemical Hole Burning (NPHB) Imaging for discerning differences in cellular ultrastructures due to cancer development is possible. The means by which this has been accomplished have involved culturing carcinoma and temperature sensitive SV40 transfected normal analog cell lines of ovarian surface epithelial origin, and the application of a fluorescent mitochondrial specific dye (Molecular Probes MitoFluor Far Red 680 (MF680), commonly known as rhodamine 800) that exhibits efficient NPHB. Upon incubating cell cultures with the probe dye briefly and subsequently freezing the culture, differences were found with respect to dispersive hole-growth kinetics parameters, with the surprising finding that the carcinoma cells exhibit a difference in structural heterogeneity suggestive of the dye probe being oriented with a higher degree of order relative to the normal cells. Differences were also found in the probe dye molecules response to applied external electric fields, with the carcinoma cells exhibiting a more pronounced change (1.5-fold increase) in permanent dipole moment change relative to the normal analogs which have been temperature treated to denature the SV40 antigen. A final interesting observation is the similarity in values of permanent dipole moment change measured between carcinoma cells and non-temperature treated normal analogs, where the SV40 antigen is still present and functioning. As the SV40 antigen interacts with many of the same proteins found to be errant in cancer cells, this finding was a positive corroboration.

Results are also briefly presented in Appendix A showing the possibility for NPHB to be applied to cells cultured on coverslip glass, mounted in a cryostat, and

subsequently hole-burned with the fluorescence excitation signal collected with a microscope objective and sent to a CCD camera for recording. This system has potential implications for being used with smears of cells, however minor difficulties still need to be addressed in the system (see Appendix A).

Future studies based on this system could broaden into several areas, such as testing for NPHB agreement in tissue samples (a study is currently in development) as well as testing alternative dye molecules, either continuing to target mitochondria or choosing an alternative organelle. The list of candidates is long, and could include targeting the structural foundations of cells such as the cytoskeleton, microfilaments, or microtubules. Certain factors must always be considered, however, the most notable of which are the possible existence of anomalies created due to carcinogenesis, the necessity for a fluorophore probe to bind intimately with the target structure, and the necessity for the fluorophore to hole-burn efficiently. In many respects, mitochondria present the ultimate in encompassing all of these requirements, as well as providing further NPHB application in association with other disease detection such as Alzheimer's, Parkinson's, and diabetes to name a few of the major afflictions which have been implicated to arise due in part to mitochondrial abnormalities.

It is hoped that the research advanced in this thesis may someday prove useful in the development of early diagnostics for disease detection. In the case of cancer, this has been shown to be an instrumental asset in treatment success, and this may very well prove to be the case with the other diseases mentioned.

ACKNOWLEDGEMENTS

This work was performed at Ames Laboratory under Contract No. W-7405-Eng-82 with the U.S. Department of Energy. The United States government has assigned the DOE Report number IS-T 1967 to this thesis.

Although it is not possible to convey my gratitude to all those who have had an impact on my graduate career, I would like to give a brief mention of those which are most significant. First, I would like to mention my gratitude to members of the group of the late Therese Cotton, who passed away on October 26, 1998. Thank you for all you did for me, Dr. Cotton, Dr. George Chumanov, Dr. Morgan Sibbald, and Dr. Albert Avila. I am sure we all share the same thought: Dr. Cotton's passing came far too early.

I am also forever indebted to Dr. Gerald Small, who accepted me into his group after Dr. Cotton's passing with little knowledge of my abilities. Fortunately, Dr. Small has shown extreme patience in working with me as I struggled in getting worthwhile results. I only hope he is as proud of the outcome as I. Of course, none of this work would be possible without the additional helpful guidance of Dr. John Hayes, Dr. Ryszard Jankowiak, and the master of the laboratory Dr. Tonu Reinot, who will not miss hearing the phrase, "Tonu, the laser's on the fritz again!" or any of the other numerous phrases that make him visibly shudder. Other group members that have been instrumental in helping me are Dr. Nebojsa "Nick" Milanovich, Dr. Kenneth Roberts, Dr. Walter Zazubovich, Sathoshi Matsuzaki, and the "Doctors in waiting" Nenad Grubor and Nhan Dang. Outside of the chemistry department, I must acknowledge the help of Dr. Paul Kapke and Dr. Donhui Cheng, both of whom

were extremely generous with their time in helping to explain the many aspects of cell biology, cell culture, and flow cytometry. Dr. Robert Doyle was instrumental in assisting with confocal microscopy studies, and I am truly grateful for his help.

Personal friendships have also been instrumental in my success, and I must thank both Dr. Tony Layson and (soon to be Dr.) Brett Simpson for the numerous dog-sitting weekends and for great golfing and imbibing sessions, among other activities. I will certainly miss having you guys around, and not just to watch the dogs! I also would like thank my "Minnesota Crew" gang of friends (Mike, Beth, Joe, Christa, Pat, Gary, Cathi, Joel, Mick, and Mike), for their annual visits and the fun that ensued, and to Mark and Andy for stopping by as well.

Lastly, the true secret behind my source of strength, determination and ability to continue, no matter how bleak things ever looked, is my best friend and spouse, Crista. Without a doubt, she has been the greatest asset I could ever have in achieving my goals, and never gave up believing in me even if I had. For this, I am forever indebted and owe more gratitude than I can ever express!

APPENDIX A. SINGLE CELL HOLE-BURNING IMAGING

One of the original objectives set forth for the work presented in this thesis was to investigate the possibility of NPHB comparisons at the scale of individual cells. By comparison, the previously presented cellular NPHB studies (chapters 4, 5) were performed utilizing samples with cell populations ranging from 5×10^5 to 2×10^6. Only recently has the original objective been met, and the preliminary results are presented in this appendix to further elaborate the possibilities of NPHB in cellular anomaly detection.

A system has been devised as depicted in Figure A.1. Cells are cultured on a poly-L-lysine coated coverslip glass, which is then suspended over a 25X reflecting microscope objective and illuminated by a fiber optic, all of which is housed in a cryostat. The subsequent fluorescence signal is collected by the microscope objective, redirected out of the cryostat via a prism, and the signal is detected by a liquid nitrogen cooled charge coupled device (CCD) camera.

In order to minimize alignment errors made by inserting and removing samples, a method by which both cell types could be grown on the same coverslip was developed. Rubber culture chambers were created with Sylgard 184 (Dow Corning, Midland MI). The rubber was cured in a 35 mm plastic petri dish, and subsequently cut to fit a square 18 mm coverslip. Culture wells were created with a cork borer, so that each line could be placed in an individual well with its respective medium. When the rubber is placed on glass, it forms a watertight seal, containing the cells and their growth medium. The rubber is autoclavable. Further, the sample

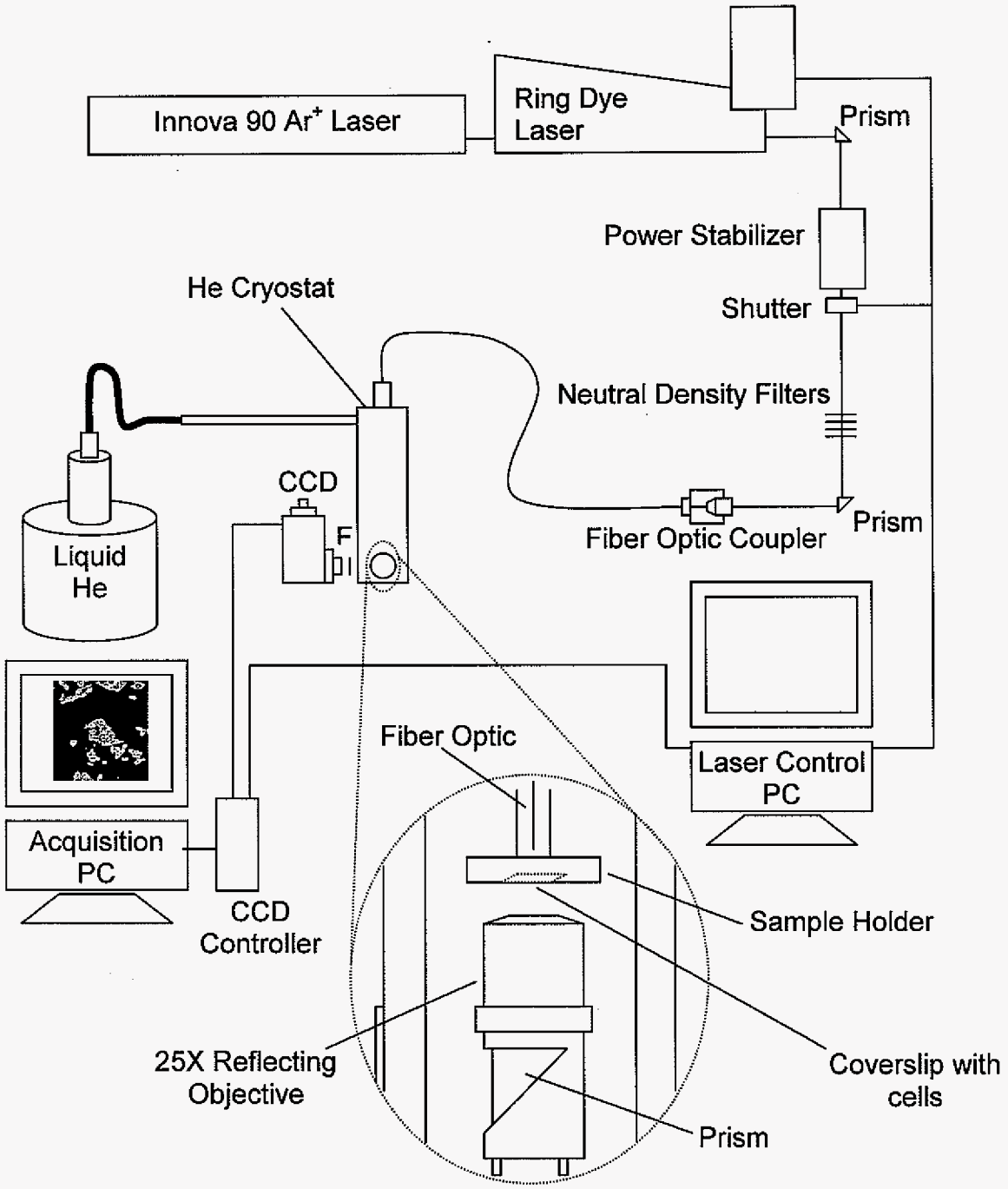

Figure A.1. Schematic for single cell hole burning. "F" refers to a low pass filter.

holder depicted in Fig. A.1. allows for x-, y-, and z-axis manipulation of the sample, and both cell lines could be maneuvered into the focal plane of the objective, although not concurrently. After a series of burns were performed on one cell line, the sample was warmed to 140 K before performing burns on the other cell line to erase resulting ZPHs and PSBHs.

Representative data collected by this method are presented in Figure A.2, with an image of numerous cells displaying the first of 900 total images taken at a rate of 1 s^{-1} presented in A.2.A. In A.2.B, an individual cell (corresponding to the cell contained in the white box in A.2.A) is tracked by frame number as it is exposed to 710 nm light at 6.8 K. For simplicity, the time used to collect each frame can be set equivalent to the frame number, corresponding to 1 s in the present case. However, this does not include the time taken to read and report the CCD chip, which is a significant time contribution. For a frame with 1 s exposure, 0.1 - 0.4 s of additional time is added by the read and report process, dependent on the size of the image frame (regions of the CCD chip can be ignored during data collection, thus the region of interest must be set the same for accurate comparisons). The data presented in this case has not been corrected for this additional time. However since all data presented here was collected under identical conditions, using identical frame sizes, this is not seen as a significant problem. The subsequent hole growth kinetics curve in A.2.C was generated by summing the pixels selected in the black box (of the first image in A.2.B.) in each frame. Experimental conditions are described in the figure, and color has been added artificially to show signal intensity gradients. Notably, there is a striking difference in the fluorescence signal of the cell

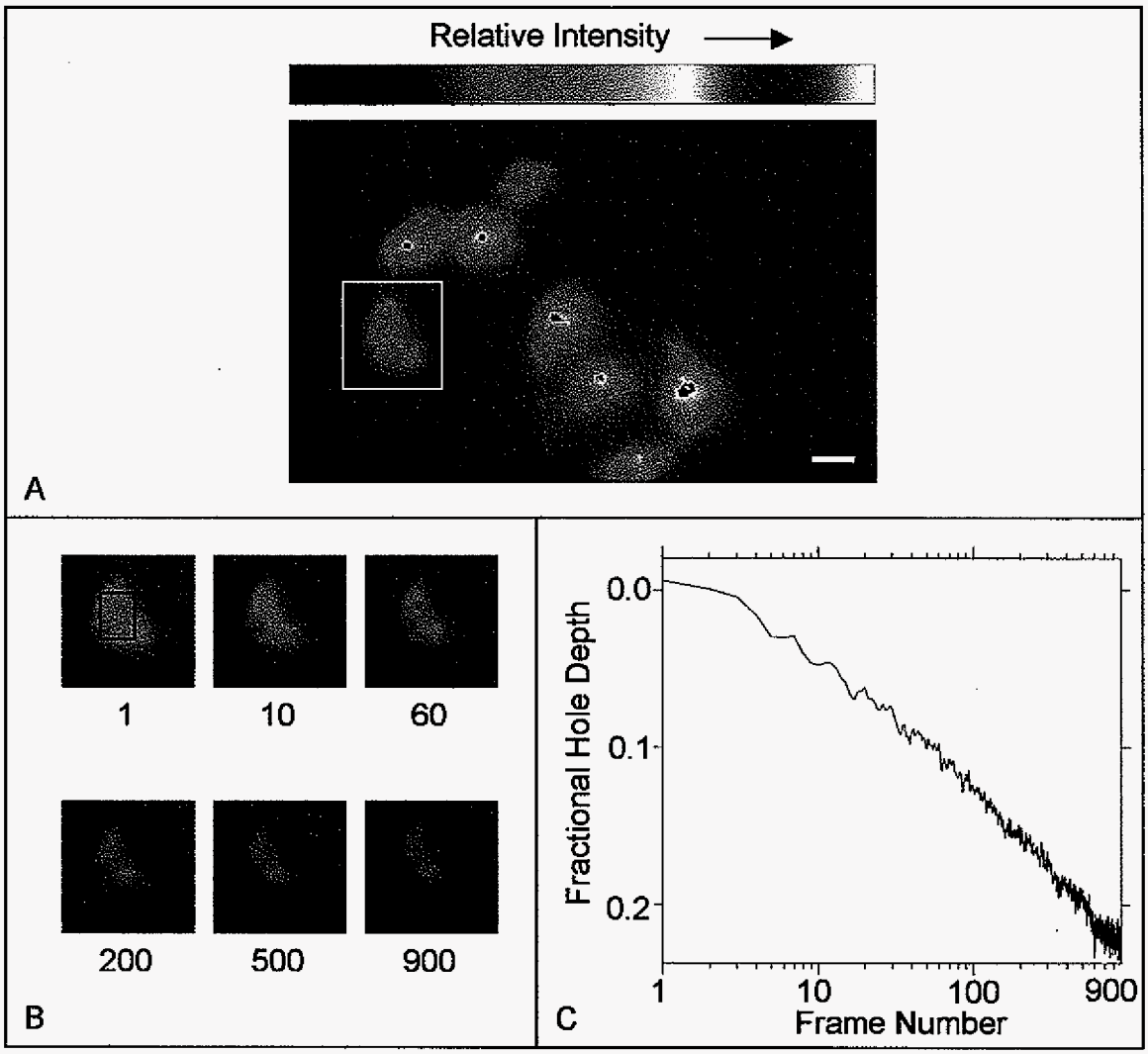

Figure A.2. Initial image (A) of OV167 cells stained with MF680 and burned at λ_B = 710 nm. The white bar represents approximately 20 μm. In B, individual images of the same cell at increasing frames are shown, exhibiting the burn over time. The cell shown corresponds to the white box shown in A. In C, a hole growth kinetics curve has been created from the individual cell shown in B by summing the pixels contained within the box over the cell image at 1 s and repeated for each of the 900 image frames. Other conditions: T = 6.8 K; total exposure time: 900 s; time for each exposure: 1 s; fluence: 1 mJ/cm^2.

in B as time progresses, as would be expected from the burning of MF680. 900 images were collected in this burn, with 1 s separating each frame.

Most significantly, the data presented in Figure A.3. shows that individual cells burn with the same characteristics as the bulk samples presented in chapters 4 and 5. Clearly, the carcinoma cell line burns at a faster average rate. An interesting observation of the data is exhibited in Fig. A.3.A, as individual cells are observed to burn at slightly different rates – indicative of heterogeneous burn rates between cells in the same line. As there appeared to be a slightly brighter background in the center of the image relative to the sides, this effect might be attributable to non-uniform illumination from the fiber optic. However, cells located at various positions in the image (not all cells are shown in Fig. A.2.A.) were analyzed for a possible position - burn rate dependence, with the finding that burn rates were not dependent on location, confirming heterogeneities in burning between individual cells.

In both Figures A.3.A and B, fits from the hole growth kinetics (HGK) equation given in chapter 5 (Equation (1)) are superposed with the data presented. Analysis of 16 individual cells HGK curves produced λ_o and σ_λ values for the OSE(tsT)-14 normal line of 9.2 ± 0.6 and 3.3 ± 0.5, respectively, and λ_o and σ_λ values for the OV167 carcinoma line of 8.8 ± 0.3 and 1.7 ± 0.2, respectively. Although these values are much larger than those presented in chapter 5 for each cell line, the trend is identical in that the carcinoma line exhibits lower σ_λ values, attributable to decreased structural heterogeneity in the carcinoma cell line. A possible reason for the σ_λ value increases is due to the loss of signal sampling sensitivity that is

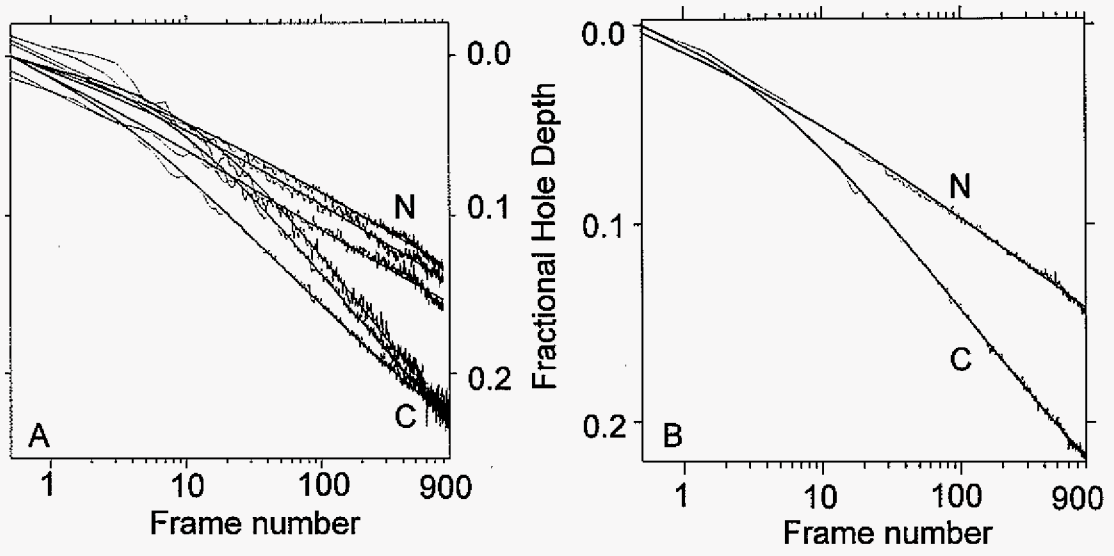

Figure A.3. Hole growth kinetics curves for each cell type, OSE(tsT)-14 normal (N) and OV167 carcinoma cells (C). In A, six curves of representative data with superposed theoretical fits (three from each cell type) are presented, exhibiting the degree of variance in burn rates within each cell line and in comparison between the cell lines. In B, 16 different cells for each cell line were analyzed and summed to produce each curve, with the resulting curves of data and superposed fits averaging the variance exhibited by individual cells.

possible with detection by photomultiplier tube. In the experiments conducted for chapters 4 and 5, HGK data points were collected every 0.1 s for the first 30 s, providing high resolution of 30-50% of the entire burn depth. After 30 s, data points were collected less frequently (1 s^{-1}). In the present case, however, images are collected about every second for the entire burn, thus limiting the resolution of the initial section of the burn, and in turn fitting of the curves suffers. Improvements to the system are being performed to overcome this problem, as described below. A second HGK comparison was also conducted by summing all of the kinetics curves (see Fig. A.3.B) and fitting the resulting curve, with the result of σ_λ = 3.1 and λ_o = 9.6 for the OSE(tsT)-14 cells and σ_λ = 1.7 and λ_o = 8.8 for the OV167 cells. These values are within the experimental uncertainty of the individual cell evaluations, exhibiting good agreement between the two methods used. A third comparison was conducted by summing the entire image frame, including background areas where no cells were present. As a result of fitting the curves generated, values of σ_λ = 3.7 and λ_o = 10.1 for the OSE(tsT)-14 cells and σ_λ = 2.3 and λ_o = 9.5 for the OV167 cells were produced. Based on this result, background contributions were determined to be a significant source of difference between the comparisons, and it is evident that this last method does not provide accurate determinations of cellular HGK. For all fits generated, the Huang-Rhys factor, S, was set at 1.1 and the laser intensity was set to 230 μW.

Most significantly, this data presents the finding that HGK for individual cells follow the same trends as those measured in bulk samples, effectively lowering the limit of detection to the single cell scale. Further, the data presents the possibility of

a very simple system by which HGK measurements for the determination of cellular anomalies could be made. The necessary equipment is inexpensive, requiring only a diode laser of a single wavelength, a cryostat and cooling system, and a method of detection. This system could be used for analysis of either individual cells or bulk tissues, exhibiting a large working range of sample size. However, testing to this point has been limited to cell cultures, and tissue experiments are to be completed in the future.

Limitations of the present system will also be addressed in future experiments. Namely, the aforementioned use of a fiber optic and resulting uncertainty in fluence uniformity will be addressed by eliminating the use of a fiber optic altogether. The system depicted in Figure A.1 is being modified to locate the microscope objective outside of the helium chamber of the cryostat, thus allowing illumination from a laser beam spot on the backside of the sample. Further, this system will be vacuum capable, allowing the sample to be suspended in sub-lambda point liquid helium, lowering the boiling temperature of the helium and concurrently lowering the sample temperature to 2.0 K. Lastly, a newly acquired intensified CCD camera may allow lower fluences to be successfully applied, lowering the average burn rate and increasing the overall resolution, providing improved fits of HGK curves. Alternatively, the frame exposure times can be decreased, providing a similar result.

APPENDIX B. CELL CYCLE PHASES

As cell cycle phases have received significant attention throughout this thesis, it is important to be familiar with the classifications of the life cycle of the cell, which in this case will be assumed to be that of a standard eukaryotic cell. What follows is summarized from ref.[B1]. The cell cycle is broken into two different events of a circular loop, called interphase and division. Division is the most easily observed phase under a microscope, however this phase only encompasses one of the subdivisions of the standard cell cycle, the M (mitosis) phase. There are three other phases, designated as G_1, S, and G_2, all of which can occur during interphase and are not as easily identified as the M phase. The cycle period varies for different types of cells, but in a typical dividing mammalian cell is about 24 hours.

The G_1 phase is noted as beginning at the completion of mitosis but before the beginning of DNA synthesis. The cell is afforded time for growth during this period, before going into a new reproductive cycle. Entry into S phase marks the start of the latter, where DNA synthesis is begun and completed. G_2 serves as an internal checkpoint for the cell, to assure that it is prepared for division by ensuring that DNA replication is complete and that the cell has increased its size enough (roughly doubled its mass) to continue with division. Although it is beyond the scope of this discussion, it is important to note that a central control system is in control of transitions into each of the succeeding cycles, albeit with numerous checks and controls. An illustration of this cycle is provided in Figure B.1.

[B1] Alberts, B.; Bray, D.; Roberts, K.; Watson, J. D. *Molecular biology of the cell*, Third ed.; Garland Publishing, Inc.: New York, **1994**

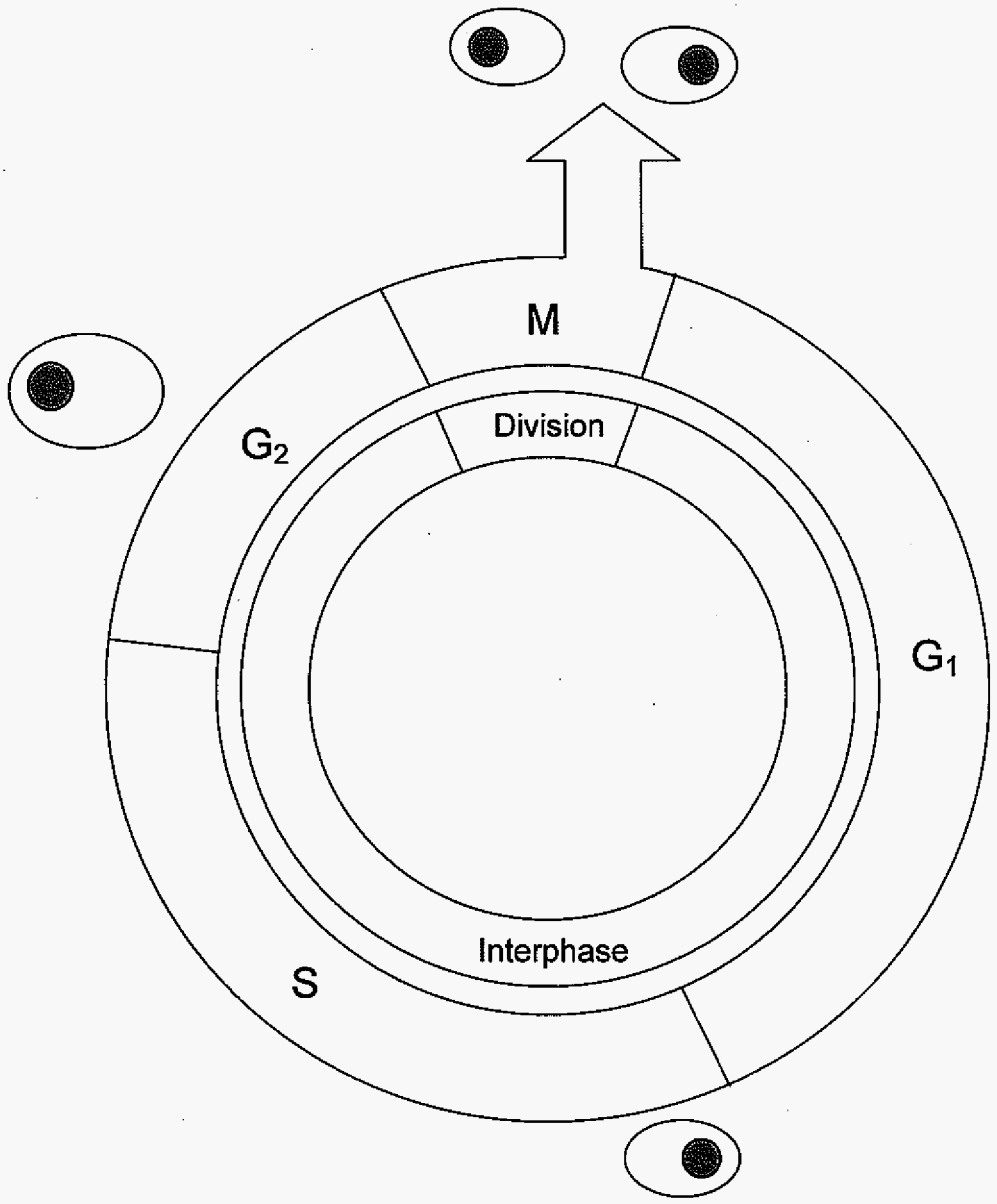

Figure B.1. The four successive life cycle phases of a standard eukaryotic cell cycle. Cells grow continuously during interphase, and division occurs during M phase. The typical cycle of an adult eukaryotic cell is ~24 hours.

APPENDIX C. LABORATORY SCHEMATIC

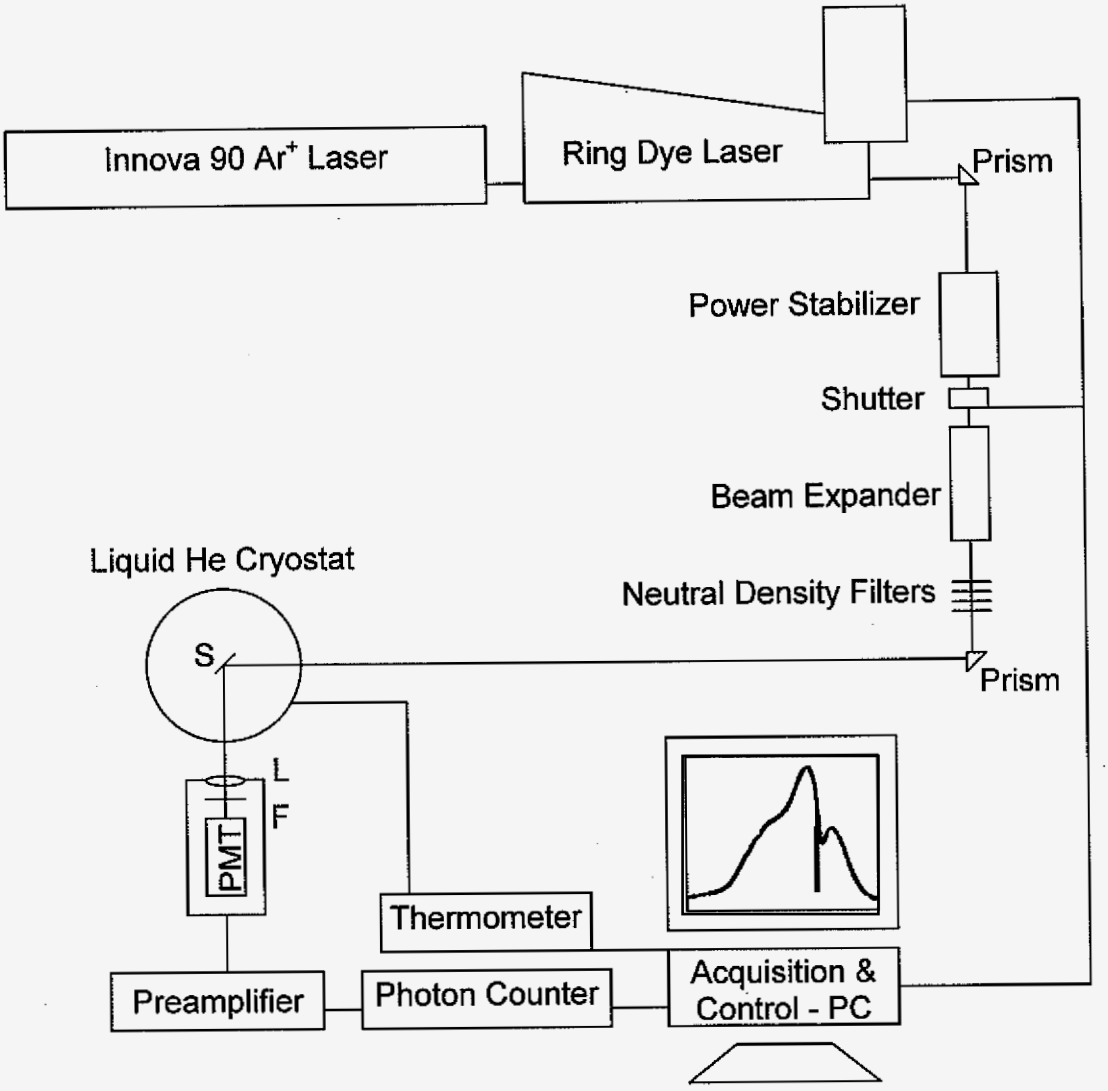

Figure Legend. F: longpass filter; L: light collecting lens (*f* 1.3, 80 mm focal length); S: sample. In-house software (written by Tonu Reinot) to control ring dye laser and interface with photon counter.

APPENDIX D. ADDITIONAL SPECTROSCOPIC INFORMATION REGARDING IN VITRO CELLS AND MF680

Portions of data not included in the previously presented manuscripts are still important to the understanding of MF680 NPHB characteristics *in situ*. Namely, measurements made pertain to the optimal burn regions of MF680, ZPH FWHM's of MF680 in each cell line for comparably burned holes, and temperature dependence of MF680 ZPH FWHM. Each will be addressed briefly, with further explanation of the experimental conditions and results obtained.

Figure D.1 displays the "action spectrum" for MF680 located in each cell line. This spectrum provides a measure of the ZPH formation efficiency for selective burning at various wavelengths with a fixed burn fluence[D1]. From the figure, it is evident that ZPH burning efficiency decreases at wavelengths < 704 nm for both cell lines. Also noteworthy is the observation that hole depth does not differ greatly for wavelengths > 704 nm, within experimental uncertainty. Spectra were burned and scanned without the inter-cavity etalon installed, which is to say the laser is in a lower resolution mode than typically used, and the holes are thus laser linewidth limited. The average minimum step size of the laser is about five times larger than the effective linewidth and prone to omit or misrepresent ZPH depth occasionally. Nonetheless, the action spectrum still provides adequate indication of optimal burn ranges.

Figure D.2 displays data for ZPHs burned at identical fluences to investigate the possibility of differences in ZPH FWHM in each cell line. From the data, there is

---

[D1] Wu, H. M.; Reddy, N. R. S.; Small, G. J., *J. Phys. Chem. B* **1997**, *101*, 651

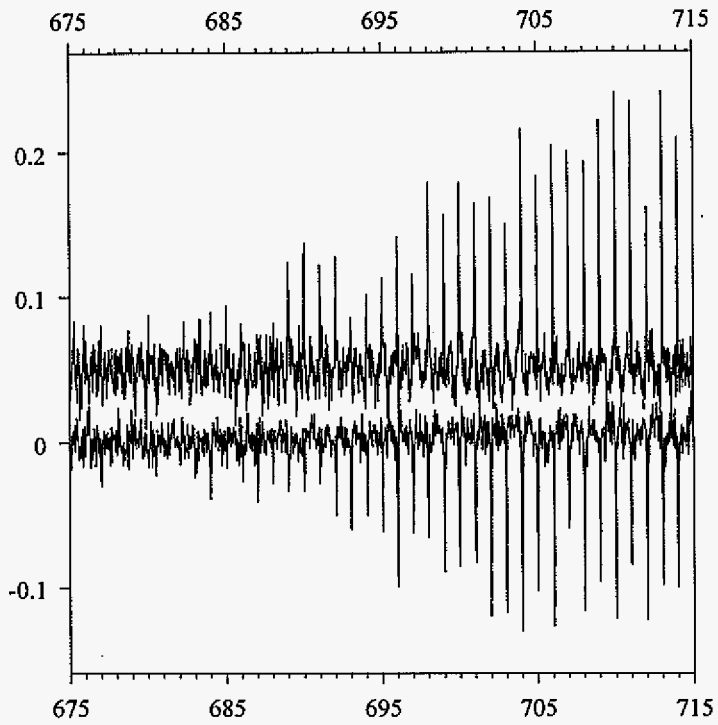

Figure D.1. Zero-phonon hole action spectra (arbitrary units) of MF680 in OSE(tsT)-14 normal (N) and OV167 carcinoma (C) cells. Each ZPH was burned with a fluence of 10 mJ/cm^2 at 1 nm intervals. The spectrum for C has been inverted for the sake of comparison.

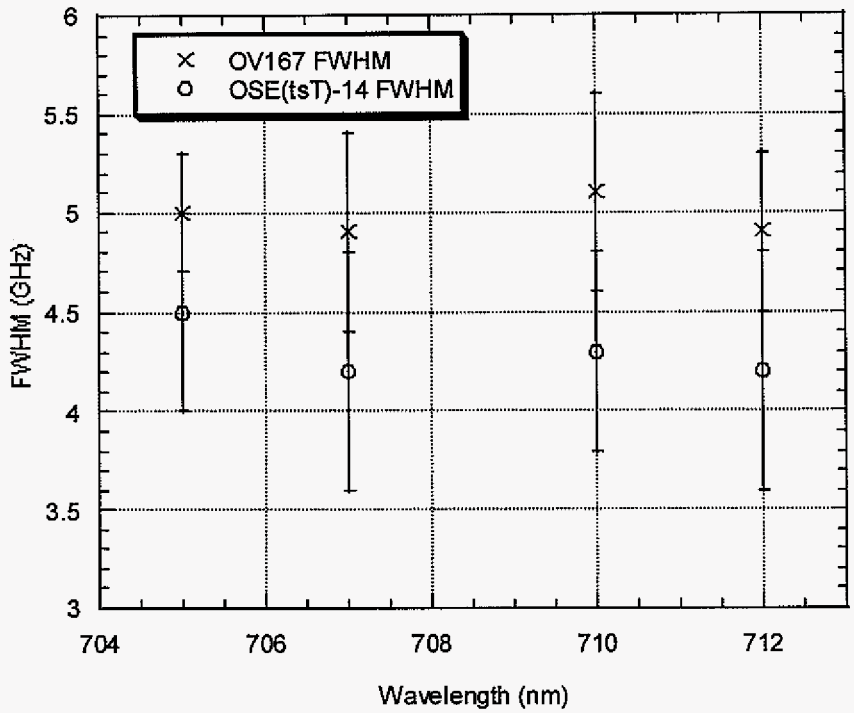

Figure D.2. Zero-phonon hole widths burned at identical fluence and various wavelengths. Burn temperature: 1.4 K; fluence: 2.5 mJ/cm^2.

a tendency for the normal cell line to have slightly narrower ZPHs, however the average difference is within experimental uncertainty and cannot be considered significant for determining discernable differences. Noteworthy from the figure is the observation that ZPH FWHM displays no wavelength dependence (within uncertainty), reaffirming the conclusion drawn from the action spectrum presented in Fig. D.1.

Figure D.3 provides data from a study to investigate the possibility of variance in ZPH FWHM with burn temperature between normal and carcinoma cells. At temperatures < 10 K, the ZPH FWHM dependence on temperature is dominated by TLS_{int} glass-like matrix interactions with MF680 and might have been expected to differ between the cell lines. Burn fluences were identical for each type of sample and each temperature, with applied fluences of 10 mJ/cm^2. From the fits applied to the data, it is apparent that ZPH FWHM increases with increasing burn temperature. However there is no significant difference in the ZPH FWHM between the cell lines. This is interpreted as evidence of the density of states of TLS_{int} varying insignificantly between the cell lines.

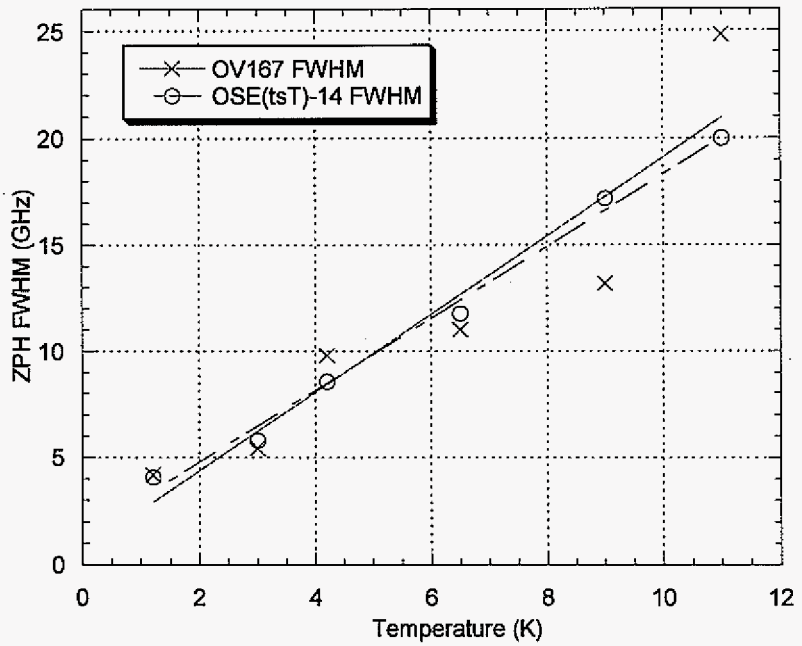

Figure D.3. Zero-phonon hole widths burned at various temperatures display no difference between each OSE(tsT)-14 normal cells and OV167 carcinoma cells. Burn fluence for each hole: 10 mJ/cm^2.

APPENDIX E. CELL CULTURE TECHNIQUES

Although any given cell culture requires a specific medium for maintaining healthy growth characteristics, this appendix is meant to explain in detail the culturing practices utilized for the research in this thesis in the event this work is to be repeated or expanded utilizing the same or different cell cultures. Therefore, the ovarian surface epithelial cell lines OV167 (carcinoma cells) and OSE(tsT)-14 (SV40 transfected normal cells) will serve as the model cells from which these procedures may be reproduced and/or adapted.

E.1. Sterility and Waste Disposal

This section has been placed first due to its extreme importance. It cannot be stressed enough: the need to pay particular attention to the sterility of all flasks, growth medium, tools, etc. is paramount to successful cell culturing. All work should be performed in a sterile laminar flow hood, which is certified and properly functioning (for the sterility of the culture and the safety of the researcher). Hoods should be inspected at least annually by the Environmental Health and Safety office (or an equivalent certified inspector). Proper hood operation encompasses turning on the flow hood and sterilizing ultraviolet (UV) light 30 minutes prior to use, and then turning off the UV light and opening the sash within given parameters (specific to every hood) to work in the hood. Personal protective equipment should be worn at all times, especially latex or nitrile gloves. Users should have a spray bottle of 70%/30% ethanol/water, to sanitize hood surfaces prior to use and also to sanitize medium bottles, gloves, etc. before placement in the hood. One time use individually wrapped plastic pipettes and flasks are commonly used, as these are

sterile and inexpensive. If sterilization is necessary, however, such as for glassware, an autoclave should be used.

Disposal of all flasks, pipettes, gloves, etc. should be in orange "Biohazardous Waste" bags. The bag should be autoclaved before disposal. Liquid wastes can be disposed of by adding bleach to the solution and subsequently disposing of the liquid, or by autoclaving the liquid and disposing. Any additional dyes, biotoxins, etc. should be handled and disposed of according to instructions.

E.2. Culture Media

OV167 cells were grown utilizing Alpha Minimum Essential Medium (MEM) with EARLE's Salts and Nucleosides. Dry powders are readily available from most chemical manufacturers, and can be made by dissolving the powder in deionized water per label instructions, with addition of sodium bicarbonate (amount also given with instructions) and adjustment of pH to 7.2 with addition of 1 M NaOH. The medium must then be sterile filtered (0.22 μm cellulose acetate) into an autoclaved container. Before use, the addition of fetal bovine serum is required at a concentration of 20% v/v. L-glutamine must also be added at 1 mL per 100 mL of medium, as well as penicillin/streptomycin at 1 mL per 100 mL medium (10,000 units/mL penicillin and 10,000 μg/mL).

OSE(tsT)-14 cells were grown in a 1:1 mixture of powdered MCDB 105 medium and powdered medium 199 (from Sigma). Powders are likewise dissolved in deionized water with the addition of 2.2 g/L sodium bicarbonate, with pH adjustment to 7.2 with 1 N NaOH. The solution was subsequently sterile filtered,

and fetal bovine serum was added at a concentration of 15% v/v. L-glutamine and penicillin/streptomycin were added at the same concentrations as the OV167 line.

E.3. Growing Cell Cultures

Storage of cells prior to culturing should be in liquid nitrogen. Cells are typically aliquoted and frozen in 1 mL amounts, and should be thawed rapidly in a 34°C or 37°C warming bath to begin culturing. Suitable culturing flasks with areas of 25, 75, and 162 cm^2 can be used to contain and grow the cells. Generally, each of these flasks holds 10, 30, and 60 mL total volume, respectively. Pre-warmed respective medium is added, and the newly thawed cells are added to the flask with medium. The flask is then placed in an incubator with relative humidity ≥ 70% and 5.5% $CO_{2(g)}$, and the flask cap is slightly opened to allow interchange of gases. In the case of the OV167 line, the cells are grown at the typical temperature of 37°C, however the case is different for the temperature sensitive OSE(tsT)-14 cells. To permit the SV40 Large T antigen to persist in the cells, the incubator must be at the temperature of 34°C and 5.5% $CO_{2(g)}$. To denature the SV40, simply increase the temperature to 39°C for 12-18 hours.

Cells should be monitored daily for growth, and "fed" after three days by removing up to 50% of the medium, followed by replacement with an equal amount of fresh medium. Depending on the cell culture, however, this cycle may be shortened or lengthened; importantly, the culture must be monitored for coverage of the flask. Confluency is usually to be avoided, especially in the case of normal cells, as this may lead to undesirable effects. In some cases, however, confluent cells

may be desired for a particular experiment (e.g. cells that are not in an active dividing stage); cell life stages can be checked via flow cytometry.

Splitting cell cultures is performed to thin the population of cells in a culture or to increase the number of flasks being used. Splitting is accomplished by adding trypsin (1X-10X) / EDTA (1 mM) to the culture flask after removing growth media and rinsing once with phosphate buffered saline (PBS). Although heavily dependent on the cells being cultured, the concentration of trypsin to be used and the time to incubate with trypsin can vary. The volume to be used should just cover the bottom of the culture flask, and as an example, 3 mL is ample for the 25 cm^2 culture flask. For particularly stubborn cells (such as the OV167 cell line), the flask can be placed back in the incubator without opening the cap. Generally, the cells should release in 5-10 minutes; longer times indicate a necessity for a stronger concentration of trypsin. Hitting the flask against the palm of the hand forcefully will also help to release the cells. The trypsin activity can be halted by adding an equal volume of fresh pre-warmed growth medium. Cell densities are often desirable to obtain at this point, and this can be performed on a cell counter (if the laboratory is so equipped) or by means of a hemocytometer. Hybridoma facility personnel can be contacted for performing these types of measurements, as full explanations are beyond the scope of this discussion.

E.4. Cryopreservation / Cryofixation

Briefly, cryofixation involves freezing a cell culture in a state that fixes the cell in its native morphological state and does not necessarily concern viability of the cell, whereas cryopreservation involves freezing a cell or cell culture so as to

preserve the viability of the cells without regard to the morphology. Commonly, the former is performed without any cryopreservatives (e.g. dimethyl sulfoxide, DMSO), and the latter relies on 5-10% DMSO. DMSO serves to permeate cell membranes prior to freezing and does not allow large ice crystals to form during the freezing process. These crystals rupture cell membranes and in turn kill the cell when the cell is thawed out for growth. Further, freezing rates play a large role in the success of either fixation or preservation. For fixation processes, rapid cooling (≥1000 K/s) is desirable; for preservation, a slow cooling rate (1°C/min) is desired. The latter is accomplished conveniently with a commercially available calibrated cryopreservation chamber that utilizes isopropyl alcohol to optimize the cooling rate.

In terms of experimental planning, cryopreservation plays a very important role. For the experiments conducted in this thesis, it was desirable to have multiple samples with cells in similar proportions of growth stages and at the same passage number. In order to accomplish this, large numbers of cells were cultured and subsequently cryopreserved in 1 mL aliquots. Using a 75 cm^2 culture flask, an initial aliquot was grown and split into three 75 cm^2 flasks, which in turn were harvested to provide 54 aliquots of cells. Each aliquot contained 50,000-100,000 cells, an adequate number from which to start new cultures.

For individual experiments, cells were cultured approximately 6-7 days before staining and processing. Staining was accomplished by simply adding the dye to the medium, as the dye used in this thesis was membrane permeable. After a set incubation time, the cells were rinsed three times with PBS and trypsinized; once lifted, the trypsin was halted with growth medium and the suspension placed in a

centrifuge tube and spun to form a pellet. The supernatant was poured off, and the cells were re-suspended in 120 µL medium and 6 µL DMSO. This mixture was then placed into a #5 gelcap, which was then placed in a #4 gelcap (the #5 gelcaps dissolve rapidly in medium, typically before freezing). The gelcap was then placed in a cryovial and placed in the aforementioned calibrated cryopreservation chamber in a –70°C freezer for at least 4 hours.

E.5. Cell Culturing for Microscopy

It is sometimes desired to have cells remain attached to a microscope coverslip or coverglass for use in a microscope, and this creates some procedural additions. Cells typically adhere poorly to glass, so that any time glass is to be used it must be coated with poly-L-lysine, which reverses the inherent negative charge of the glass and fosters cell attachment. The procedure for creating such glass is to begin by cleaning the glass in a cleanser and then thoroughly rinsing, with the final rinses in nanopure water. The glass should then be dried and sterilized in a sterile hood with UV light for approximately 30 minutes per side. A 5% solution of poly-L-lysine can be made by diluting the poly-L-lysine in sterile water, and the glass submerged in this solution overnight at 4°C. After soaking, the glass should be removed and thoroughly rinsed once again with sterile water (deionized). The glass can be used wet or allowed to dry; cell suspensions should be placed directly on the glass, and subsequently submerged in growth medium.